Interactions of Multiple Market-Based Energy and Environmental Policies in Transmission - Constrained Competitive National Electricity Markets

Final Project Report

Power Systems Engineering Research Center

Empowering Minds to Engineer
the Future Electric Energy System

Interactions of Multiple Market-Based Energy and Environmental Policies in a Transmission-Constrained Competitive National Electricity Market

Final Project Report

Project Team

Project Leader: William Schulze, Cornell University

Team Members: Ward Jewell, Wichita State University, and Daniel Tylavsky, Arizona State University

Graduate Students:

John Taber and Jubo Yan
Cornell University

Di Shi and Nan Li
Arizona State University

Yingying Qi, Trevor Hardy and Zhouxing Hu
Wichita State University

PSERC Publication 12-25

September 2012

For information about this project contact:

William Schulze
Dyson School of Applied Economics and Management
Cornell University, Ithaca NY 14853
Email: wds3@cornell.edu
Phone: (607) 227-9895

Power Systems Engineering Research Center

The Power Systems Engineering Research Center (PSERC) is a multi-university Center conducting research on challenges facing the electric power industry and educating the next generation of power engineers. More information about PSERC can be found at the Center's website: http://www.pserc.org.

For additional information, contact:

Power Systems Engineering Research Center
Arizona State University
527 Engineering Research Center
Tempe, Arizona 85287-5706
Phone: 480-965-1643
Fax: 480-965-0745

Notice Concerning Copyright Material

Acknowledgements

This is the final report for the Power Systems Engineering Research Center (PSERC) research project titled Interactions of Multiple Market-based Energy and Environmental Policies in a Transmission-Constrained Competitive National Electricity Market (PSERC Project M-24). We express our appreciation for the support provided by PSERC's industry members, by the Department of Energy CERTS program and by the National Science Foundation under the Industry / University Cooperative Research Center program.

We would also like to thank Energy Visuals for providing much of the data used in this study. Daniel Shawhan (RPI) and Ray Zimmerman (Cornell) have made enormous contributions to this research through work on the related CERTS project. Timothy Mount, Richard Schuler, and Robert Thomas (Cornell) have also contributed greatly to this work. We are very grateful to Jim Price (California ISO) for developing the network reduction for WECC used in this study. We would like to thank Shmuel Oren (UC Berkeley), James Bushnell (UC Davis), and Siny Joseph (Kansas State Univ.) for their contributions as well as our industry team members, Hamid Elahi (GE), Michael Swider (New York ISO), Jim Price (California ISO), Floyd Galvan (Entergy), Robert Ethier (ISO New England), Mark Westendorf and Rao Konidena (Midwest ISO), Lisa Beard (Quanta Technology), Gary Stern (Southern California Edison), and Ray Williams (PG&E).

Executive Summary

Energy futures for the United States depend critically on the electric power system. Goals of energy independence, cleaner energy sources for industry, commercial and residential uses, as well as transportation, are in great part determined by investment in the future power system. A planning tool that optimizes investment in generation is needed because the electric power industry faces the possibility of increased loads from energy users trying to find cleaner sources of energy, including transportation, renewable portfolio standards, and integration of a smart grid that allows for demand response. These challenges need to be met while maintaining reliability and with a $1000 bid cap for generators (in areas with markets) that may limit a free market solution for new investment in generation. Both reliability and investment require planning. This report uses an integrated engineering, economic and environmental modeling framework for the electric power system (the SuperOPF Planning Tool), developed with support from the Department of Energy CERTS program. The model maximizes the net expected benefits of electricity production, optimizes investment in new generation, and includes environmental and other regulations and incentives. This report examines alternative futures for the electric power industry for the continental United States over the next 20 years by using the SuperOPF Planning Tool to analyze plausible policy and fuel price scenarios.

This research depends critically on detailed network reductions for the ERCOT (Texas), WECC (Western States), and EI (Eastern Interconnection) systems. To maintain acceptable accuracy in line flows for the Eastern Interconnection needed, for optimal investment in generation, the research showed that a model with more than 5,200 busses was necessary. Since the full EI network is much more tightly connected than the ERCOT and WECC systems, it is expected that the errors in the PF and OPF solutions for the equivalent for EI will be larger than that for the ERCOT and WECC systems when the percentage of buses retained for the equivalent is the same for each model. The results of the model evaluations demonstrated that a 279-bus equivalent for ERCOT has more than acceptable accuracy in terms of both PF and OPF solutions, indicating that even a smaller equivalent would likely be acceptable. For the WECC system, a similar size system, a 300-bus equivalent, is adequate for performing an optimal generation investment study.

To assess the response of long-term generation investment to alternative future natural gas prices, environmental regulations and renewable incentives, studies are conducted using six possible scenarios. Each future (case) consists of three simulation years: 2012, 2022 and 2032, an interval which is based on the assumption that each investment cycle takes ten years and generation is optimized in 2022 and 2032 for conditions in that year. The simulation year 2012 is assumed to have generation as built today.

The cases studied in this report are described as follows. The first case is referred to as the base case. In the base case, no environmental regulation or subsides for renewable energy are included.

In the second case, a CO_2 emissions price is added to represent a cap-and-trade auction for CO_2. This cap-and-trade auction for CO_2 is assumed to have a price cap similar to that

proposed in the Kerry-Lieberman Bill. This case is referred to as the cap-and-trade (C&T) case. In the C&T case, the CO_2 price starts at 36.94 $/ton in 2022 and rises to 60.18 $/ton in 2032, equivalent to the Kerry-Lieberman price cap. Besides modeling CO_2 emissions prices, subsides for wind and solar generation are included. An incentive of 22 $/MWh for wind and solar generation is included to model the Federal Renewable Electricity Production Tax Credit [28].

Similar to the C&T case, the third case also includes the production tax credit incentives for wind and solar generation. However, instead of cap-and-trade, the EPA proposed rule aimed at regulating CO_2 emissions from power plants is included, a rule that is expected to be finalized later in 2012. This rule requires all new fossil-fuel-fired generation of 25 MW or larger to emit no more than 1000 lbs. of CO_2 per MWh. Since coal-fired plants cannot meet this standard, the standard effectively prohibits the construction of new coal plants. Therefore, in the third case, no new coal-fired plants can be built in 2022 and 2032. The third case is referred to as the EPA case.

All of the three cases are simulated with two different sets of gas prices, yielding six futures in total. The first set of gas prices is referred to as the high gas price set, which is 2.5 $/MMBTU in 2012, 7 $/MMBTU in 2022 and 14 $/MMBTU in 2032. The low gas price of 2.5 $/MMBTU modeled in 2012 is based on the current availability of shale gas but it is possible that the costs of extracting shale gas will start to rise by 2022 and so the gas price increases to 7 $/MMBTU. Then in 2032, the gas price converges to a world price of about 14 $/MMBTU. The natural gas price of 14 $/MMBTU may seem large, but the gas price was in the neighborhood of 15 $/MMBTU in 2005.

The second set of gas prices is referred to as the low gas price set, which is 2.5 $/MMBTU in 2012, 4.77 $/MMBTU in 2022 and 5.86 $/MMBTU in 2032. This set of gas prices is based on estimates by the EIA [27].

Based on the different sets of gas prices used, the scenarios studied can be categorized into two groups. The cases that are run with the high gas price set are referred to as high-gas-price cases (HG) and similarly the cases that run with low-gas-price set (LG) are referred to as low gas price cases.

The results suggest that alternative policies may have very different outcomes in terms of electricity prices and CO_2 emissions that vary across regions of the continental United States.

First consider fossil fuels. For natural gas, only combined cycle plants are constructed across all scenarios with substantial retirements of single cycle plants by 2022. There is no new construction in ERCOT until 2032 and then only in the scenario with low gas prices and cap-and-trade. There is no new gas generation constructed in WECC under any scenario. The EI is a different story with combined cycle plants constructed both under high and low gas price cases for all scenarios in 2022 and 2032 with the most construction occurring under cap-and-trade. However, retirements generally exceed new construction in 2022 but the reverse is true for cap-and-trade in 2032 and more balanced in the other scenarios. Surprisingly, no new coal is constructed in any of the scenarios, even the base case with high gas prices. Retirement of both existing coal (and single-cycle natural gas plants) is accelerated by low gas prices, the production tax credit for

wind and solar, and by cap and trade. No new oil units are built and retirements are substantial over the 20-year time horizon of the study.

For renewables, wind and solar are encouraged by high gas prices, cap-and-trade, and the production tax credit. No wind is retired under any of the scenarios. In ERCOT, wind is added by 2022 in all but the low gas price base case, but more is added in all cases by 2032. For WECC, wind is added in all cases, mostly by 2022. For the EI there are very large additions under all scenarios, mostly in Kansas and Oklahoma, but some additions in all states except Florida. Note that the model assumes that the existing high voltage network is in place with no new high voltage lines. The geographic distribution of additional wind is likely to change if new high voltage lines are put in place. For solar, by 2022, small amounts are constructed in ERCOT only if cap and trade is implemented, and small amounts are constructed in WECC only in the high gas, cap-and-trade scenario. But, surprisingly, by 2022 in the EI solar is constructed in all cases except the low gas price base case. In the EI by 2032 solar is added in all cases, but the most is added in cases with the production tax credit. Solar investment occurs mostly in Florida, but with the production tax credit, solar is built throughout the southeast. It should be noted that, though no nuclear construction takes place by 2022, substantial nuclear construction takes place by 2032, but only with high gas prices and cap-and-trade. Thus, policies can change how much new generation is built, what types of plants are built, and what types of plants are retired.

Across all regions, electricity prices are highest under cap-and-trade combined with high natural gas prices and lowest with the production tax credit for wind and solar combined with low natural gas prices. CO_2 emissions are lowest with low natural gas prices combined with cap-and-trade and the production tax credit for wind and solar, and highest with high natural gas prices under the base case.

A number of caveats are important in interpreting these results. First, the model assumes that a smart grid is in place in 2022 and 2032 that allows demand response. Second, capital costs are estimated far into the future and, for example, while the costs of wind are well understood, recent cost decreases for solar may, or may not, continue. This study assumes that they do. Similarly, there are several technologies proposed that may lower the costs of nuclear plants. If that were to occur, and nuclear became politically feasible, the results would be quite different than those shown here.

Finally, this study represents the first step in making the SuperOPF Planning Tool publically available as open source software similar to MatPower, since the tool has now been used at both Arizona State and at Wichita State to analyze energy futures for ERCOT and WECC respectively for this report.

Project Publications:

J. Taber, D. Shawhan, R. Zimmerman, C. Marquet, M. Zang, W. Schulze, R. Schuler, S. Whitley, “Mapping Energy Futures Using The SuperOPF Planning Tool: An Integrated Engineering, Economic and Environmental Model,” HICSS 46 Proceedings, Jan 2013.

D. Shi, D. J. Tylavsky, "An Improved Bus Aggregation Technique for Generating Network Equivalents," 2012 IEEE Power Engineering Society General Meeting, San Diego, CA.

Y. Qi, D. J. Tylavsky, "Impact of Assumptions on DC Power Flow Accuracy," North American Power Symposium 2012, Champaign Illinois, Sep. 2012, pgs. 6.

N. Li, D. Shi, D. Shawhan, D. J. Tylavsky, J. Taber, R. Zimmerman, "Optimal Generation Investment Planning: Pt 2:, Application to the ERCOT System," North American Power Symposium 2012, Champaign Illinois, Sep. 2012, pgs. 6.

D. Shi, D. Shawhan, N. Li, D. J. Tylavsky, J. Taber, R. Zimmerman, "Optimal Generation Investment Planning: Pt 1:, Network Equivalents," North American Power Symposium 2012, Champaign Illinois, Sep. 2012, pgs. 6.

Z. Hu, W. T. Jewell, "Optimal Power Flow Analysis of Energy Storage for Congestion Relief, Emissions Reduction, and Cost Savings," *2011 Power Systems Conference and Exhibition*, Phoenix, March 2011.

Student Theses:

John Taber, *Essays on Carbon Abatement and Electricity Markets*, PhD thesis at Cornell University, Aug. 2012.

Di Shi, *Power System Network Reduction for Engineering and Economic Analysis*," PhD thesis at Arizona State University, Aug. 2012.

Nan Li, *A Modified Ward Equivalent of ERCOT for Power System Planning Studies*, Masters of Science thesis at Arizona State University, expected in Dec. 2012.

Zhouxing Hu, *Optimization of Electric Power System Operation with Renewables and Energy Storage*, PhD thesis at Wichita State University, expected in December 2012.

Table of Contents

Table of Contents (continued)

List of Figures

List of Figures (continued)

List of Figures (continued)

List of Tables

1. INTRODUCTION

1.1 Background

Energy futures for the United States depend critically on the electric power system. Goals of energy independence, cleaner energy sources for industry, commercial and residential uses, as well as transportation, are in great part determined by investment in the future power system. A planning tool that optimizes investment in generation is needed because the electric power industry faces the possibility of increased loads from energy users trying to find cleaner sources of energy, including transportation, renewable portfolio standards, and integration of a smart grid that allows for demand response. These challenges need to be met while maintaining reliability and a $1000 bid cap for generators (in areas with markets) that may limit a free market solution for new investment in generation. Both reliability and investment require planning. This report uses an integrated engineering, economic and environmental modeling framework for the electric power system (the SuperOPF Planning Tool), developed with support from the Department of Energy CERTS program. The model maximizes the net expected benefits of electricity production, optimizes investment in new generation, and includes environmental and other regulations and incentives. This report examines alternative futures for the electric power industry for the continental United States over the next 20 years by using the SuperOPF Planning Tool to analyze plausible policy and fuel price scenarios.

1.2 Overview of the Problem

This research depends critically on detailed network reductions for the ERCOT (Texas), WECC (Western States), and EI (Eastern Interconnection) systems. Research was conducted to develop equivalents that maintain acceptable accuracy in line flows needed for optimal investment in generation. To assess the response of long-term generation investment to the future environment, an environment that is uncertain, studies are conducted using six possible scenarios. Each future (case) consists of three simulation years: 2012, 2022 and 2032, an interval which is based on the assumption that each investment cycle takes ten years and generation is optimized in 2022 and 2032 for conditions in that year. The simulation year 2012 is assumed to have generation as built today.

The cases studied in this report are described as follows. The first case is referred to as the base case. In the base case, no environmental regulation or subsides for renewable energy are included.

In the second case, a CO_2 emissions price is added to represent a cap-and-trade auction for CO_2. This cap-and-trade auction for CO_2 is assumed to have a price cap similar to that proposed in the Kerry-Lieberman Bill. This case is referred to as the cap-and-trade (C&T) case. In the C&T case, the CO_2 price starts at 36.94 $/ton in 2022 and rises to 60.18 $/ton in 2032, equivalent to the Kerry-Lieberman price cap. Besides modeling CO_2 emissions prices, subsides for wind and solar generation are included. An incentive of 22

$/MWh for wind and solar generation is included to model the Federal Renewable Electricity Production Tax Credit [28].

Similar to the C&T case, the third case also includes the production tax credit incentives for wind and solar generation. However, instead of cap-and-trade, the EPA proposed rule aimed at regulating CO_2 emissions from power plants is included, a rule that is expected to be finalized later in 2012. This rule requires all new fossil-fuel-fired generation of 25 MW or larger to emit no more than 1000 lbs. of CO_2 per MWh. Since coal-fired plants cannot meet this standard, the standard effectively prohibits the construction of new coal plants. Therefore, in the third case, no new coal-fired plants can be built in 2022 and 2032. The third case is referred to as the EPA case.

All of the three cases are simulated with two different sets of gas prices, yielding six futures in total. The first set of gas prices is referred to as the high gas price set, which is 2.5 $/MMBTU in 2012, 7 $/MMBTU in 2022 and 14 $/MMBTU in 2032. The gas price of 2.5 $/MMBTU modeled in 2012 is based on the assumption that the costs of extracting shale gas start to rise by 2022 and so the gas price increases to 7 $/MMBTU. Then in 2032, the gas price converges to the world price of about 14 $/MMBTU. The gas price of 14 $/MMBTU may seem large, but the gas price was in the neighborhood of 15 $/MMBTU in 2005.

The second set of gas prices is referred to as low gas price set, which is 2.5 $/MMBTU in 2012, 4.77 $/MMBTU in 2022 and 5.86 $/MMBTU in 2032. This set of gas prices is based on estimates by the EIA [27].

Based on the different sets of gas prices used, the scenarios studied can be categorized into two groups. The cases that are run with the high gas price set are referred to as high-gas-price cases (HG) and similarly the cases that run with low-gas-price set (LG) are referred to as low gas price cases.

1.3 Report Organization

Chapter 2 of this report describes the methods used and network reductions developed for ERCOT, WECC, and the EI. Chapter 3 presents results from applying the SuperOPF Planning tool to the cases described above. Chapter 4 draws conclusions from the study.

2. NETWORK EQUIVALENTS

This chapter shows the network equivalents for ERCOT, WECC and the EI respectively. For ERCOT, a validation check was also conducted in the second part of this chapter to confirm that the reduced network is actually reasonable approximation of the full network model. For WECC, the network reduction is taken from existing literature so the third part of this chapter only briefly describes the reduction and refers to different literatures.

2.1 A Modified Ward Equivalent for ERCOT System

The first part of this chapter presents the method used for developing a backbone equivalent for a large-scale power system and then the method is applied to the ERCOT system. Several prevailing network reduction techniques are first reviewed. A brief introduction to ERCOT system is given in this chapter. The equivalents generated are validated using different metrics and promising results are obtained.

2.1.1 Literature Review on Network Equivalencing Techniques

Depending on the application of the equivalent, the network equivalencing technique can be generally divided into two categories: static and dynamic equivalencing. For dynamic reduction, the focus is to capture the dynamic characteristics of the full system, and the reduced model is intended for system dynamic analysis, such as real-time power system transient stability assessment [2]. For static reduction, the reduced model is intended for static power flow studies, such as online contingency evaluation, market-based system analysis and system-planning studies. Since the focus of this report is on system planning, only the static equivalencing technique is reviewed and the term “network reduction” refers only to static power system reduction. Currently there exist several prevailing classes of equivalents. One of them is the REI (radial equivalent independent) equivalent, which was first proposed in [3] and further discussed in [4] and [5]. The REI equivalent aggregates power and current injections at designated external buses on to a fictitious ‘REI’ node, and the designated group is then replaced by a fictitious bus in the reduced model. The REI nodes are connected to boundary buses through a radial network called the REI network. The criteria for aggregating buses can be selected based on generation and load conformity, or electrical, geographical, ownership groupings, etc.

REI equivalent may have some limitations. One limitation is that the fictitious ‘REI’ nodes may suffer from low bus voltage magnitude. To solve this problem, solutions were proposed in [5] to improve the REI equivalent. The performance of the improved REI equivalent was compared against other types of equivalents and promising results were observed.

Another limitation with REI equivalent is that the REI equivalent is operating point dependent: the admittances of the REI network are functions of operating condition at which REI equivalent is constructed. Therefore, as the operating point moves away from the base case, the accuracy of the REI equivalent will in general deteriorate.

The REI equivalent also has the limitation that it lacks the ability to preserve low degree of sparsity of the reduced model. Due to the extra interconnections introduced by REI

network, an REI equivalent always tends to be denser than its Ward equivalent counterpart. This limitation decreases the computational efficiency of the REI equivalent, and may limit its applicability in problems where high computational efficiency is required.

Another widely used type of equivalencing method is the Ward equivalencing technique, which was first proposed by Ward in [6] and further discussed in [7]-[10]. The basic idea of Ward reduction method is to eliminate the buses in the external subsystem through Gaussian elimination, while keeping the internal subsystem intact.

The classic Ward reduction method has two versions [9], differing in the ways that they model bus injection at each node. The first version of classic Ward reduction is referred to as Ward Injection method. In this method, the power injection at each bus is converted to injected current before eliminating the external buses. After the external buses are eliminated, current injection is converted back to power injection at each bus. The second version of classic Ward reduction is referred to as Ward Admittance Method. In this method, power injection at each bus is converted to constant shunt admittance instead of current injection before reduction. The second version is less preferable than the first version, because it may yield unrealistic admittance in the equivalent, and the shunt-admittance modeling of bus injections may not be appropriate for all loads.

The classic Ward equivalent also has its limitations. One such lies in its inability to accurately model the reactive power response from the external buses. In order to overcome this limitation, several modified versions of classic Ward equivalent were discussed in [8]-[13]. In [8], a Ward-PV equivalent was proposed. In this model, all the external PQ buses are eliminated while the external PV buses are retained. However, retaining of all the external PV buses increases the size of the equivalent and thereby decreases the computational efficiency of the equivalent. To further improve the Ward equivalent, an extended Ward equivalent for static security analysis was proposed in [12]. In the extend Ward equivalent, a fictitious PV bus is attached to each boundary bus. This fictitious PV bus contributes no active power injection but provides adjustable reactive power injection to the system. The reactive power provided by the fictitious is zero under base case and will vary as operating point moves away from base case.

In [14], J. Mochowski et al. proposed a reduced Ward-PV equivalent. In this method, all the external generator nodes are retained and aggregated into several groups. After generator aggregation is done, each group is replaced by an equivalent generator node using Zhukov method [15]. Therefore, the number of nodes retained is reduced. By using the Zhukov method, the dynamic properties of the system can also be maintained, which make the reduced Ward-PV equivalent also applicable in dynamic studies.

Other limitations of the traditional Ward equivalent make its application to the optimal power flow problematic. It is well known that the traditional Ward equivalent may “smear” the injections of external generators over a large number of boundary buses. For system planning studies and market-based analysis, modeling of fractions of generators at different buses is not practical. To overcome this limitation, authors in [16] proposed a “combined” equivalent for the Northeast part of the U. S. power grid. To generate such a “combined” equivalent, the classic Ward Injection Method is first applied to eliminate all external buses except those that are generator buses. Then based on “electrical distance”,

external generators are “moved” to the closest retained buses. The Ward reduction is continued to eliminate the external generator buses that have become vacant. With generators retained as whole, the original generator cost functions can be directly applied and the equivalent can be used in market analysis. However, the internal-system power flows and bus voltages in this equivalent are very different from that in the original system.

In recent years, several network reduction techniques were proposed for system planning and market analysis [17]-[20]. The methods proposed in [18]-[20] are based on DC power flow assumptions and power transfer distribution factors (PTDF). The fundamental concept of these two methods is to aggregate buses while keeping the inter-zonal topology the same as the original (full) system. However, the equivalents generated by these methods contain only equivalent lines with no MVA ratings on them, and currently no existing methods in the literature discusses how the line limits should be assigned for these equivalent lines. Therefore, these two methods may not be applicable in market based analysis where congestion information is required.

2.1.2 Objective of the Study and Requirements for Equivalent

The objective of this study is to develop a DC backbone equivalent for the entire ERCOT system to be used in a system planning tool for making policy and investment decisions that take into account of the market structure and greenhouse gas (GHG) regulations. A DC rather AC model was chosen for the equivalent because the PF problem becomes linear under DC assumptions and therefore the solution requires much less execution time and convergence is guaranteed. The assumptions used to justify using any of the various Ward equivalents in traditional applications are violated when applied to developing such a backbone equivalent.

First, in the traditional scenario, the internal area is geographically and electrically localized, and the external area is electrically remote from the internal area. However, in the equivalent to be used in this study, the internal area is neither geographically nor electrically localized. Also, for the external network, most parts of it are not electrically remote from the internal area.

Second, in the traditional scenario, the generators in the external area are either eliminated or replaced by equivalent generators. The injections from external generators are either modeled as small pieces of injections over a large number of buses, or aggregated to equivalent generators. However, for system planning studies to be carried out in this paper, all the generators participate in the market should be retained and each generator should be retained as whole.

Therefore, a novel modified Ward equivalent [21] that can meet these requirements is implemented in this study.

2.1.3 Brief Introduction to Ward-Type Equivalent

In the Ward (bus elimination) approach, the power system under consideration is usually separated into two parts: the studied system and the external system, as shown in Figure

2.1. The studied system can be further partitioned into internal buses and boundary buses. The internal buses are interconnected with external system through the boundary buses.

During the reduction process, the external buses are collapsed and the branches are eliminated via partial triangular factorization of the network matrix and the eliminated branches are replaced by equivalent lines between (collapsed) boundary buses. The electrical power injected at the external buses is first modeled as equivalent current injections at the boundary buses and then converted back to power injections based on the bus voltage at boundary buses. After elimination, the internal system remains unscathed while the external subsystem is eliminated.

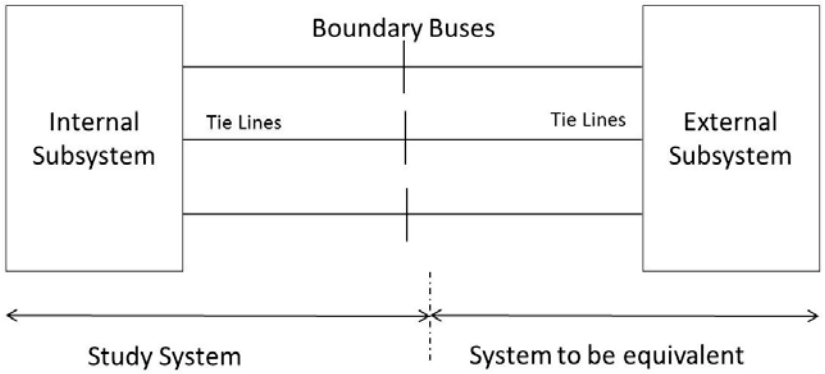

Figure 2.1: Partitioning of the System

2.1.4 A Modified Ward Reduction for ERCOT System

2.1.4.1 Selecting Buses to Retain

The first step in conducting a network reduction is to select the study system. Since the equivalent to be generated will be used to conduct optimal generation investment planning that taking into account of the environmental regulations, it is important that the system congestion information be retained in the reduced system.

The congestion information was obtained from the *ERCOT Planning and Operation Information Database* (the database is proprietary), which includes not only the ERCOT congestion reports from year 2000 to 2008, but also the transmission planning reports for year 2010 to 2015. These data bases were used to identify congested lines and congested paths, which were retained in the model.

Another criterion for selecting retained buses is the voltage levels of the buses. In general, high-voltage buses are more important to retain since these are the electrical nodes through which bulk power flows. Therefore, besides the congested transmission lines/paths, we experimented with retaining different sets of high-voltage buses using voltage level as the criterion.

2.1.4.2 Modeling of Special Elements

Specific elements in the system need special handling before the process of network reduction is conducted. In the ERCOT system, the elements need to be handled are HVDC lines. Prior to the process of reduction, each HVDC line in the system is replaced by a pair of generators connected to the "from" and "to" bus as shown in Figure 2.2. If DC lines and converters are assumed to be lossless, the following relationship can be obtained:

$$p_{ac\_from} = p_{ac\_to} \tag{2.1}$$

and the outputs of the two generators are given by:

$$p'_{ac\_from} = p_{ac\_from} \tag{2.2}$$

$$p'_{ac\_to} = p_{ac\_to} \tag{2.3}$$

where p_{ac_from} and p_{ac_to} are the power injections at the "from" end and "to" end of the HVDC line, and both p_{ac_from} and p_{ac_to} are at the AC side of the converters; P_{Loss} is the power loss on the HVDC line; and p_{dc_from} and p_{dc_to} are the power flow at the DC side of the converters.

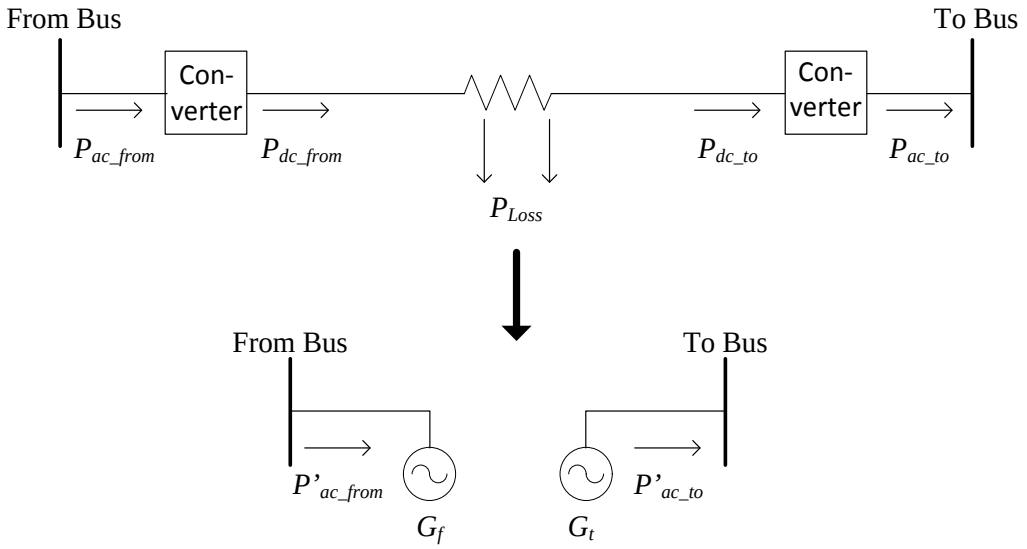

Figure 2.2: Handling of HVDC Lines

After the handling of special elements is completed, a base case can be obtained which will be later used for comparison with reduced models and conducting network reductions.

2.1.4.3 Eliminating External Subsystem and Moving Generators

After the retained buses are selected, the network reduction proceeds in the following steps. First, the Ward network reduction described in [6]-[9] is applied to the entire ERCOT system to remove all external buses. Since most of the retained lines in the reduced model have impedances smaller than 0.01 p.u., equivalent lines with impedances larger than 5.0 p.u. can be removed in the equivalent without significant degradation of the model.

In the second step, the Ward network reduction is conducted again but with a new set of buses retained: the buses retained in the first step and all the generator buses. This model is referred to as the "reduced model with all generators" and will be used in the next step to determine the movement of external generators.

The third step is to assign external generators to retained buses. To demonstrate the procedure of moving generators, a small portion of the reduced model with all generators is shown in Figure 2.3: Reduced Generator Model with All Generators. As shown in, generators *G1* and *G2* are connected to internal system through multiple paths. For example, *G1* is connected to internal buses through transmission line 1-3, transmission line 1-4, or the combination of transmission line 1-2 and 2-5, etc. It should be noted that the actual reduced model with all generators is much more complicated than what is illustrated in Figure 2.3.

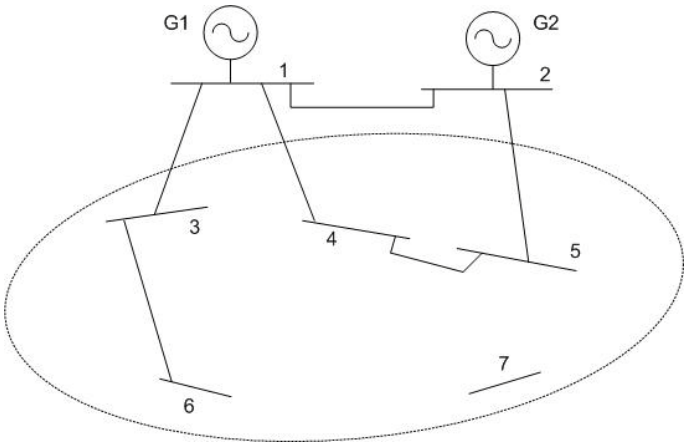

Figure 2.3: Reduced Generator Model with All Generators

The electrical distance between two buses *A* and *B* is defined as

$$Dis_{AB} = \min_{k\in\{k_1\ldots k_n\}}\left(\sum_{k_i=1}^{k_i=m}\sqrt{r_{k_i}^2 + x_{k_i}^2}\right) \qquad 2.4$$

where m is the number of transmission lines that connected bus *A* and *B* in path k_i, and n is the number of paths that between bus *A* and *B*.

Assume the transmission lines that connected generator *G1* to the internal buses in Figure 2.3have the impedances listed in Table 2.1:

Table 2.1: Impedance of Transmission Lines in Figure 2.3

Transmission Line	$\sqrt{r^2 + x^2}$ **(p.u.)**
1-2	0.01
1-3	0.02
1-4	0.01
2-4	0.02
2-5	0.01
3-6	0.015
4-5	0.04

Based on 2.4, the electrical distance between generator *G1* and internal buses can be calculated as

$$Dis_{G1-3} = 0.02$$

$$Dis_{G1-4} = \min\{0.01, 0.06\} = 0.01$$

$$Dis_{G1-5} = \min\{0.05, 0.02\} = 0.02$$

$$Dis_{G1-6} = 0.035$$

From the above calculations, generator *G1* is electrically closest to bus *#4* and should be moved to bus *#4*. Following the similar approach, all the generators in the system can be moved to their electrically closest buses. After the movement of the external generators is determined, the external generators are attached to their corresponding internal/boundary buses in the equivalent produced in step one.

In the equivalent model, generators' real power limits remain the same as in the full system. Since the equivalent is intended to be used with system planning tools for DC OPF based studies, the reactive power limits will play no role in the solution process.

2.1.4.4 Moving Load

In the classical Ward equivalent, the retained-line flows are exactly the same as the corresponding lines in the full model. This is achieved by breaking-up each external generator and load into multiple fractions with each fraction moved to a different boundary bus. However, in the modified Ward equivalent used here, each generator is moved integrally to a retained bus. To maintain the retained-line flows the same as those in the full model, a procedure called the "inverse power flow" is designed to compensate the movement of generators.

The objective of the inverse power flow program is to move the load in the system so that the retained-line MW flows in the reduced system exactly match those in the full system. It is assumed in the "inverse power flow" program that the bus voltage angles in the reduced model are the same as those at the corresponding buses in the full system.

The inverse power flow program proceeds in the following steps. First, the admittance matrix Y is constructed based on the equivalent network model. In the second step, the power injection at each bus in the reduced system is calculated by using the Y matrix and bus voltage angle vector. Once the power injection at each bus is obtained, the nodal power injection is used to determine the amount of load assigned to each bus based on the existing generation at each bus. By using this approach, the flows on retained lines match exactly those on the corresponding lines in the full model. And the sum of load added at each bus in the equivalent equals the total load in the original system.

2.1.5 Introduction to the ERCOT System

Figure 2.4shows the one-line diagram of the ERCOT system, which contains 6072 buses, 687 generators, 7504 branches, and 3 HVDC lines. The lines shown in Figure 2.4are transmission lines whose voltage levels range from 69 kV to 345 kV. The total generation and load for the 2011 summer-peak case are 72826 MW and 71204 MW, respectively, with a loss of 2.22% (of the total generation).

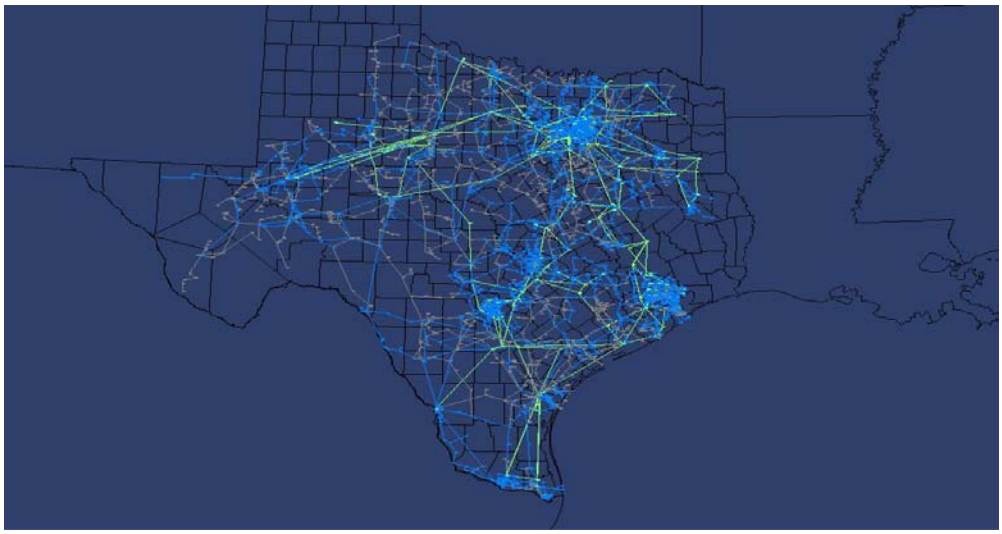

Figure 2.4: One-line Diagram of the Full ERCOT System

2.1.6 279-Bus Equivalent of ERCOT

Following the procedure described above, a 279-bus DC equivalent (shown in Figure 2.5) of the ERCOT system is first produced. In this equivalent, all the 230 kV-and-above buses are retained, which means all 230 kV-and-above congested lines/paths are retained, while congested lines/paths operating at less than 230 kV are ignored. In particular, this equivalent model consists of 1279 TLs, among which 414 lines are physical lines while the remaining 865 lines are equivalent/fictitious TLs generated in the reduction process.

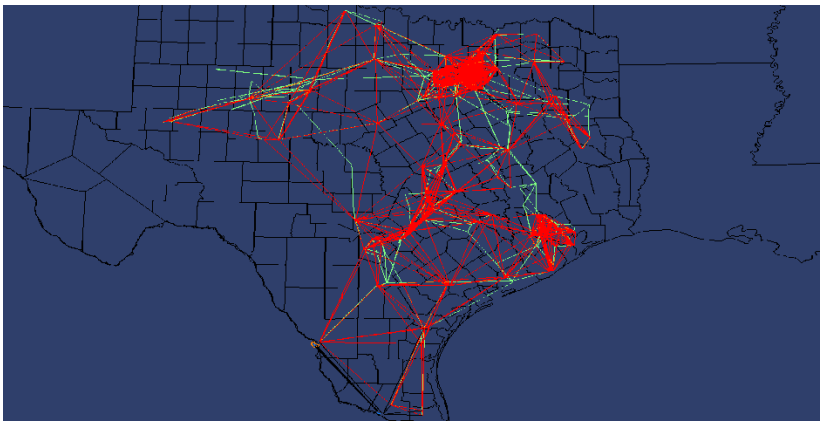

Figure 2.5: One-line Diagram of the 279-bus Reduced Model

2.2 Validation of the Reduced ERCOT Model

In this section, the accuracy of the equivalent generated in section 2.1 is evaluated. Metrics are developed to evaluate the error between the equivalent and full model under the base case and the changed generation case. Conflicts between accuracy and size exist when generating equivalents: generating a small equivalent sacrifices accuracy; generating a large equivalent gains accuracy but sacrifices computational efficiency. To study the relationship between the accuracy and size of an equivalent, several equivalents were generated and their accuracy was tested and compared. The performance of the equivalent was also tested in terms of DC optimal power flow.

2.2.1 Reduced Model Evaluation in Terms of Power Flow Solutions

In the base case, the power flows (PFs) on the retained lines of the equivalent exactly match those in the full model. For changed cases this is not true. As the operating point is moved away from the base case, e.g., the generator power orders in the reduced models are changed, it is necessary to quantify the difference between the full and the reduced models. The test to examine the changed dispatch involves decreasing the coal generation by increasing amounts and then picking up the decrease with increases in power orders to the natural-gas units. This test is simulates, in an approximate way, the potential generation-mix changes under environmental regulations. It is likely that under CO_2 cap-and-trade schemes that coal-fired generation will be reduced at times when CO_2 emissions threaten the cap and the system will thus require a concomitant increase in gas fired generation. In this subsection, the 279-bus equivalent generated in 2.1is used to evaluate the performance of the equivalent.

Several metrics are used to determine the accuracy of the model for changed cases. One is the magnitude of the retained-line-flow errors, i.e., difference between line flows (in MW) calculated using the full and the reduced equivalent models. The second one is the error of these line flows in percentage based on the corresponding lines' MVA ratings. These two metrics are shown in 2.5 and 2.6.

$$Error_i = \left| Pf_i^{full} - Pf_i^{reduced} \right| \tag{2.5}$$

$$Error_i\% = \frac{\left| Pf_i^{full} - Pf_i^{reduced} \right|}{(Lim_{MVA})_i} \tag{2.6}$$

where Pf_i^{full} and $Pf_i^{reduced}$ represent the PFs on retained line *i* from the full model and the reduced model, respectively; the variable $(Lim_{MVA})_i$ is the MVA rating of the retained line *i*.

Another metric used is the average error in the retained-line flows. The average error calculated in MW and in percentage is shown in 2.7 and 2.8.

$$Error_{Avg} = \frac{\sum_{i=1}^{N} \left| Pf_i^{full} - Pf_i^{reduced} \right|}{N} \tag{2.7}$$

$$Error_{Avg}\% = \frac{\sum_{i=1}^{N} \left| Pf_i^{full} - Pf_i^{reduced} \right| / (Lim_{MVA})_i}{N} \tag{2.8}$$

where *N* is the number of retained lines.

Generators in ERCOT are summarized in terms of fuel types in Table 2.2 (based on the 2011 summer peak case). It is shown in the Table 2.2 that the coal generation contributes 27.4% and the natural gas generation contributes 62.5% to the total MW generation in the ERCOT.

Table 2.2: Generator Information in ERCOT System

Gen Fuel Type	Num. of Gens	Generation (MW)
Coal	41	19,961.3
Distillate Fuel Oil (Diesel, FO1, FO2, FO4)	2	0
Hydro	27	0
Natural Gas	477	45,535.0
Nuclear	4	5,131.0
Wind	107	1552.9
Wood or Wood Waste	2	50.0
Waste Heat	2	29.0
Other/Unknown	25	567.6
TOTAL	687	72826.8

The aforementioned test is conducted using the following steps. First, the coal generation is decreased by 1.0%, which is 199.6MW. Then, to compensate the decrease in coal generation, the natural gas generation is increased by 199.6MW, which corresponds to 0.44% of the total generation of natural gas. After the generation of coal and natural gas are changed, the DC power flow is solved for both the full and reduced model. Then the line flows on the retained transmission lines in the equivalent are compared against the same flow in the full model.

Taking the MW flow on the retained lines in the full model as the reference, errors in retained-line flows are calculated with their absolute values plotted in Figure 2.6 versus retain branch/line ID's whose values were assigned arbitrarily, but contiguously. These errors, in percentage of the corresponding lines' MVA ratings, are shown in Figure 2.7.

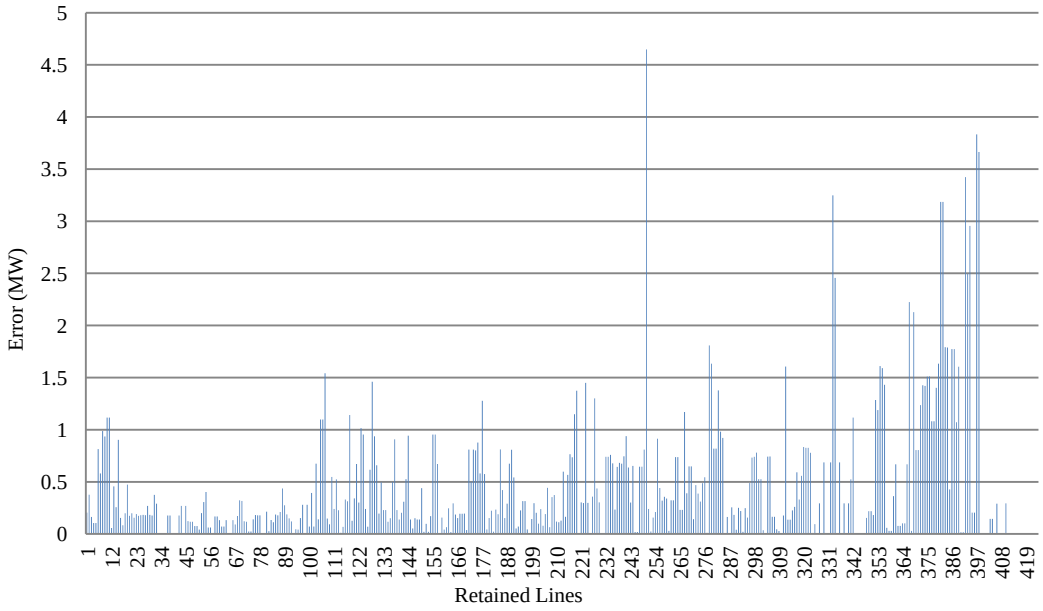

Figure 2.6: Retained Line Flow Errors in MW

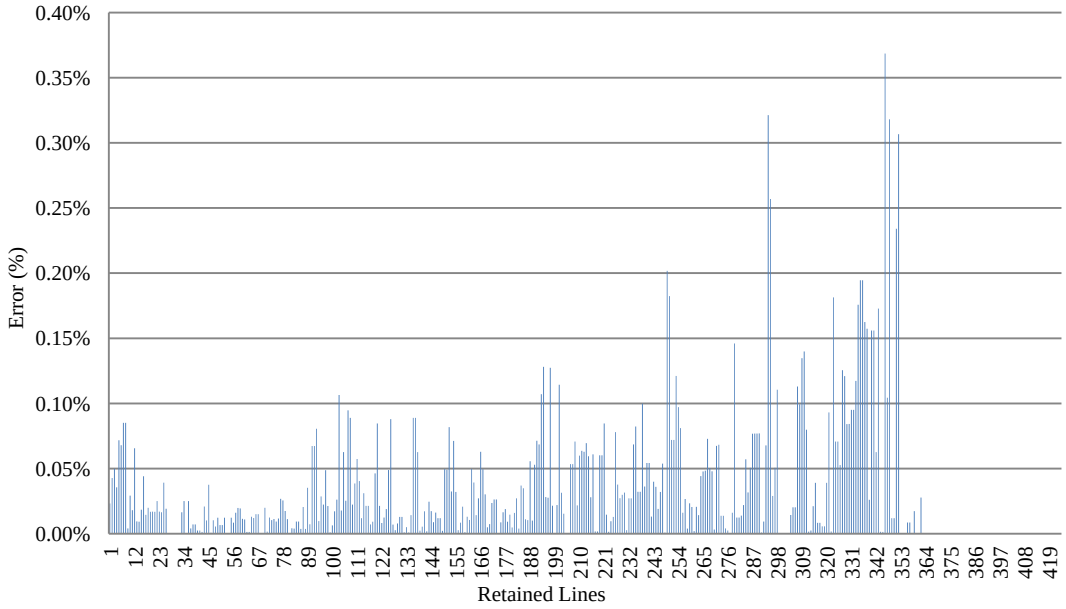

Figure 2.7: Retained-line Flow Errors in Percentage

From Figure 2.6 and Figure 2.7, it can be seen that, when the coal generation is decreased by 1%, the largest error in the retained-line flows is around 4.6 MW, or 0.36% of the corresponding line rating. Most of the errors are smaller than 2.5 MW with only a few lying between 2.5 MW and 4 MW, or between 0.15% and 0.35% of the line rating.

For this 279-bus equivalent, the average error in the retained-line flows is 0.45 MW for a 1% decrease in coal. As we further decrease the coal generation (while increasing the gas generation) the average errors on the retained-line flows are depicted in Figure 2.8.

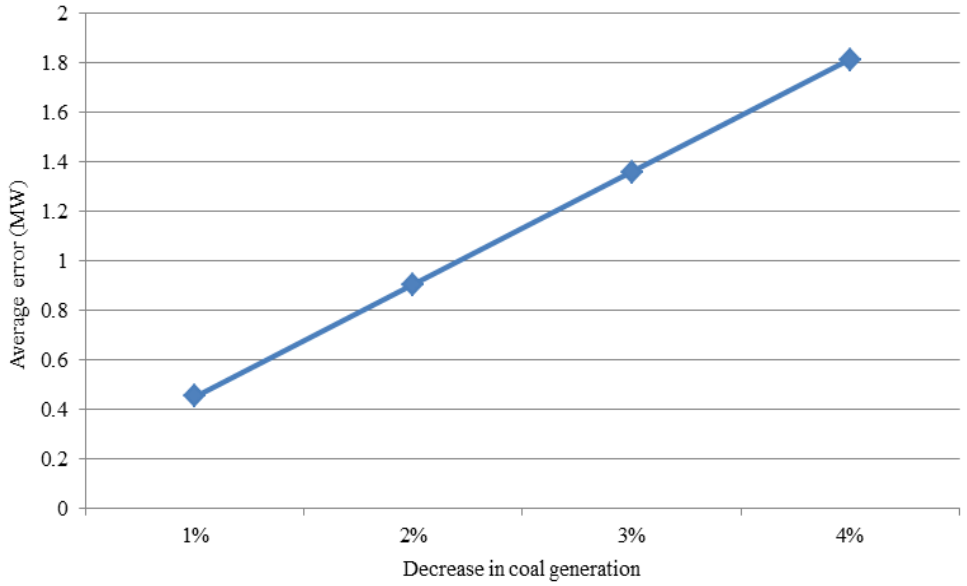

Figure 2.8: Average Errors (MW) in Retained-line Flows vs. Decrease (%) in Coal Generation

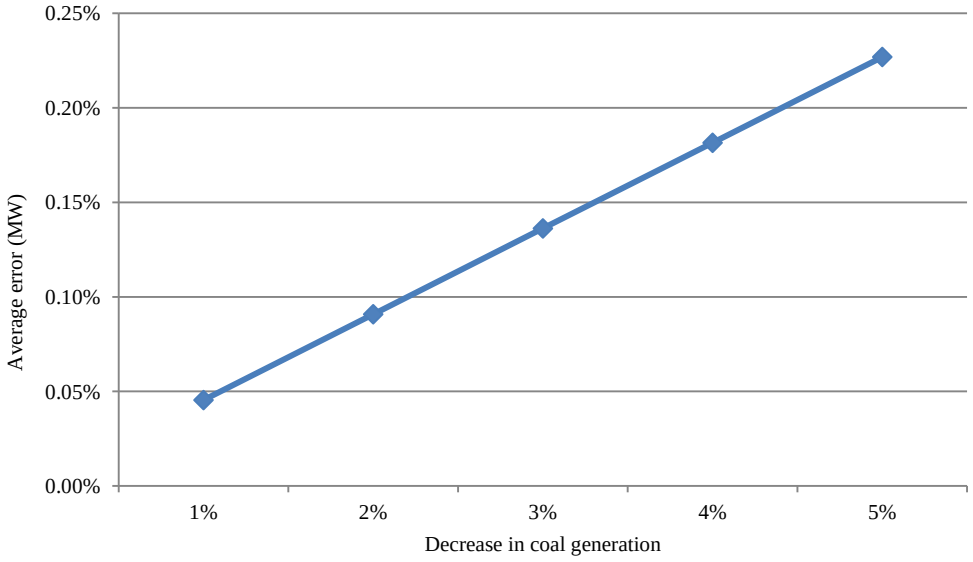

Figure 2.9: Average Errors (%) in Retained-line Flows vs. Decrease (%) in Coal Generation

As Figure 2.8 and Figure 2.9 show, a 4% decrease in the coal generation will result in an average error of 1.8MW, or 0.23% in terms of the corresponding MVA rating in the retained-line flows.

Intuition suggests that the accuracy of an equivalent is related to its size: the more buses the equivalent retains, the more accurate the equivalent is; however, increasing the size of the equivalent will increase the computational burden. Balancing these conflicting criteria requires engineering judgment. To study the relationship between size and accuracy, two larger equivalents were generated for the ERCOT system:

- 424 bus model: retain all 138 kV and above congested lines/paths plus 230 kV and above buses.
- 1036 bus model: retain all 138 kV and above congested lines/paths, all the 230 kV and above buses, and all the generator buses.

The schematics of the two equivalents are shown in Figure 2.10 (a) and (b). The red and yellow lines in these figures represent equivalent lines while other colors represent physical lines.

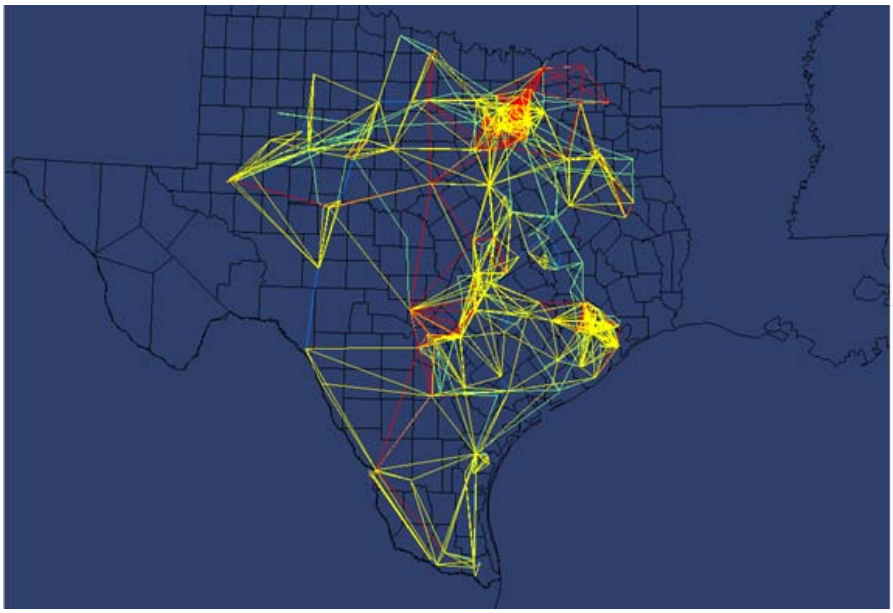

(a) ERCOT 424-bus Equivalent

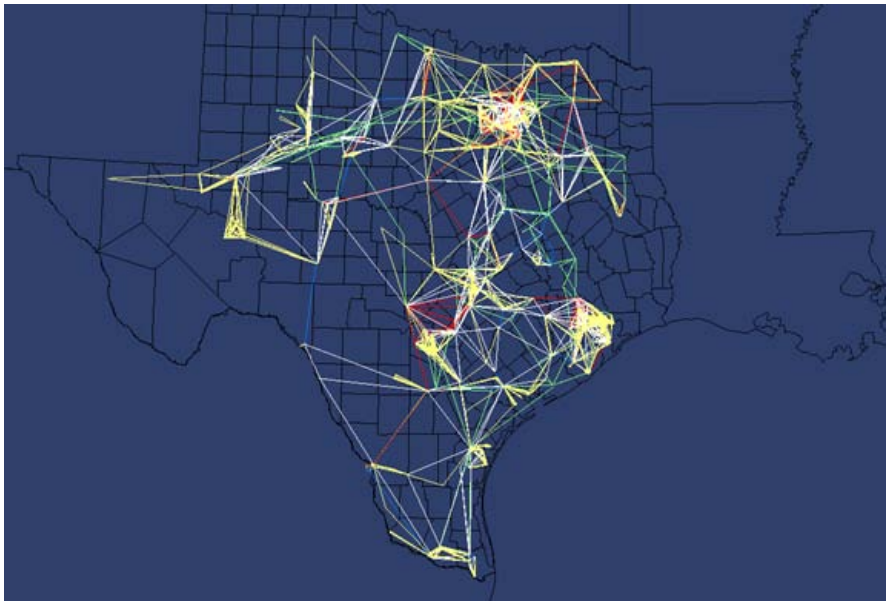

(b) ERCOT 1,036-bus Equivalent

Figure 2.10: Schematics of ERCOT Equivalents

The same sets of tests described above are conducted using these two equivalents and the average errors on the retained-line flows are plotted versus coal reduction as shown in Figure 2.10.

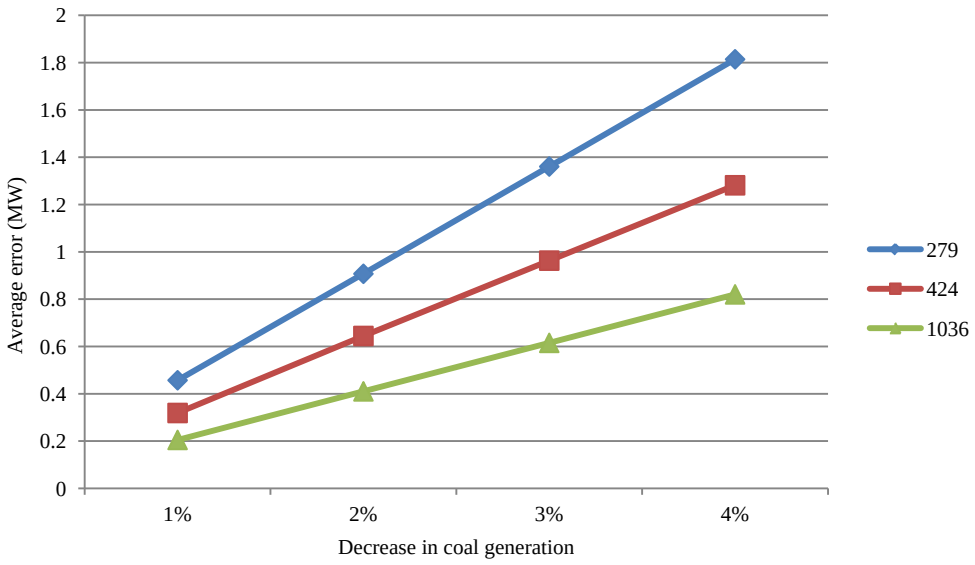

Figure 2.11: Average Errors (MW) in Line Flows for ERCOT Equivalents

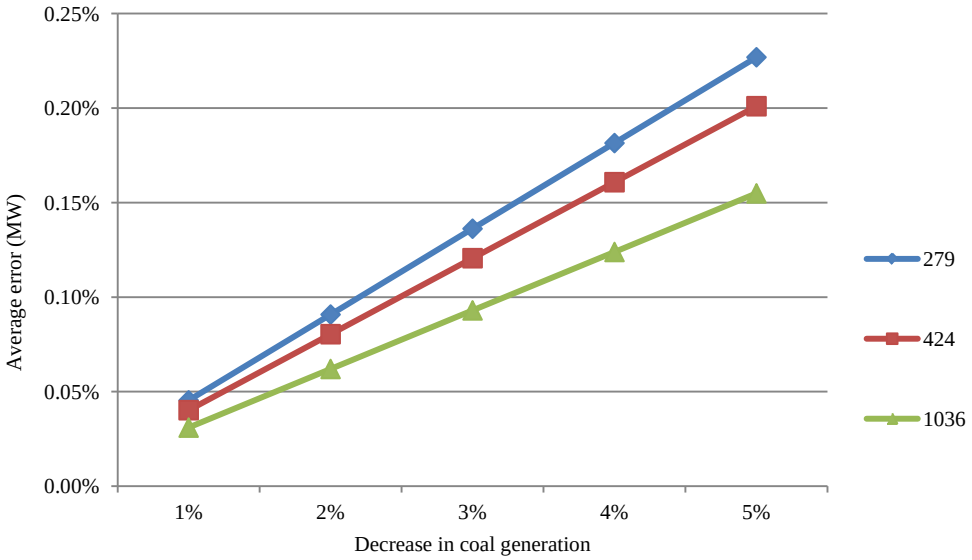

Figure 2.12: Average Errors (%) in Line Flows for ERCOT Equivalents

As shown in Figure 2.10 and Figure 2.12, for the 1,036-bus equivalent, when coal generation is reduced by 4%, the average error in the retained-line flows is very small, 0.8 MW, or 0.03% of the corresponding lines' MVA limits. And for the 424-bus and 279-bus equivalents, this error increases to 1.3 MW and 1.8 MW, or 0.04% and 0.045% of the line rating, respectively, still well within the range of acceptability. This pattern of increasing error with reduction in number of retained buses is consistent with intuition and is used as a sanity check. Furthermore, the effectiveness of the proposed network

reduction scheme is validated in terms of the line-flow metrics associated with power flow solutions under changed dispatches.

In OPF studies, a metric that takes into account maximum line-flow ratings, which are more critical to LMP calculations, is an important criterion. This is addressed in the next section.

2.2.2 Evaluation of the Reduced Model in Terms of Optimal Power Flow Solutions

Ultimately, the equivalents generated are to be used in OPF studies. Two metrics useful in comparing the accuracy of the full and equivalent models' OPF solutions are the total operating cost difference (error) and average difference in the LMP's, both of which include the effects of constrained lines/paths.

In addition to the network data, generator cost functions were needed and obtained to perform an OPF solution. Since the equivalent will also be used in optimal generation investment studies in which the real-load data are used, it is important to use the real load data rather than the modeled data in the OPF solution comparison. Therefore, the load in the aforementioned ERCOT database is scaled based on the hourly load data obtained from *ERCOT Hourly Load Data Archives* [21]. Solutions from OPF executions using both the equivalent DC model and the full DC model were obtained and the two solutions were compared. One important metric, and the impetus for creating an equivalent, is the OPF execution time. For the 424 bus equivalent, the DC OPF converged about 6 times faster than when using the full model. The total operating costs, and average LMPs from the two DC OPF solutions for the 424-bus and full models are listed in the second and third columns of Table 2.4, while the corresponding error metrics are shown in the fourth and fifth columns. The test was conducted in Matpower [22] with the Mosek [23] default LP solver.

Table 2.3: Comparison between the DC OPF Solutions of the Full and 424-Bus-Equivalent ERCOT Models

	Full Model	**424-bus Equivalent**	**|Errors (MW)|**	**|Errors (%)|**
Convergence	Y	Y	NA	NA
Total Cost ($/Hour)	1,363,111	1,360,559	2552	0.19%
Average LMP ($/MWh)	25.6163	25.6337	0.0174	0.068%

Table 2.4: Comparison of the Generator Dispatch between the Full and 424-Bus-Equivalent ERCOT Models Based on a DC OPF Solutions

Fuel Type	Equivalent (MW)	Full System (MW)	|Errors (MW)|	|Errors (%)|
nuclear	5,131	5,131	0.0	0.0%
coal	19,576	19,577	1.0	0.005%
natural gas	26,041	25,952	89.0	0.342%
wind	9,380	9,468	88.0	0.949%
distillate fuel oil (diesel,FO1,FO2,FO4)	-2	-2	0.0	0.000%
hydro	0	0	0.0	0.000%
waste heat	14	14	0.0	0.000%
wood or wood waste	50	50	0.0	0.000%
unknown	568	568	0.0	0.000%

From Table 2.3, it can be seen that the error in the total operating costs between the two models is 0.19% of the total operating cost. The average LMPs differed by 0.0174 $/MWh, which corresponds to an error of 0.068%.

Another metric used to compare the DC OPF solutions of the full model and 424-bus equivalent is the generator dispatches by fuel type. Generator dispatches and differences (errors) in dispatches are shown in Table 2.4.

It can be seen from Table 2.4 that except for natural gas and wind generators, all the other fuel types have essentially the same total dispatch in the full and equivalent models. The error in dispatch for the natural gas generators is 0.342% of the total natural gas generation. The error in the wind generator dispatches is 0.949% of the total wind generation, values well within the bound of acceptability.

To sum up, the simulation results shown in this section support the conclusion that the 424-bus equivalent is acceptable for DC OPF studies.

2.3 Western Electricity Coordinating Council (WECC) Model

The Western Electricity Coordinating Council (WECC) system is the “western interconnect” of North America. As shown in Figure 2.13, the WECC region covers all or part of 14 western US states, the Canadian provinces of Alberta and British Columbia, and the northern part of Baja California, Mexico. The full WECC system model is not available for general research use, and a reduced model was desired for practical reasons such as computing time and software limitations on model size. Dr. James Price of the California ISO (CAISO) developed a 240-bus model from publicly-available data and validated it using the full WECC models [29].

Development of the model began with a 179-bus model [30] used for multi-agent research. The model was extended to 225 buses [31] to conform the model’s topology to that of models used in CAISO [32] and other organizations’ [33] transmission planning studies. The 240-bus model adjusted a few aggregated transmission line impedances to

produce power flow results that better agree with full planning models [29]. It also includes transmission wheeling charges [29].

The topology of the 240-bus model is shown in Figure 2.14: 240-bus WECC Model Topology [29]. Colored blocks within the diagram are constrained load and generation pockets. Solid red lines signify significant transmission constraints between CAISO and other areas. The complete data set for the model is available online [34]. Hourly aggregated base-case (2004) and future (2015) data are provided with the model:

- Loads for eleven areas within CAISO and for sub-regions outside CAISO.
- Wind and solar resources for 16 wind resource and five solar resource areas.
- Geothermal resources at the North Bay/Geisers area in CAISO. Four geothermal resource areas outside CAISO are assumed to operate at constant 80% of maximum capacity.
- Biomass generation at three buses within CAISO.
- Hydroelectric generation. While hydro should be modeled as dispatchable, the complexities of hydro dispatch will prevent realistic modeling in most research applications, so representative hydro output values are provided.

Other generation resources are modeled as follows:

- Eleven generic renewable resource areas, representing mixed renewables, and including a limited amount of biomass outside CAISO, operate with constant output of 80% of maximum capacity.
- Gas-fired generation is dispatchable. To allow for unit commitment and dispatch within aggregated generators, a minimum output of 5% of capacity is assumed.
- Coal-fired generation is aggregated at 17 sites outside of CAISO and operates at constant load of 85% of capacity.
- Four nuclear generators are operated at 100% capacity, but may be reduced to 90% for congestion management.

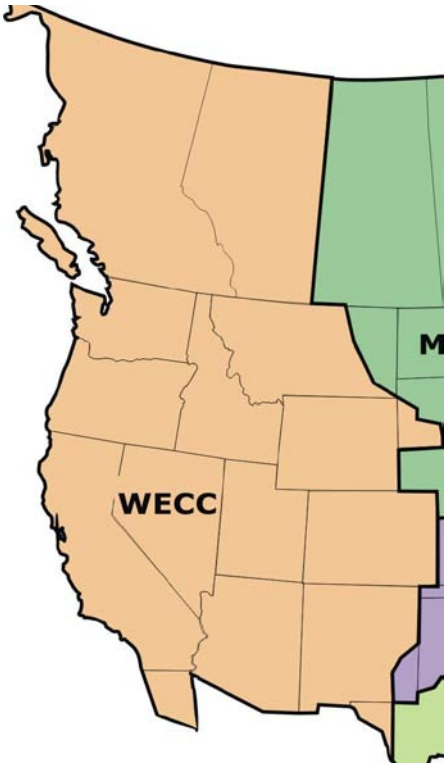

Figure 2.13: WECC Region

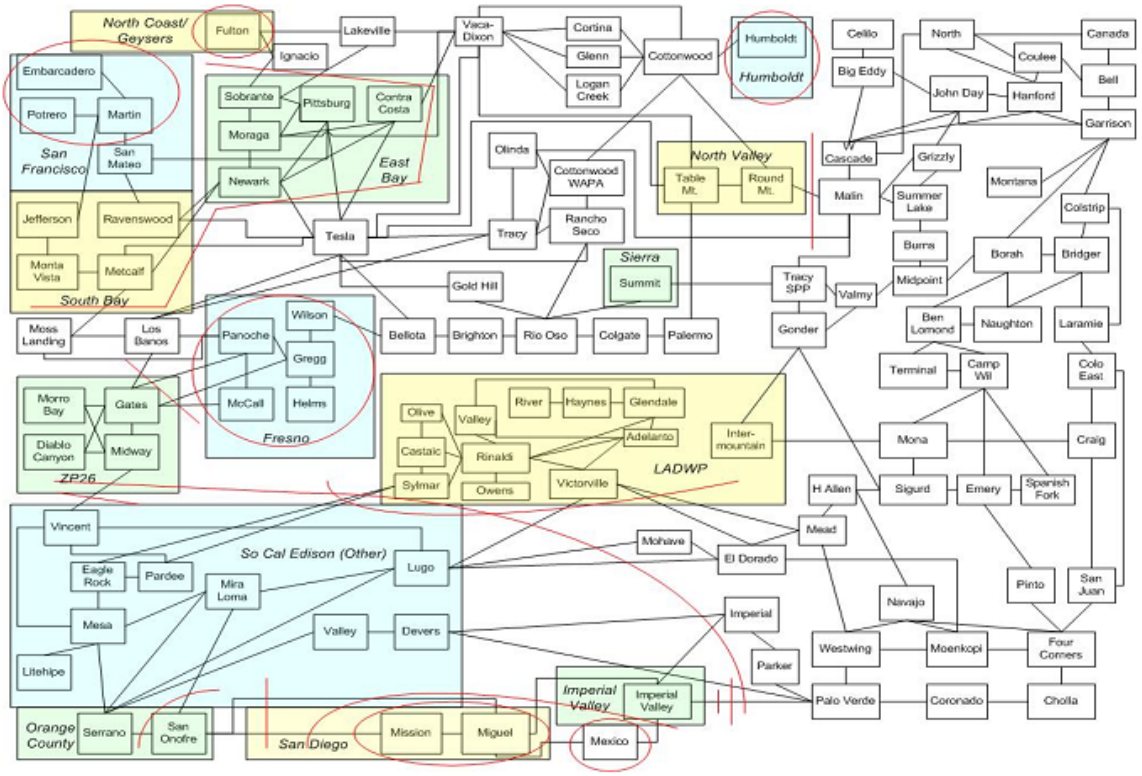

Figure 2.14: 240-bus WECC Model Topology

2.4 Equivalent for Eastern Interconnection (EI)

2.4.1 Reduced Model

Using the model reduction procedure described earlier, network equivalent models of the three synchronous islands in the US were constructed. The following describes the models and acceptance testing done for the 62,000 bus Eastern Interconnection (EI) model.

The full EI model is shown Figure 2.15. This model includes 62,013 buses, 8,190 generators, 79,766 branches, and 24 HVDC lines.

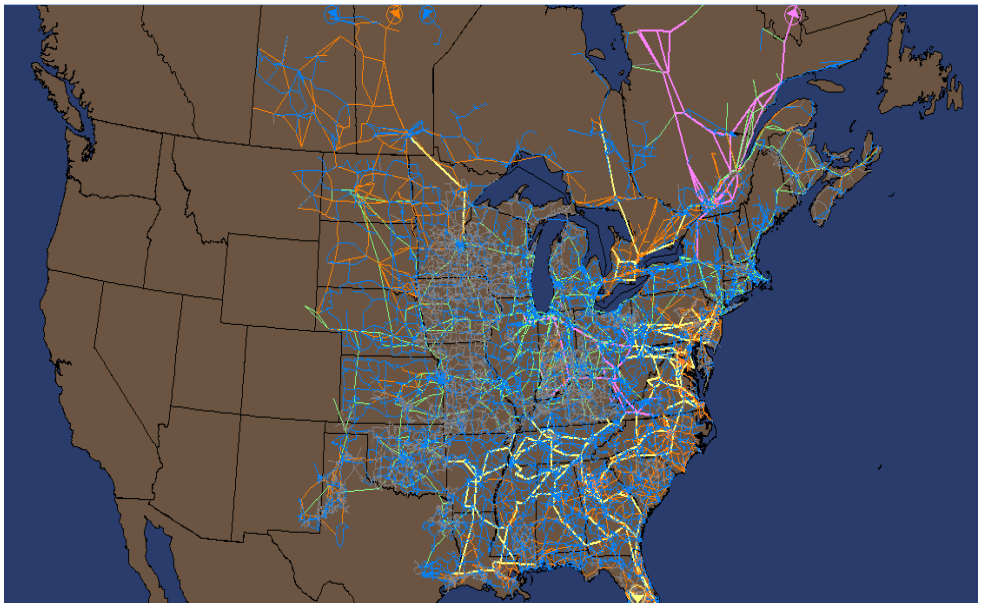

Figure 2.15: The Full Eastern Interconnection (EI) Model

Several models of the EI were built and evaluated to determine the smallest model that we could use in our simulations while retaining the needed fidelity. The first model built, a 273-bus reduced EI model, is shown below in Figure 2.16. As shown in the figure, there are two islands in the reduced model: the island in the Hydro Québec area located in the top right corner of the figure, and the main island of the EI. The island in the Hydro Quebec area contains 26 retained buses and a total generation is about 23,200 MW. The main island of the EI contains 247 retained buses with a total generation of 637,000 MW. The slack buses for the two islands are selected to be bus 84755 in the database (bus name: CANTON, nearest city: Montreal, CA), and bus number 18018 (bus name: H1 CHEOH, nearest city: Johnson City, TN), respectively, which offer the best numerical convergence during the reduction process because they are generator buses with a large amount of generation. There are 1,653 TLs in the reduced model, among which 273 lines are the retained TLs from the original model while the rest of the lines (1380) are equivalent TLs produced in the reduction process. Also, the TLs are shown in different colors in the figure to represent lines with different voltage rating, which are summarized in Table 2.5.

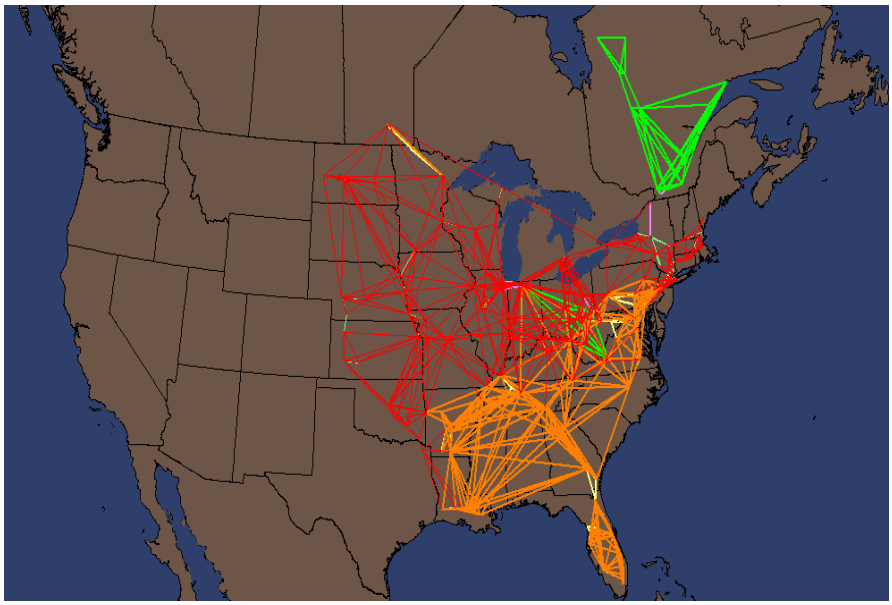

Figure 2.16: A 273-bus Reduced Equivalent for the EI

Table 2.5: Correspondence between Colors of the Lines and their Voltage Levels

Line color	**Voltage level (kV)**
Red	345
Orange	500
Yellow	500 (retained TLs)
Green	735, 765
Purple	765 (retained TLs)

2.4.2 Evaluation of the Reduced Model in Terms of Power Flow Solution

In this subsection, the generation pattern of the EI is changed and the power flows on the retained TLs between the full model and the reduced model are compared. The same test conducted on the ERCOT system is carried out in subsection 2.2.

Generators in the EI, in terms of fuel types are summarized in Table 2.6 (based on the 2008 summer peak case). It is shown in the Table 2.6 that the coal generation contributes 40.6% and the natural gas generation contributes 28.6% to the total MW generation in the EI. Several changed cases are generated by reducing coal generation in a range between 1% and 5% while increasing the gas generation by the corresponding amount.

Table 2.6: Generator Information in the EI

Gen Fuel Type	Num. of Gens	Generation (MW)
Coal	1,158	261,931.5
Distillate Fuel Oil (Diesel, FO1, FO2, FO4)	831	10,042.5
Hydro	1,584	66,825.5
Jet Fuel	17	241.4
Natural Gas	2,884	184,717.5
Nuclear	116	96,786.9
Residual Fuel Oil (FO5, FO6)	115	22,408.5
Wind	126	1,765.8
Wood or Wood Waste	177	332.1
Other/Unknown	242	578.2
TOTAL	7,250	645,629.9

Two metrics are used to determine the accuracy of the model for changed cases. One is the magnitude of the retained-line-flow errors, i.e., difference between line flow generated by the full and equivalent models in MW and percent as shown in 2.9- 2.10.

$$Error_i = \left| Pf_i^{full} - Pf_i^{reduced} \right| \quad 2.9$$

$$Error_i\% = \frac{\left| Pf_i^{full} - Pf_i^{reduced} \right|}{(Lim_{MVA})_i} \quad 2.10$$

The errors in the retained-line flows in MW and percentage are shown in Figure 2.17 and Figure 2.18.

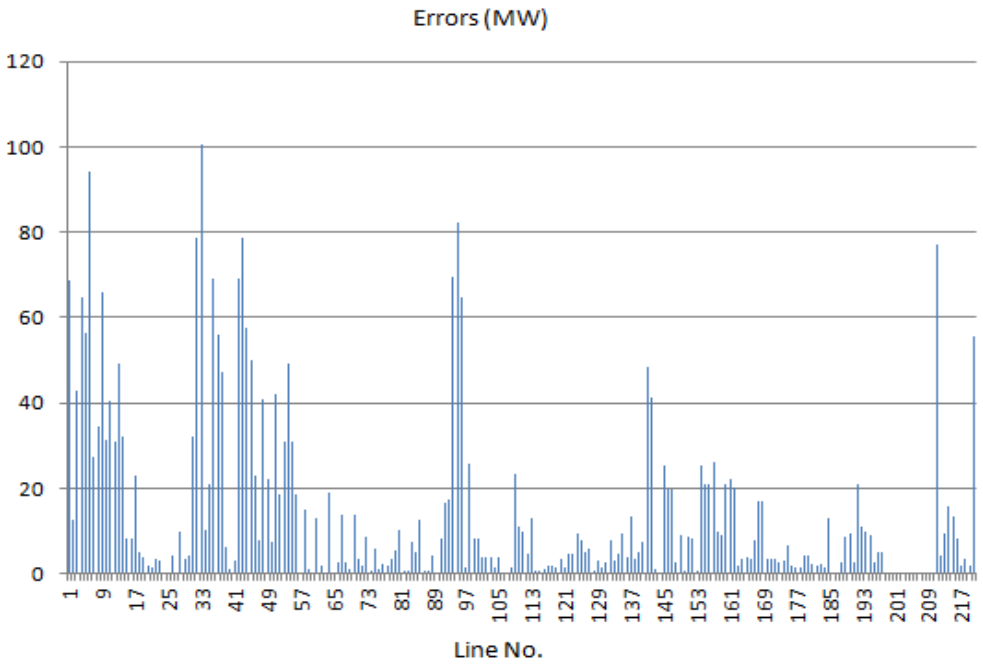

Figure 2.17: Errors (MW) in the Power Flow on Retained TLs (MW)

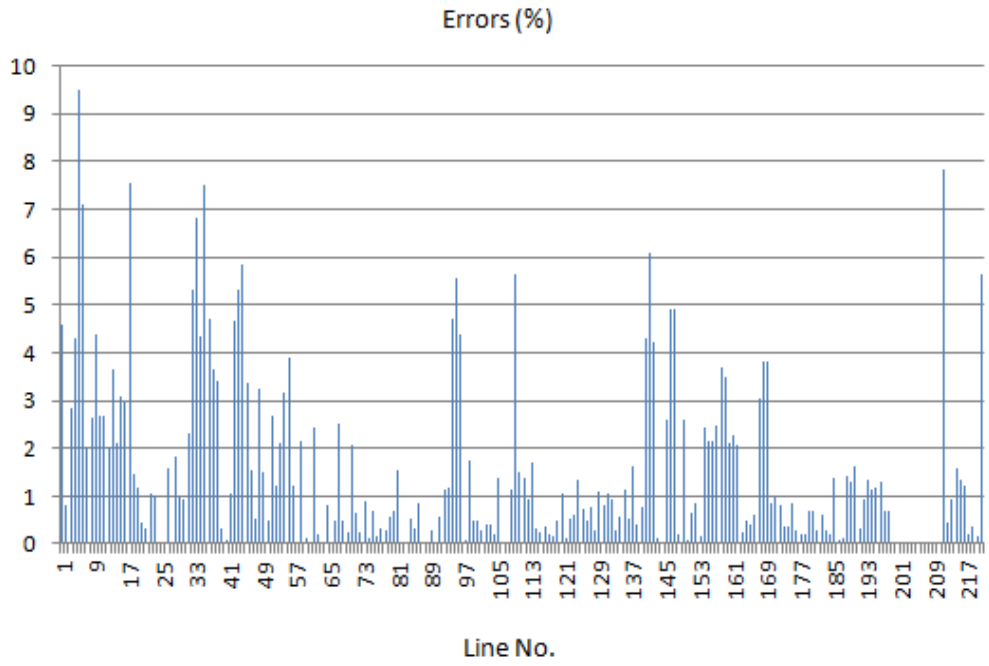

Figure 2.18: Errors (%) in the Power Flow on Retained TLs

From Figure 2.17 and Figure 2.18, it can be seen that, when the coal generation decreases by 1%, the largest error in the power flows on retained TLs reaches 100 MW, or 9.7% in terms of the MVA rating of the TL. About 1/3 of the errors are larger than 4% of the lines' MVA ratings.

Another metric used for acceptability testing is the average line-flow error. The average line-flow error in WM and percentage is calculated as follows:

$$Error_{Avg} = \frac{\sum_{i=1}^{N} \left| Pf_i^{full} - Pf_i^{reduced} \right|}{N} \quad 2.11$$

$$Error_{Avg}\% = \frac{\sum_{i=1}^{N} \left| Pf_i^{full} - Pf_i^{reduced} \right| / (Lim_{MVA})_i}{N} \quad 2.12$$

The average error in the line flows for a 1% decrease (26,193 MW) in the coal generation with a corresponding increase in gas-fired generation is calculated to be 10.31 MW or 4.375% of the line MVA ratings, indicating that the power flows on the retained TLs are quite sensitive to the change in the generation pattern.

As we further decrease the coal generation and increase the gas generation, the average errors in percentage of the TL MVA ratings are calculated as shown in Figure 2.19.

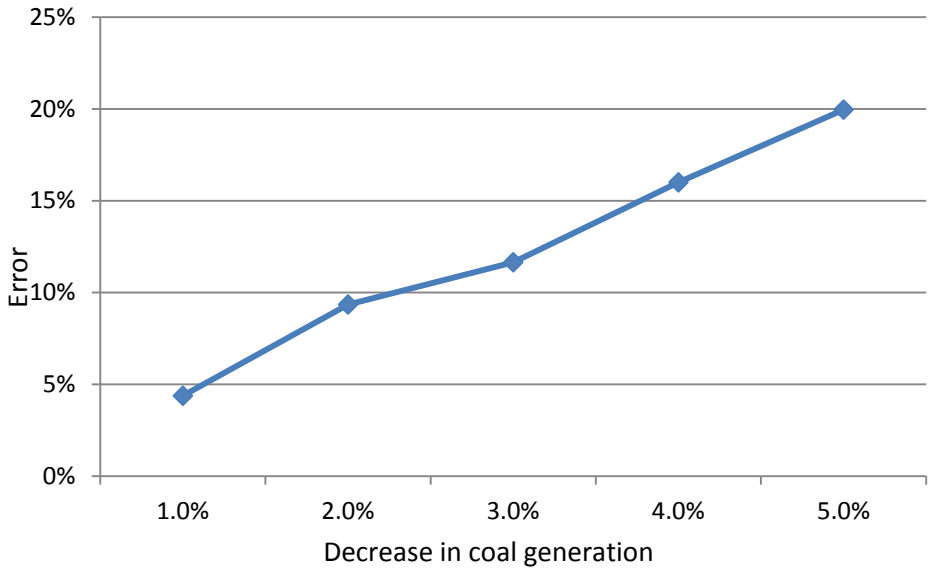

Figure 2.19: Average Errors (%) in Line Flows vs. Decrease (%) in Coal Generation

As Figure 2.19 shows, a 5% decrease in the coal generation will result in an average error of 20% in the line-flows. Based on this observation, the 273-bus reduced model is not acceptable.

To get an appropriate equivalent model for the EI, two conflicting factors need to be weighted:

- Accuracy (the larger the reduced system, the more accurate it is)
- Efficiency (the smaller the reduced system, the less the computational burden.)

It is necessary to strike a balance between accuracy and efficiency by selecting a proper size for the reduced system. To study the relationship between the accuracy and size of the reduced system, we generate different reduced models and checked their performance. The equivalents generated along with the criteria used for selecting buses to retain are:

- 300 bus model: retain all the congested lines
- 650 bus model: retain congested lines plus 500 kV and above buses
- 1400 bus model: retain congested lines plus 345 kV and above buses
- 2800 bus model: retain congested lines plus 345 kV and above buses and part of 230 kV buses
- 4400 bus model: retain congested lines plus 230 kV and above buses

Figure 2.20 shows the EI equivalents generated with these different numbers of buses.

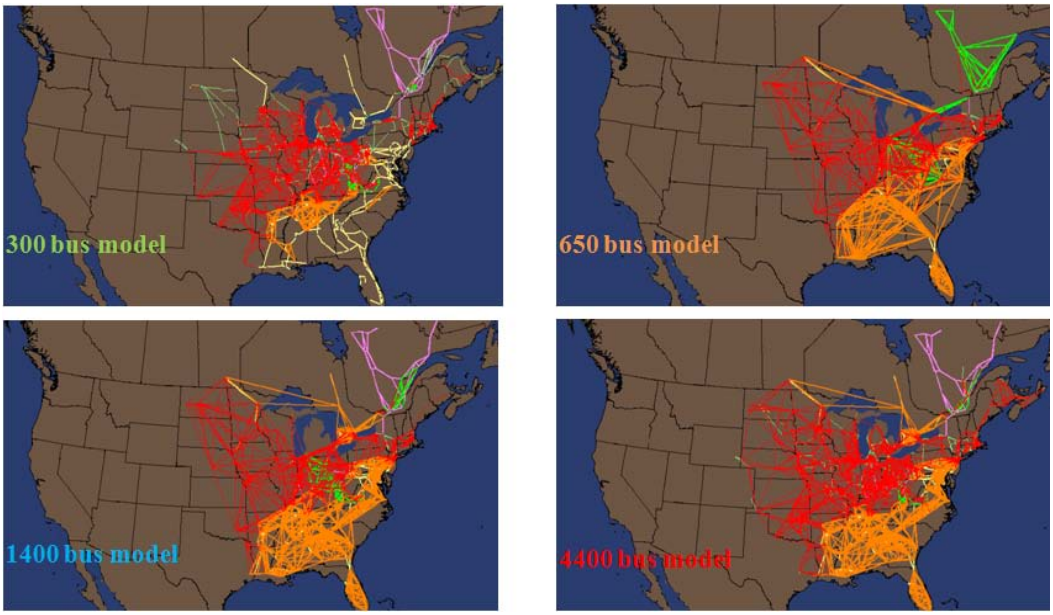

Figure 2.20: Equivalent of EI with Different Number of Buses

Performance of the reduced equivalents is evaluated using the same metrics described earlier. The simulation results for these reduced models under different generation patterns are shown in Table 2.7.

Table 2.7: Average Errors (%) in the Line Flows for Different EI Equivalents

Decrease in coal gen. / Bus #	1%	2%	3%	4%	5%
300	4.38	9.35	11.65	16	19.96
650	2.71	5.38	8.01	9.96	12.97
1400	1.75	3.68	4.93	7.23	8.77
2800	1.21	2.40	3.67	4.79	5.53
4400	0.79	1.73	2.38	3.05	3.88

Results in Table 2.7 can be summarized as plots shown in Figure 2.21.

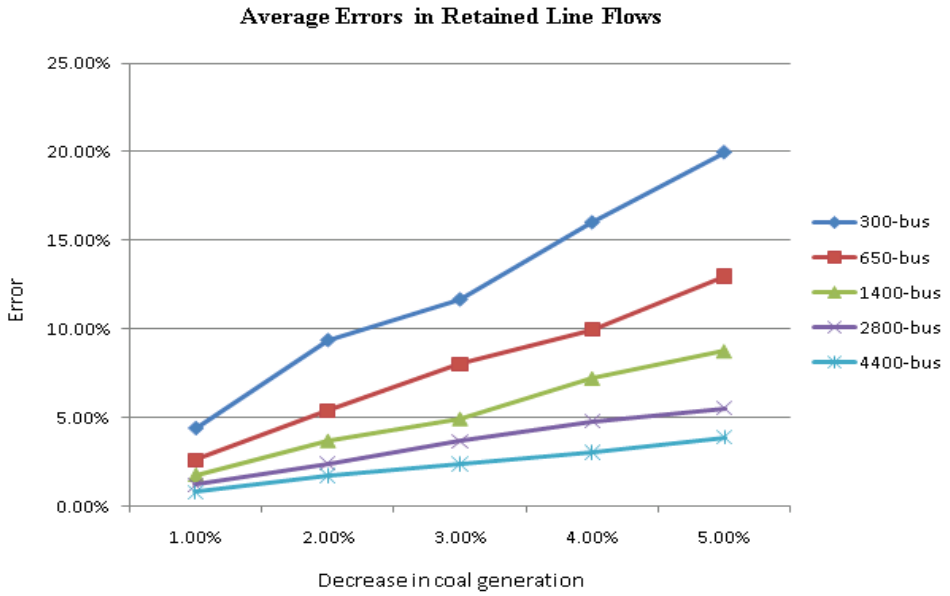

Figure 2.21: Average Errors (%) in Line Flows for Different EI Equivalents

As Table 2.7 and Figure 2.21 show, the average error in the retained-line flows decreases as the size the equivalent increases, something not unexpected. For the 4400-bus equivalent, when the decrease in the coal generation is 5%, the average error in the retained-line flows reaches 3.88%. For the 2800-bus equivalent, this average error reaches 5.53%. As a result, the size of the equivalent can be determined based on the acceptable errors in the line flows.

2.4.3 Evaluation of the Reduced Model in Terms of Optimal Power Flow Solutions

In the previous section it was shown that a 4400-bus equivalent met the first set of acceptability tests. To improve performance further, a larger 5222-bus equivalent was

generated by keeping all the high voltage buses and transmission lines above 230 kV. This improved equivalent was then evaluated using the next acceptability test, that is, the solution of an OPF problem is obtained for the full model and the reduced equivalent and the results are compared using several metrics.

The full EI system and the 5222-bus EI equivalent system are shown below in Figure 2.22.

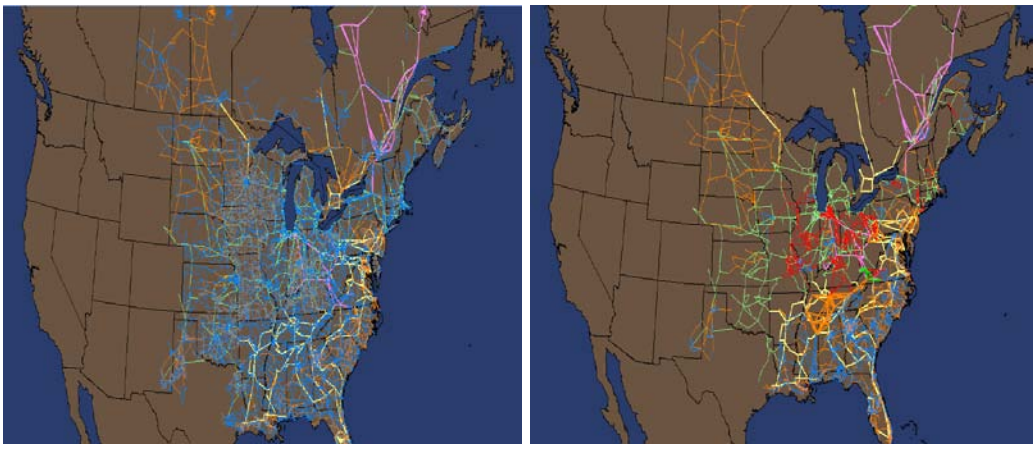

(a) full EI model (b) 5222-bus equivalent of EI

Figure 2.22: Full EI System and the 5222-bus Equivalent

In the test, generation cost functions were obtained from Energy Visuals **Error! Reference source not found.** [35]. A sample of the generator cost data can be found in Appendix 1. The cubic generator fuel cost model is employed. The relationship between the hourly fuel cost at generator i, $C(p_{Gi})$, is determined by its output p_{Gi} as:

$$C(p_{Gi}) = a_i + b_i p_{Gi} + c_i (p_{Gi})^2 + d (p_{Gi})^3 \qquad \$/Hour \qquad 2.13$$

where a_i, b_i, c_i and d_i are constant coefficients that determine the cubic fuel cost model. As can be seen from Appendix 1, for all the generators in the data base, a, c, and d are zero. As a result, all the generators in the EI have linear fuel cost functions as shown in 2.14.

$$C(p_{Gi}) = b_i p_{Gi} \quad \$/Hour \qquad 2.14$$

The OPF test is conducted in Matpower [36] with the default LP solver of Mosek [23]. When the DC OPF is executed on the full EI system model, the program converges with an optimal solution obtained in 35.89 seconds. A summary of the solution is shown Figure 2.24. The LMPs on each bus in the full EI system are calculated and plotted in Figure 2.25.

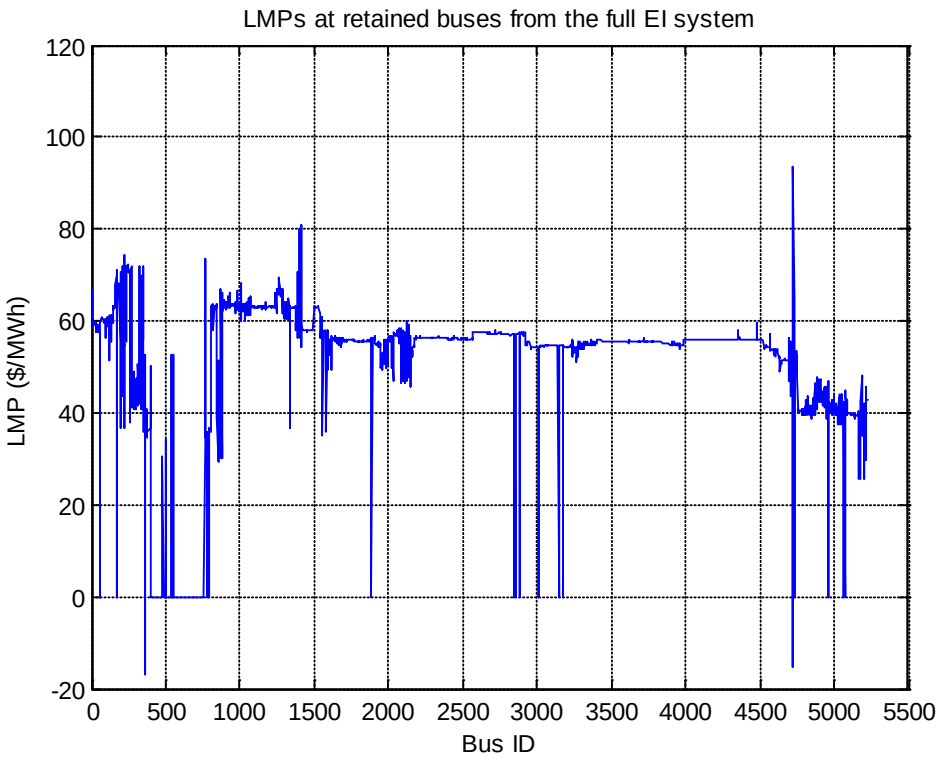

Figure 2.23: LMPs at Retained Buses from the Full EI System

```
The solution is optimal.

Converged in 35.89 seconds
Objective Function Value = 16244321.51 $/hr
================================================================================
|     System Summary                                                           |
================================================================================

How many?                How much?              P (MW)            Q (MVAr)
---------------------    --------------------  -------------  -----------------
Buses            62013   Total Gen Capacity    872591.0          0.0 to 0.0
Generators        8152   On-line Capacity      717190.0          0.0 to 0.0
Committed Gens    5474   Generation (actual)   648157.7              0.0
Loads            30052   Load                  647872.3              0.0
  Fixed          30026     Fixed               647800.5              0.0
  Dispatchable      26     Dispatchable          71.8 of 525.5      -0.0
Shunts            3870   Shunt (inj)            -285.5               0.0
Branches         79222   Losses (I^2 * Z)         0.00               0.00
Transformers     79222   Branch Charging (inj)     -                 0.0
Inter-ties        2477   Total Inter-tie Flow  253099.4              0.0
Areas              136

                         Minimum                      Maximum
                  -------------------------  --------------------------------
Voltage Magnitude   1.000 p.u. @ bus 100001      1.000 p.u. @ bus 100001
Voltage Angle    -130.08 deg   @ bus 129106     177.54 deg   @ bus 669755
Lambda P          -86.45 $/MWh @ bus 602025     265.42 $/MWh @ bus 200541
Lambda Q            0.00 $/MWh @ bus 100001       0.00 $/MWh @ bus 100001
```

Figure 2.24: Summary of the DC OPF Results on the Full EI System

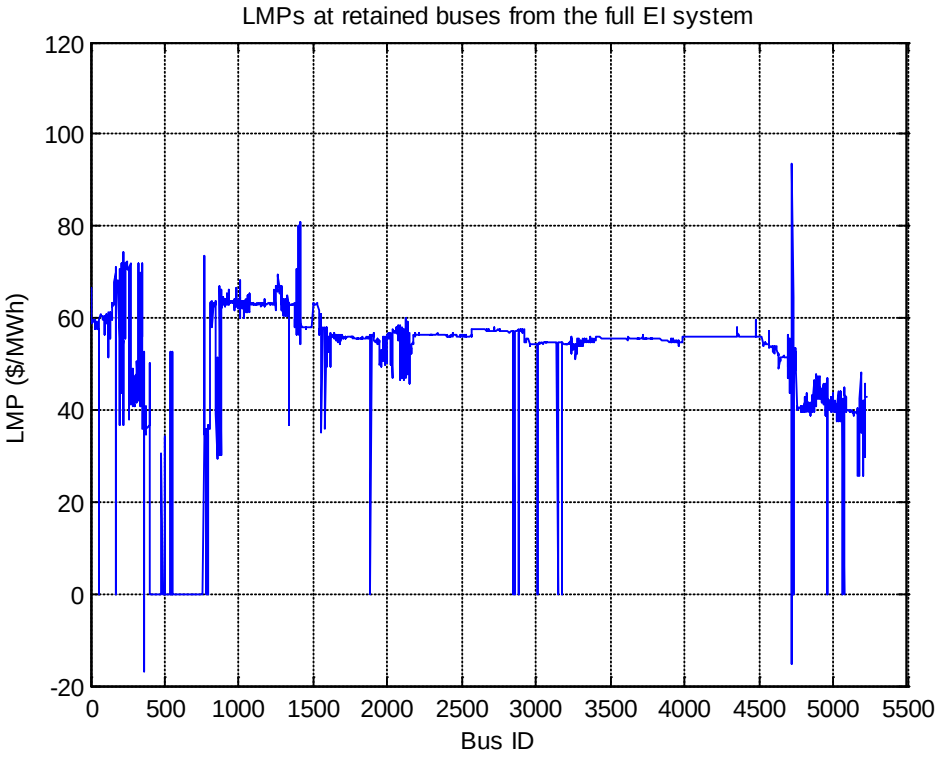

Figure 2.25: LMPs Calculated at Retained Buses in the Full EI System

When the DC OPF is run on the 5222-bus EI equivalent; the program converges in 2.18 second with an optimal solution. A summary of the solution is shown Figure 2.26. The LMP calculated at each bus is plotted in Figure 2.27.

```
Converged in 2.18 seconds
Objective Function Value = 16193495.27 $/hr
================================================================================
|     System Summary                                                           |
================================================================================

How many?                How much?              P (MW)            Q (MVAr)
---------------------    -------------------  -------------  -----------------
Buses             5222   Total Gen Capacity   872732.0           0.0 to 0.0
Generators        8152   On-line Capacity     717331.0           0.0 to 0.0
Committed Gens    5474   Generation (actual)  648110.7               0.0
Loads             4124   Load                 648110.2               0.0
  Fixed           4098     Fixed              648086.2               0.0
  Dispatchable      26     Dispatchable         24.0 of 525.5       -0.0
Shunts               3   Shunt (inj)             -0.5                0.0
Branches         14225   Losses (I^2 * Z)         0.00               0.00
Transformers     14225   Branch Charging (inj)     -                 0.0
Inter-ties        2027   Total Inter-tie Flow 197695.9                0.0
Areas              104

                         Minimum                      Maximum
                 -------------------------  --------------------------------
Voltage Magnitude   1.000 p.u. @ bus 100001      1.000 p.u. @ bus 100001
Voltage Angle     -85.35 deg   @ bus 126304    209.51 deg   @ bus 667016
Lambda P          -19.28 $/MWh @ bus 155073    109.56 $/MWh @ bus 130764
Lambda Q            0.00 $/MWh @ bus 100001      0.00 $/MWh @ bus 100001
```

Figure 2.26: Summary of the DC OPF Results on the 5,222-bus EI Equivalent

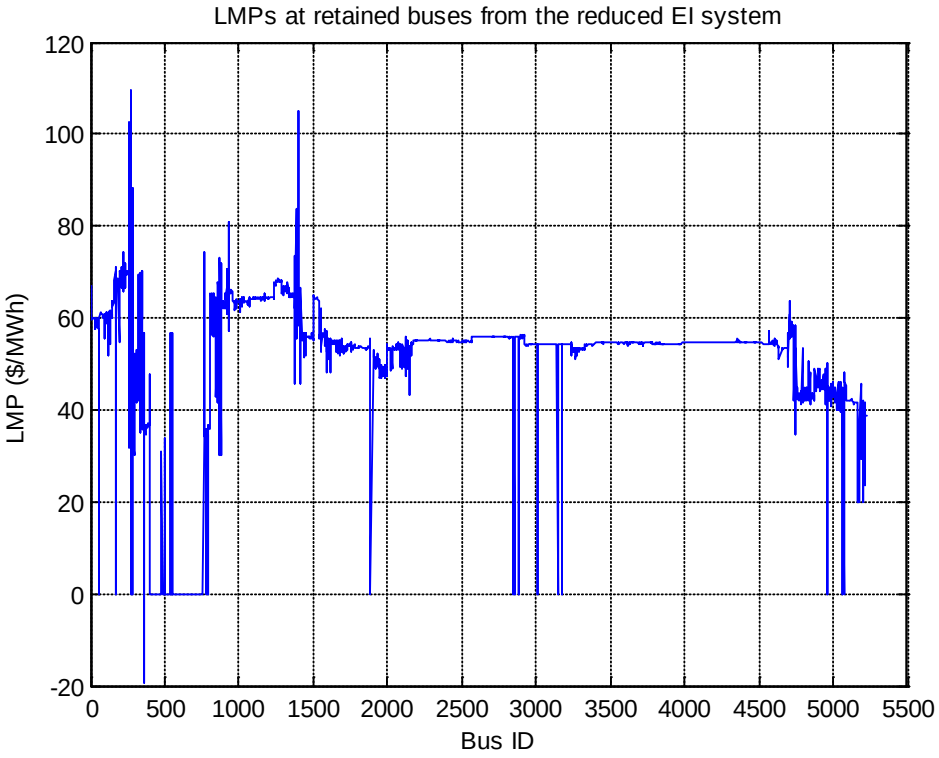

Figure 2.27: LMPs Calculated at Retained Buses in the EI Equivalent

In order to better compare the performance and results of the DC OPF on the full EI and equivalent EI system, some metrics are provided in Table 2.8.

Table 2.8: Comparison between the DC OPF Solutions of the Full and Equivalent EI Models

	Full EI Model	**Equivalent EI Model**
Convergence of the solution (Y/N)	Y	Y
Time for Convergence (sec)	35.89	2.18
Total Generation (MW)	648,157	648,110
Total Load (MW)	647,872	648,110[1]
Total Cost ($/Hour)	16,244,322	16,193,495
Average LMP ($/MWh)	50.6938	50.7067

[1] The total load in the reduced system is slightly greater than that of the original model because the corona losses in the original model are lumped parameter elements, while this power is modeled as MW load in the reduced model.

The following conclusions can be drawn based on the simulation results shown above.

- By reducing the full EI model from about 60,000 buses to 5,000 buses, the computational efficiency for running DC OPF is greatly improved with a speedup factor of 16.5.
- The calculated total operational costs from the two models are 16,244,321.51 $/Hour in the full system and 16,193,495.27 $/Hour in the equivalent. This corresponds to an error of 0.31%.
- The average LMP values calculated by the two models differ by 0.0129 $/MWh, which corresponds to an error of 0.0254%.

- The LMPs at each retained bus in the equivalent were compared to the ones obtained from the DC OPF solution using the full model. The errors in the LMP in the reduced system are plotted as shown in Figure 2.28. The Average LMP Difference at each retained bus is found to be 1.6841 ($/MWh). Only about 3.3% of the Average LMP.

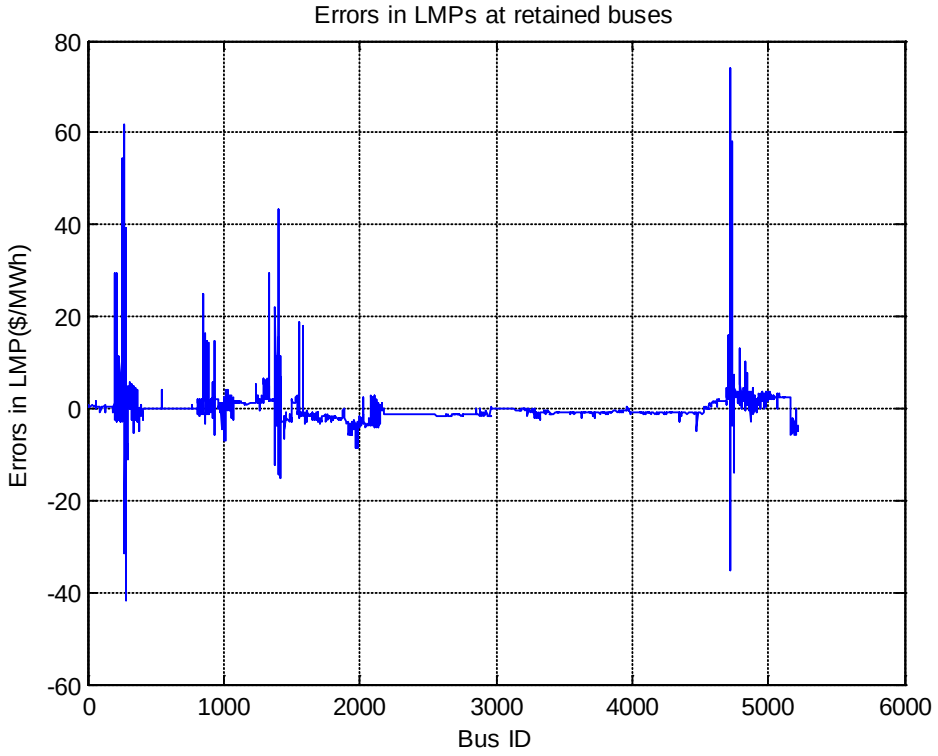

Figure 2.28: Errors in LMP for the Reduced Equivalent ($/MWh)

2.4.4 Loss Compensation in DC Power Flow Modeling

The DC power flow has found favor in LMP-based market applications because of its speed and robustness [37]-[38]. Although some authors have shown impressive accuracy with DC power-flow formulations, others are not so optimistic about its accuracy [39] [39]. Presently, many versions of DC power-flow formulations exist. In general, these

different formulations are characterized by different definitions of active power injections, loss compensation and branch admittances [39]-[41].

In the previous section, errors between the DC PFs on the equivalent and the full EI models have been quantified. More light can be shed on the feasibility of using DC network equivalents if the difference between the AC and DC PFs on the full EI system can be quantified. Also, it is of interest to examine the influence of different assumptions so that better (EI) DC network equivalents can be created.

Equivalent DC PF models are inherently approximate, and, as is well known, their accuracies are very system and case dependent [39] [39]. Given the limits of theory and applied mathematics in formulation-acceptability analysis, this section experimentally explores the influence of loss compensations on the accuracy of DC PF formulations for system as large as the EI.

2.4.4.1 Formulations of DC Power Flow Models

Four DC PF formulations are discussed in this section: the classical DC PF model, DC PF model with a single multiplier for loss compensation, DC PF model with zonal multipliers for loss compensation, and DC PF model with loss compensation for each line. A general transmission line (*I*, *j*) model is shown in Figure 2.29.

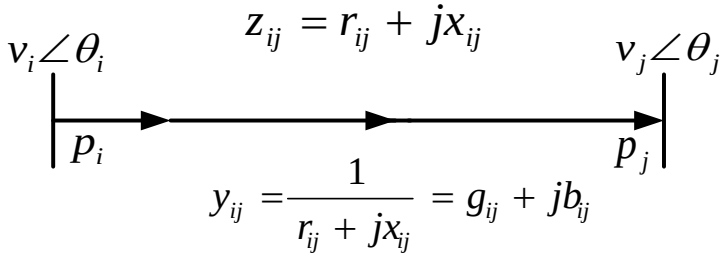

Figure 2.29: A General Transmission Line Model

The DC power-flow modeling starts from the AC power-flow equations. As shown in Figure 2.29, based on the AC PF formulation, the real power flows at sending end and receiving end of the line are:

$$\begin{aligned} p_i &= \mathrm{Re}\left\{v_i \angle \theta_i \cdot \left[(g_{ij} + jb_{ij}) \cdot (v_i \angle \theta_i - v_j \angle \theta_j)\right]^*\right\} \\ &= g_{ij}\left[v_i^2 - v_i v_j \cos(\theta_i - \theta_j)\right] - v_i v_j b_{ij} \sin(\theta_i - \theta_j) \end{aligned} \qquad 2.15$$

$$p_j = -g_{ij}[v_j^2 - v_i v_j \cos(\theta_i - \theta_j)] - v_i v_j b_{ij} \sin(\theta_i - \theta_j) \qquad 2.16$$

2.4.4.2 Classical DC Power-Flow Model

A general branch model used in DC PF is shown in Figure 2.29, in which l_i and l_j are parameters representing the loss on transmission line (i, j) at terminal i and j, respectively.

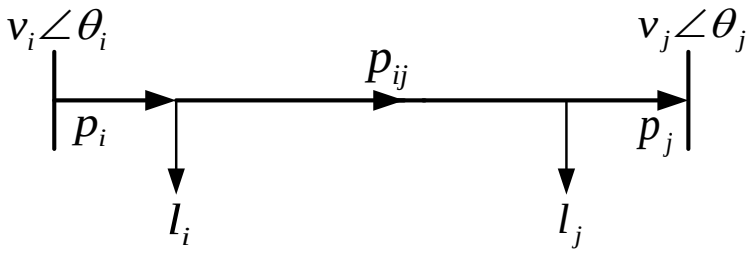

Figure 2.30: A General Branch Model Used in DC Power Flow

In the classical DC power-flow model, four assumptions are made. First, loss is neglected:

$$l_i = l_j = 0 \quad so \quad that \quad p_i = p_j = p_{ij} = -b_{ij} v_i v_j \sin(\theta_i - \theta_j) \tag{2.17}$$

Second, the voltage angle across each branch is very small:

$$\theta_i - \theta_j \approx 0 \quad so \quad that \quad p_{ij} \approx -b_{ij} v_i v_j (\theta_i - \theta_j) \tag{2.18}$$

Third, voltages at all buses are close to 1 p.u.:

$$v_i, v_j \approx 1 \quad so \quad that \quad p_{ij} = -b_{ij} (\theta_i - \theta_j) \tag{2.19}$$

Finally, branch resistance is small compared to reactance and thus, is neglected:

$$r_{ij} \approx 0 \quad so \quad that \quad p_{ij} = (\theta_i - \theta_j) / x_{ij} \tag{2.20}$$

2.4.4.3 DC PF Model with a Single Multiplier for Loss Compensation

In this DC PF model, the same assumptions are used as those for the classical model except that a single multiplier is used to scale-up the entire load to compensate for the losses in the system. This single multiplier λ is calculated as the ratio of the total generation to total load in the system based on the AC power flow solution:

$$\lambda = \frac{\sum P_G}{\sum P_L} \tag{2.21}$$

where $\sum P_G$ and $\sum P_L$ are the total generation and total load in the system, respectively.

2.4.4.4 DC PF Model with Zonal Multipliers for Loss Compensation

In this DC PF model, the same assumptions are used as those for the DC PF model with a single multiplier except that a different loss distribution assumption is used. Basically, the load in each zone is scaled up by a different multiplier. The zonal loss multiplier for zone *m* is calculated as:

$$\lambda_m = \frac{\sum_m P_{Loss} + \sum_m P_L}{\sum_m P_L} \qquad 2.22$$

where $\sum_m P_{Loss}$ and $\sum_m P_L$ are the total losses and total load within zone *m*.

2.4.4.5 DC PF Model with Loss Compensation for Each Line

In this DC PF model, loss is compensated on a line-by-line basis. Based on 2.15-2.16, the loss-approximating parameters for line (*i*, *j*) are calculated as:

$$l_i = g_{ij}[v_i^2 - v_i v_j \cos(\theta_i - \theta_j)] \qquad 2.23$$

$$l_j = -g_{ij}[v_j^2 - v_i v_j \cos(\theta_i - \theta_j)] \qquad 2.24$$

For a transformer with off-nominal tap and (or) non-zero phase shift, the loss compensation is a bit more complicated. A general PF model for phase-shifter branches is shown in Figure 2.31. Based on the AC PF, the real PF at the sending end and receiving end are:

$$\begin{aligned} p_i = {} & g_{ij}[(v_i / t_{ij})^2 - (v_i / t_{ij}) v_j \cos(\theta_i - \theta_j - \delta_{ij})] \\ & - (v_i / t_{ij}) v_j b_{ij} \sin(\theta_i - \theta_j - \delta_{ij}) \end{aligned} \qquad 2.25$$

$$p_j = -g_{ij}[v_j^2 - (v_i / t_{ij}) v_j \cos(\theta_i - \theta_j - \delta_{ij})] - (v_i / t_{ij}) v_j b_{ij} \sin(\theta_i - \theta_j) \qquad 2.26$$

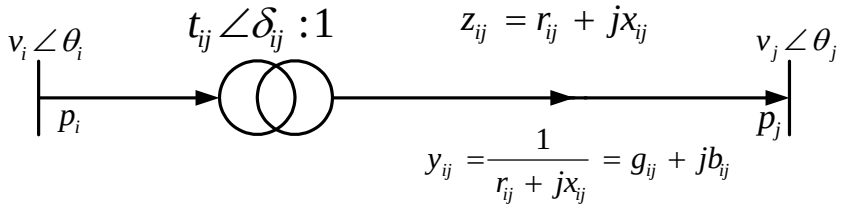

Figure 2.31: A General Transformer Model with Off-nominal Tap and (or) Non-zero Phase Shift

For the general transformer branch shown in Figure 2.31, the following loss compensation factors are selected:

$$l_i = g_{ij}[(v_i / t_{ij})^2 - v_i v_j \cos(\theta_i - \theta_j - \delta_{ij})] \qquad 2.27$$

$$l_j = -g_{ij}[v_j^2 - (v_i / t_{ij}) v_j \cos(\theta_i - \theta_j - \delta_{ij})] \qquad 2.28$$

2.4.4.6 Comparison of DC Power-Flow Models of EI

An AC PF solution is first obtained for the EI under the base case. This AC PF solution is used to construct the four DC PF models based on 2.17-2.28. For each of the four DC models, the PF is solved and compared with the original AC PF solution. Figure 2.32 summarizes numerical simulations conducted.

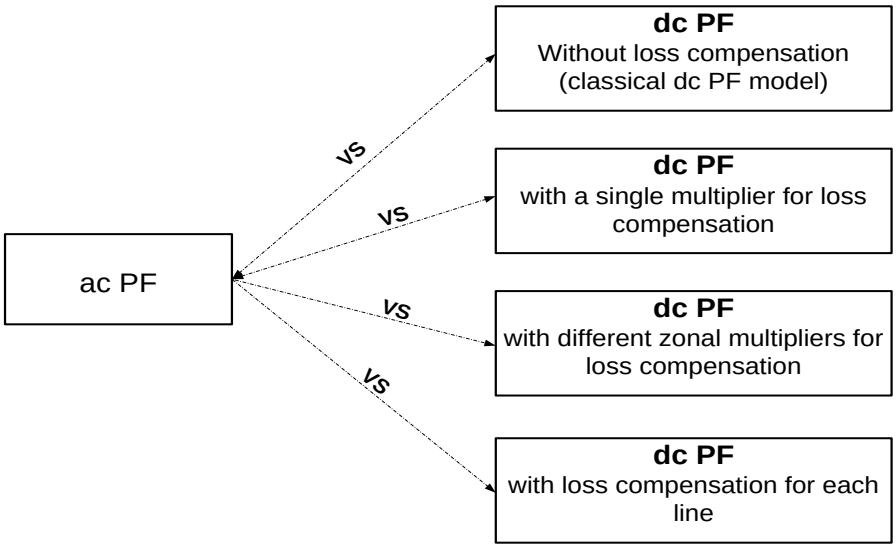

Figure 2.32: The Numerical Simulations Conducted

In all the tests below, the same testing methods as discussed in [39] are followed. In determining the branch-flow errors, the following assumptions are used:

- all branches with PF below 50 MW are neglected
- all branches that are loaded below 70% of their ratings are neglected
- all branches that have no MVA rating in the EI data base are neglected

The simulation results are presented below.

2.4.4.7 AC PF Model vs. Classical DC PF Model

For the full EI system, the comparison between the branch MW flows of the AC PF model and the classical DC PF model is shown in Figure 2.33. The upper part of the figures shows the actual branch MW flows of the AC and DC models while the lower part shows the difference (errors) in the branch MW flows by using the classical DC PF model.

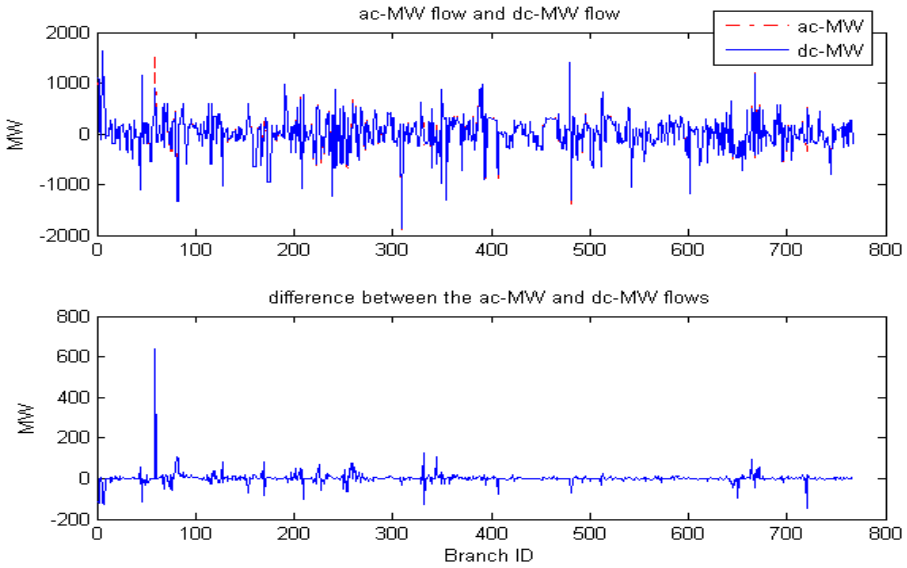

Figure 2.33: Branch MW-flow Difference Between AC and the Classical DC PF Models

As Figure 2.33 shows, the largest error in the branch PFs is about 620 MW. The average error over the all the branch flows plotted in Figure 2.33 is calculated to be 10.91 MW based on equation 2.29,

$$Error_{Avg} = \frac{\sum_{i=1}^{N} \left| Pf_i^{ac} - Pf_i^{dc} \right|}{N} \qquad 2.29$$

where Pf_i^{ac} and Pf_i^{dc} represent the PF on the i^{th} branch based on the AC PF and DC PF models, respectively; N is the total number of branches examined.

The branch MW-flow errors in percentage are calculated based on 2.30,

$$Error_i = \frac{\left| Pf_i^{ac} - Pf_i^{dc} \right|}{MVA_i} \times 100\% \qquad 2.30$$

where MVA_i is the MVA rating of line i. Based on 2.30, the branch-flow errors in percentage are shown in Figure 2.34, from which, the largest error is found to be 49.33%. The average value of the percentage errors is calculated to be 2.54%.

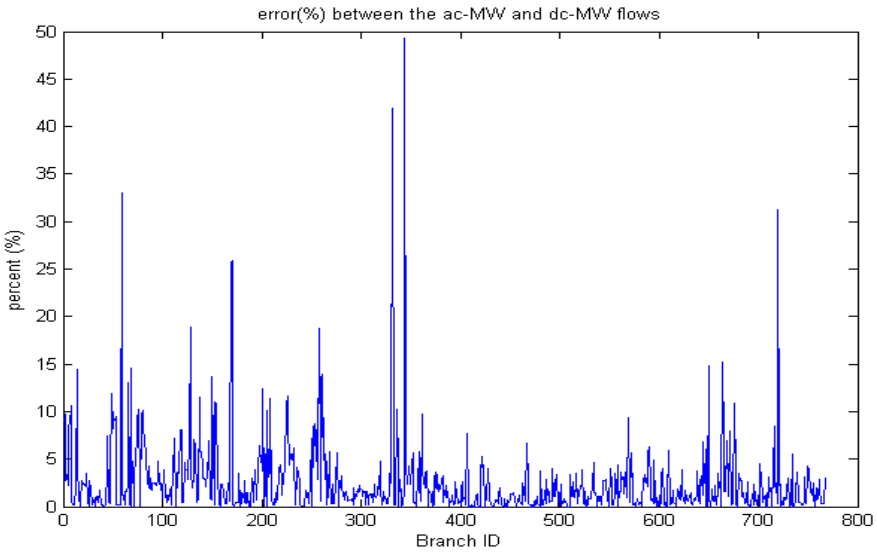

Figure 2.34: Branch MW-flow Errors (%) of the Classical DC PF Model

2.4.4.8 AC PF model vs. DC PF model with a single multiplier for loss compensation

As shown in Figure 2.35, the maximum error in the branch MW flows is 102 MW, and the average error is calculated to be 6.42 MW.

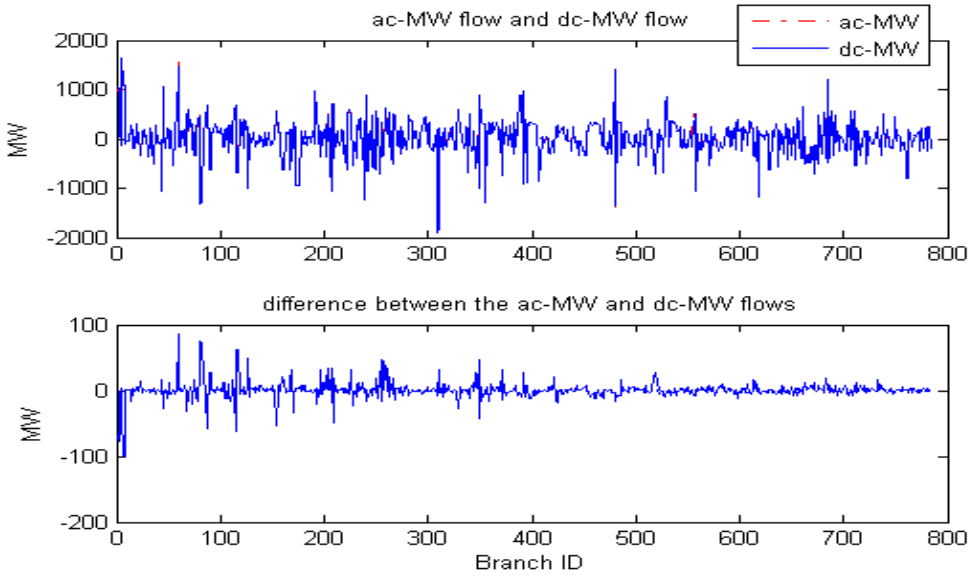

Figure 2.35: Branch MW-flow Difference Between AC PF Model and the DC PF Model with Single Multiplier for Loss Compensation

The percentage errors in the branch MW flows are shown in Figure 2.36, from which the maximum error is found to be 13.56%. The average percentage error is calculated to be 1.79%. Clearly, compensating for losses improves branch-flow errors significantly.

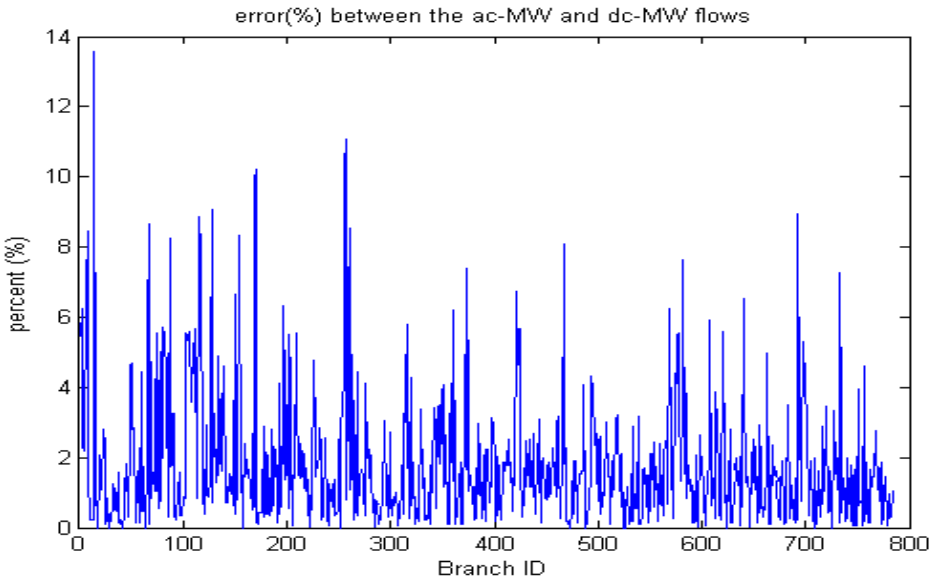

Figure 2.36: Branch MW-flow Errors (%) of the DC PF Model with Single Multiplier for Loss Compensation

2.4.4.9 AC PF model vs. DC PF model with zonal multipliers for loss compensation

As shown in Figure 2.37, the maximum error in the branch MW flows is 83 MW while the average error is calculated to be 5.62 MW when zonal loss compensation is used.

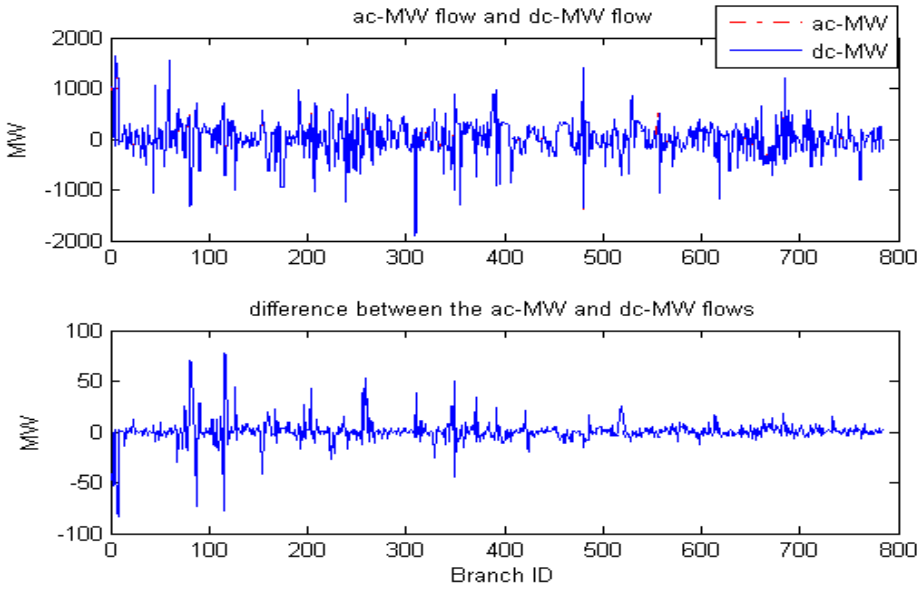

Figure 2.37: Branch MW-flow Difference Between AC PF Model and DC PF Model with Zonal Multipliers for Loss Compensation

The percentage errors in the branch MW flows are shown in Figure 2.38, based on which the maximum error is found to be 12.20%. The average percentage error is calculated to be 1.64%. These results show that using zonal multipliers is somewhat better than using a single multiplier.

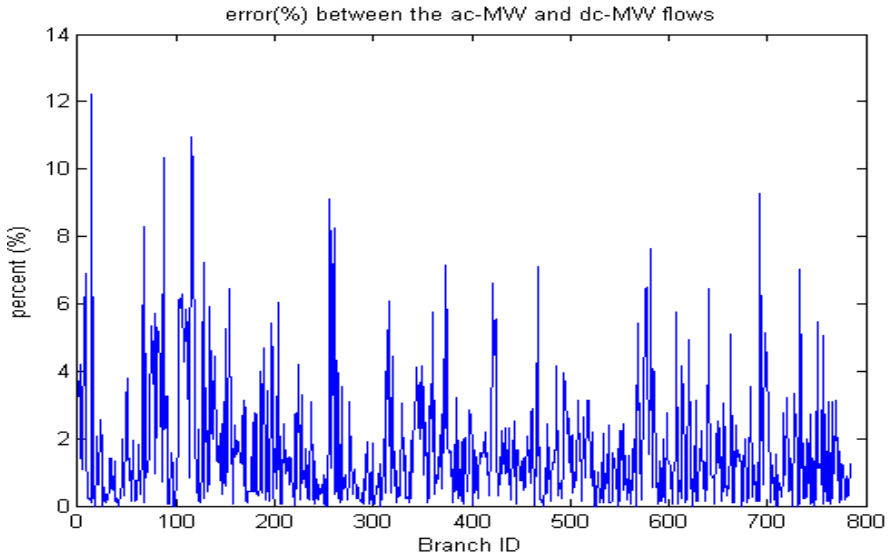

Figure 2.38: Branch MW-flow Errors (%) of the DC PF Model with Zonal Multipliers for Loss Compensation

2.4.4.10 AC PF Model vs. DC PF Model with Loss Compensation for each Line

As shown in Figure 2.39, the maximum error in the branch MW flows is 16.42 MW while the average error is calculated to be 2.98 MW.

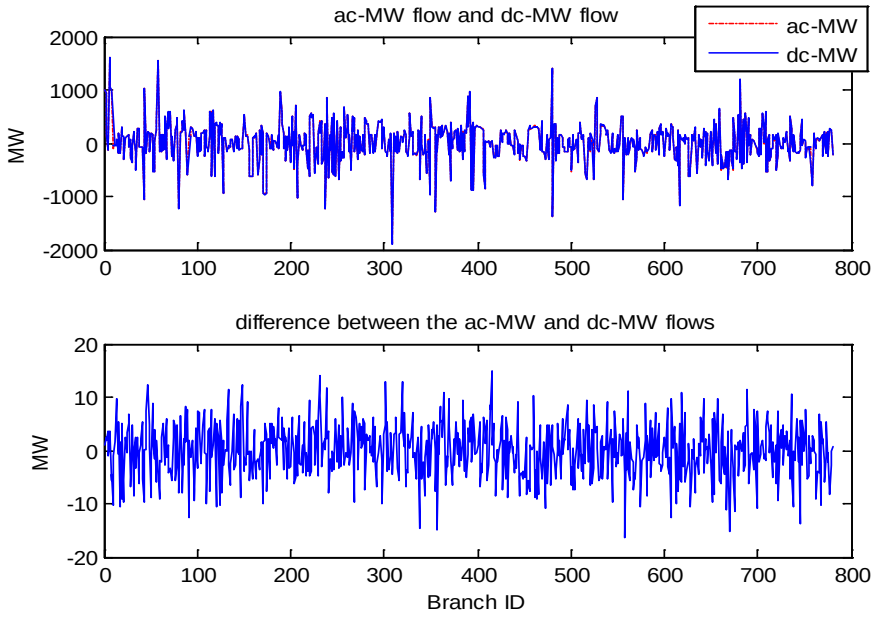

Figure 2.39: Branch MW-flow Difference Between AC PF Model and DC PF Model with Loss Compensation for Each Line

The percentage errors in the branch MW flows are shown in Figure 2.40, based on which the maximum error is found to be 2.01%. The average percentage error is calculated to be 0.31%. This shows that using compensation calculated for each line is clearly superior to all other methods.

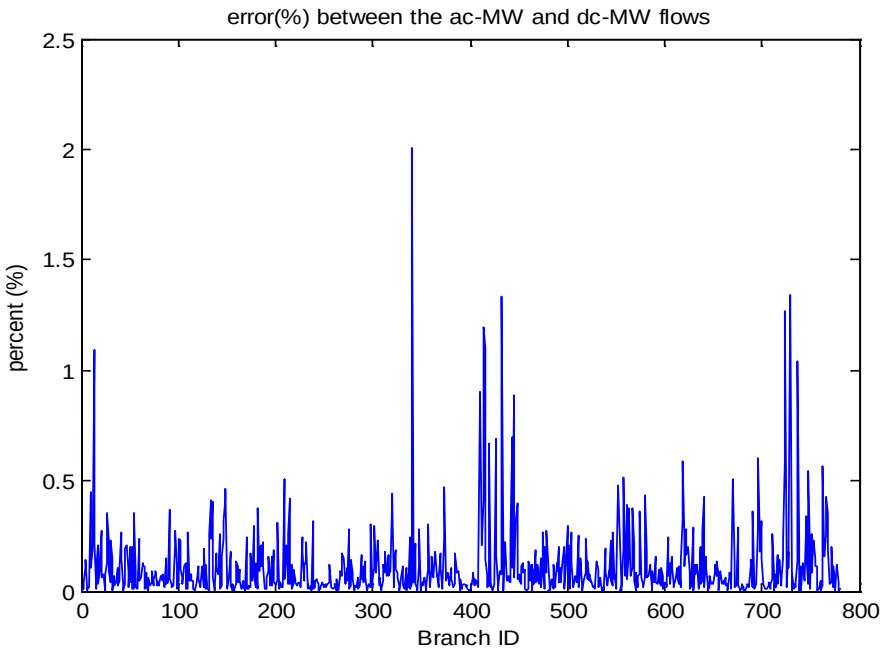

Figure 2.40: Branch MW-flow Errors (%) of the DC PF Model with Loss Compensation for Each Line

2.4.4.11 Summary of Test on EI Reduced Model

The test results are summarized into Table 2.9.

Table 2.9: Maximum and Average Branch MW flow Errors for Each DC Model

Error	Classical DC PF	DC PF-single multiplier	DC PF-zonal multiplier	DC PF-line loss compensation
Max (MW).	620 MW	102 MW	83 MW	16.42 MW
Avg. (MW)	10.91 MW	6.42 MW	5.62 MW	2.98 MW
Max (%)	49.33%	13.56%	12.20%	2.01%
Avg. (%)	2.54%	1.79%	1.64%	0.31%

The following are some conclusions drawn for the test conducted above:

- The classical DC PF model assumes no loss in the power system, and thus, it is state-independent and easy to construct. However, using the classical DC PF model for large systems, such as the EI, leads to significant branch-flow errors, and therefore, is inadvisable.
- For classical DC PF model, the branch with 620 MW flow error is close to the system slack bus. When no losses are modeled, the slack bus will pick up all of

the system losses, making the branches local to the slack bus suffer from large PF errors. A possible solution might be to use a distributed slack bus within each control area so that errors can be more evenly distributed across the entire system.

- The DC PF models with loss compensations are state-dependent models, construction of which requires a solved AC power flow solution. Compared to the classical DC PF model, DC models with loss compensation are much more accurate.
- Of all the DC models with loss compensations, the one with loss compensation for each line is closest to the AC power flow model and gives best performance for the base case.
- Compensating losses with different zonal multipliers gives slightly better performance than compensating the loss with a single multiplier.

Compensating loss with a single multiplier in DC PF is a reasonably effective and the simplest way to improve the DC PF accuracy.

2.4.5 Conclusions on EI Reduced Model

It was shown that a 5222-bus equivalent of the EI is acceptable as measured using various tests and metric. In the changed-case test and using line flows as a metric, it was found that the line flow errors were acceptable. Using LMP's, total production cost and total generation as metrics it was shown that the 5222-bus model passed the OPF-accuracy tests. It was also shown that the DC approximation of the AC model for the full EI yields acceptable results, as measured by line-flow errors. Finally, it was shown that accounting for losses in the DC model is important and various ways of accounting for losses were proposed and found to be acceptable.

3. APPLICATION OF THE EQUIVALENT IN SYSTEM PLANNING

In this chapter, the 279, 240 and 5222 bus equivalents are used in the SuperOPF Planning Tool to determine optimal generation planning in the ERCOT, WECC, and EI systems, respectively. A brief introduction to the structure and formulation of the SuperOPF Planning Tool is presented. Modeling of the data and description of the cases are provided. The results are analyzed and conclusions are drawn.

3.1 Introduction to the SuperOPF Planning Tool

The SuperOPF Investment Planning Tool, developed by Cornell, is a package whose major function is to optimize generation investment and retirement while maintaining system reliability and accounting for various system constraints such as generation building limits and environmental regulations.

Using the 279-bus ERCOT equivalent yields large execution-time savings when used in the SuperOPF environment. On a state-of-the-art PC, it takes the SuperOPF less than 10 minutes of execution time with the 279-bus equivalent, while solving the same problem with the full ERCOT model takes more than 24 hours. At the other extreme, the 5222-bus equivalent for the EI takes about 40 hours of execution time and the full EI model has never been attempted for obvious s reasons.

The formulation of the optimal generation investment problem in the SuperOPF is presented as shown in 3.1. The detail information about the SuperOPF is of less interest in this report and therefore not presented. Detail information regarding the explanation of the formulation, as well as structure and application of the SuperOPF planning tool can be obtained in [1].

$$\max_{p_{ijk}, I_{ijk}, R_{ij}} \left\{ \sum_i \sum_j \begin{bmatrix} (\sum_k H_k (B_{jk} - (c_i^F + a_{jk} e_i) p_{ijk})) \\ -(c_i^T (p_{ij}^0 + I_{ij} - R_{ij}) - c_i^I I_{ij}) \end{bmatrix} \right\} \quad 3.1$$

subject to

$$p_{ij}^0 + I_{ij} - R_{ij} \geq p_{ijk}$$
$$p_{ijk} \geq \alpha_i^{\min} (p_{ij}^0 + I_{ij} - R_{ij})$$
$$K_{ij} > I_{ij}$$
$$\sum_j L_{jk} = \sum_i \sum_j p_{ijk}$$
DC network constraints

where the following notation is used:

i: Generator index

j: Node index

k: Representative hour index

p_{ijk}: Aggregate real power output from generator i at node j during representative hour k

p^0_{ij}: Existing generator capacity

R_{ij}: Capacity requirement

I_{ij}: Capacity investment

c^F_i: Cost of fuel, operations and maintenance per MWh

c^T_i: Cost of taxes and insurance per MW

c^I_i: Annualized cost of new investment

H_k: Hours system is at load profile k

e_i: Emissions vector for generation type I, tonnes/MWh

a_{jk}: Emission cost vector at node j in hour k, $/tonne

α^{min}: Min generation for type i

K_{ij}: Max investment in fuel type I at node j

B_{jk}: Benefit function for demand response

L_{jk}: Net load

3.2 Data Preparation

The SuperOPF optimizes generation investment and retirement across multiple load scenarios. To accurately simulate the 12 representative hours that make up each year, average loads for each NERC region are calculated for each representative hour. Information from the Federal Energy Regulatory Commission, FERC Form 714, is used as a base. Form 714 Schedule 3 shows the peak hourly electricity demand for each balancing authority and electricity utility with annual peak demand greater than 200 MW. Each entity in the database is assigned to a NERC region based on its geographic location. The hourly load for each NERC region is then totaled.

Next, the data is split into seasons. Load from May-September is classified as summer, load from December-February is classified as winter, and load from the remaining four months is classified as fall and spring. Total load within each season is sorted from high to low. The top 5% of hours in each season are classified as peak, the next 25% of hours are high, the next 40% of hours are medium, and the bottom 30% of hours are low. The average load for each NERC region is averaged for all the hours in each load profile type (four seasons and four hour types.) To illustrate the results of this process, the frequency of each representative hour type and the scaling of load in each representative hour type are shown for ERCOT in Figure 3.1 and Figure 3.2.

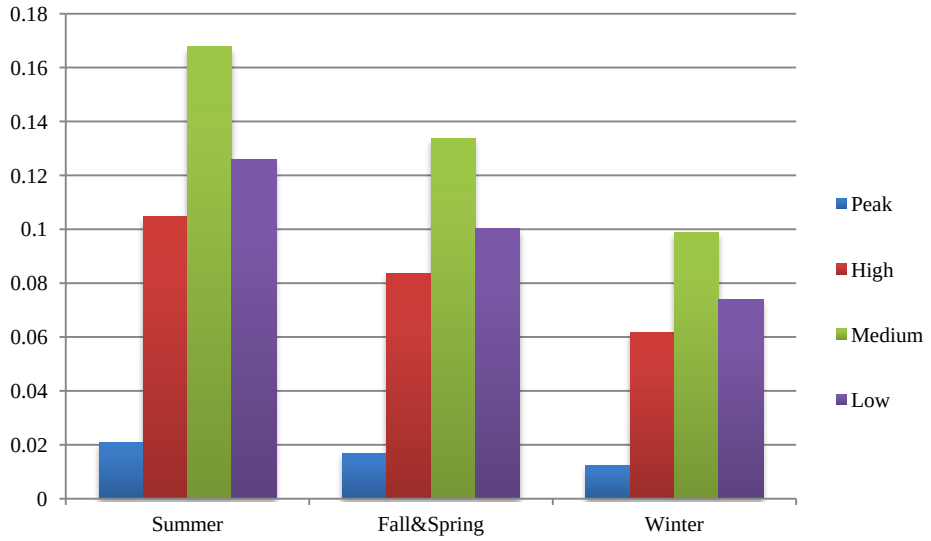

Figure 3.1: Relative Frequency of Representative Hour Types

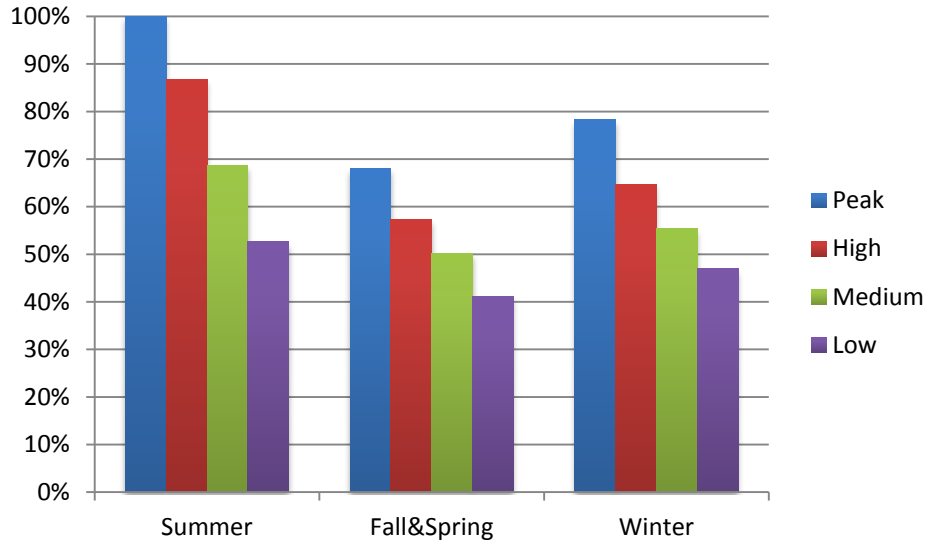

Figure 3.2: Scaling of the Load in Each Representative Hour Type

The long-run rate of growth for electricity demand in each NERC region needs to be estimated, separate from any long-run demand response (demand elasticity) that is taking place. Two sets of data are needed for this: average prices for electricity by state and quantity of electricity sold by state, for 1990-2010. These are both available from the EIA, compiled from data collected from Form EIA-861.

Using average prices for electricity, the real (adjusted for inflation) rate of price growth from 1990-2010 for each state is calculated. Similarly, the actual load growth in each state is calculated. Assuming an elasticity of 0.8, the amount of load abatement or load growth caused by increases, or decreases, in real prices is calculated. For example, if real prices increased by 10% from 1990-2010, this would have caused a decrease in electricity

sales of 8%. In the absence of any changes in price, there would have been 8% more growth than was actually observed.

In the United States as a whole, load increased 38.4% from 1990-2010, while prices (in real terms) declined by 10.2%. If prices had remained constant, load growth would have been about 30.2% over that 20-year time span, or about 1.3% each year. There is considerable variation between the states. Actual electricity sales in Washington State declined 0.7% from 1990-2010, while sales in Nevada increased by 106%. In real terms, prices decreased almost 35% in Arizona and increased by the same amount in the District of Columbia. Annual load growth factors vary from 0.02% in Maine to 3.8% in Nevada.

In order to account for reliability, a 10% reserve requirement is added to the system. To represent unit availability, generator contingencies are included in the model. This is done by de-rating a generator's maximum output capacity in each season, with each generation type de-rated by a different percentage [24].

One of the important features of the SuperOPF is its ability to study the effects of environmental regulations on optimal generation investment. In that regard, the term "emissions price" is used in this paper to refer to an emissions tax or the permit-purchasing price in a cap-and-trade program.

For investment in new generators, five fuel types of generators are considered: coal, natural gas, solar, wind and nuclear. Total capacity limits for coal, natural gas combined cycle and nuclear were calculated from historical data. Maximum growth rates for each generation type were used to set a growth rate for the entire country, which was then divided amongst the EI, WECC and ERCOT based on expected population growth rates, obtained from the US Census. A maximum of 15% of capacity can be built in ERCOT, 35% in WECC, and 50% in the Eastern Interconnect. For emerging renewable technologies, wind and solar, the capacity limit is such that each region could generate 1/3 of its electricity from wind power and 20% from solar by 2032. To illustrate the resulting limits, the total capacity addition limit for each fuel type calculated for ERCOT is listed in Table 3.1.

The SuperOPF takes into account generation marginal cost, maintenance costs, capital cost for building new plants and carrying charges. Capital recovery and fixed cost for existing and new generators were obtained from [1] as shown in Table 3.2. It should be noted that the capital recovery for solar declines from $ 590,000 to $390,000 in 2032, since it is expected that the building cost for solar units will decrease in the future. To model DOE's nuclear loan guaranty program, capital cost for nuclear generators is reduced [25]. Long and short run response to price (a.k.a., demand elasticity) is assumed to be -0.8 [26].

Table 3.1: Total Two-Decade Capacity-Addition Limit by Fuel Type by 2032

Fuel Type	Total capacity addition limit by 2032 (MW)
Coal	10,000
Natural Gas	33,000
Nuclear	5000
Wind	16,000
Solar	9,700

Table 3.2: Capital Recovery and Total Fix Costs for Different Type of Generators

Fuel Type	Capital Recovery ($/MW/Year)	Annual Total Fixed Costs($/MW)
Coal	497,201	35,255
Natural Gas	181,824	20,661
Nuclear	470,226	95,571
Wind	392,322	20,661
Solar	520,000 (in 2012 and 2022) 390,000 (in 2032)	20,661

3.3 Description of the Cases

To assess the response of long-term generation investment to the future environment, an environment that is uncertain, studies are conducted using six possible 30-year futures and predictions of generation investment are made. Each future (case) consists of three simulation years: 2012, 2022 and 2032, an interval which is based on the assumption that each investment cycle takes ten years. For all the cases, the first cycle of generation investment starts in year 2012 and ends in 2022. The simulation year 2012 is assumed to have generation as built today.

The cases studied in this report are described as follows. The first case is referred to as the base case. In the base case, no environmental regulation or subsidies for renewable energy are considered.

In the second case, a CO_2 emissions price is added to represent a cap-and-trade auction for CO_2. This cap-and-trade auction for CO_2 is assumed to have a price cap similar to that

proposed in the Kerry-Lieberman Bill. This case is referred to as the cap-and-trade (C&T) case. In the C&T case, the CO_2 price starts at 36.94 $/ton in 2022 and rises to 60.18 $/ton in 2032, equivalent to the Kerry-Lieberman price cap. Besides modeling CO_2 emissions prices, subsides for wind and solar generation are included. An incentive of 22 $/MWh for wind and solar generation is included to model the Federal Renewable Electricity Production Tax Credit [28].

Similar to the C&T case, the third case also includes the same incentives for wind and solar generation. The incentives for wind and solar used in the third case are the same as those used in the K-L case. An EPA proposed rule aimed at regulating CO_2 emissions from power plants is included in the third case, a rule that is expected to be finalized later in 2012. This rule requires all new fossil-fuel-fired generation of 25 MW or more must emit no more than 1000 lbs. of CO_2 per MWh. Since coal-fired plants cannot meet this standard, the standard effectively prohibits the construction of new coal plants. Therefore, in the third case, no new coal-fired plants can be built in 2022 and 2032. The third case is referred to as the EPA case.

All of the three cases are simulated with two different sets of gas prices, yielding six futures in total. The first set of gas prices is referred to as the high gas price set, which is 2.5 $/MMBTU in 2012, 7 $/MMBTU in 2022 and 14 $/MMBTU in 2032. The low gas price of 2.5 $/MMBTU modeled in 2012 is based on the current availability of shale gas but it is possible that the costs of extracting shale gas will start to rise by 2022 and so the gas price increases to 7 $/MMBTU. Then in 2032, the gas price converges to a world price of about 14 $/MMBTU. The natural gas price of 14 $/MMBTU may seem large, but the gas price was in the neighborhood of 15 $/MMBTU in 2005.

The second set of gas prices is referred to as the low gas price set, which is 2.5 $/MMBTU in 2012, 4.77 $/MMBTU in 2022 and 5.86 $/MMBTU in 2032. This set of gas prices is based on estimates by the EIA [27].

Based on the different sets of gas prices used, the cases studied can be categorized into two groups. The cases that are run with the high gas price set are referred to as high-gas-price cases (HG) and similarly the cases that run with low-gas-price set (LG) are referred to as low gas price cases. The summary of modeling of each case and the two sets of natural gas prices are shown in Table 3.3 and Table 3.4.

Table 3.3: Summary of the Modeling of the Cases

	Base Cases	**C&T Cases**	**EPA Cases**
CO2 emissions price	×	√	×
EPA Regulation	×	×	√
Incentives for wind and solar	×	√	√

Table 3.4: Summary of the Two Sets of Natural Gas Prices

	2012 ($/MMBTU)	**2022 ($/MMBTU)**	**2032 ($/MMBTU)**
High Gas Prices	2.50	7	14
Low Gas Prices	2.50	4.77	5.86

3.4 Results for Each Case

In this subsection, the effects that the six futures (cases) have on the investment and retirement of generation in the ERCOT, WECC, and EI systems are shown. The retirements and additions for the five fuel types—coal, natural gas, nuclear, wind and solar—considered in the investment study are presented below.

3.4.1 Natural Gas

Figure 3.3 (a) and (b) show the retirements and additions for natural gas units. As shown in Figure 3.3 (a), the C&T HG case has the largest capacity of natural gas retirement among all the cases, which is around 18.5 GW in 2022. This is the result of the high gas price (7 $/MMBTU) and CO_2 emissions penalties modeled in the C&T HG case, since together they increase the operational costs for natural gas units. About 17 GW of new natural gas units are only built in the C&T LG case in 2032, as shown in Figure 3.3 (b). In 2022 in the C&T LG case, because of the wind and solar incentives, wind and solar are built to compensate for the retirement in natural gas and to serve the assumed growth in demand. Therefore no natural gas unit is built in 2022. In 2032, as the natural gas price continues to increase, building new natural gas units becomes more economical than dispatching existing natural gas units because, while new gas natural units are expensive to build, they are relatively inexpensive to operate. In 2032, wind and solar reach their building limits (which can be seen from Figure 3.9 and Figure 3.12), and the imposition of CO_2 emissions prices forces about 16 GW of coal to retire by year 2032 (11.6 GW in 2022 and 4.4 GW in 2032), which is shown in Figure 3.6. Therefore about 17 GW of natural gas is built in 2032 in the C&T LG case.

In the three HG cases, the high gas prices increase the operating costs and decrease the competitiveness of the natural gas units. Therefore no new natural gas unit is built in any of the HG case. For the base and EPA LG cases, where CO_2 emissions prices are not imposed, it is cheaper to dispatch existing coal units than building natural gas units. Therefore no natural gas unit is built in the base LG or the EPA LG case.

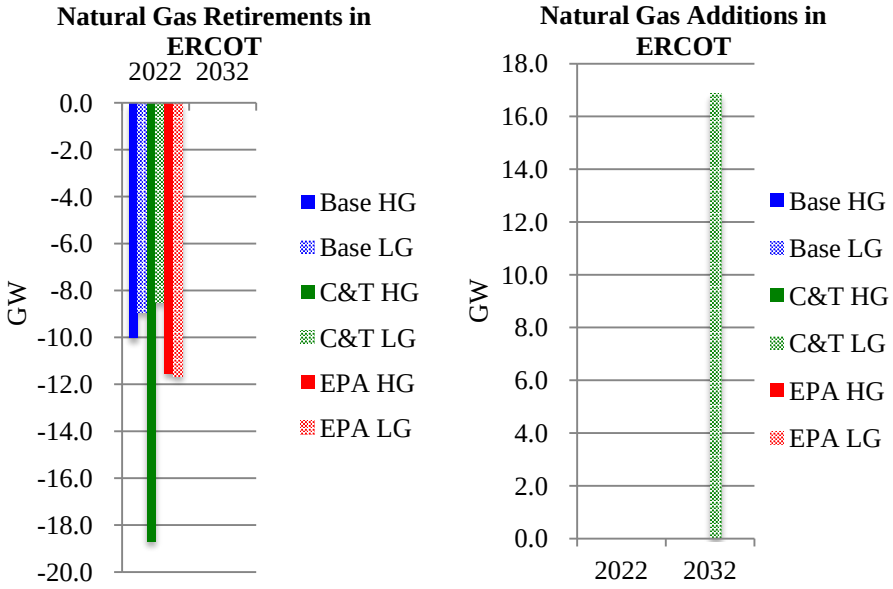

(a) Natural Gas Retirements (b) Natural Gas Additions

Figure 3.3: Retirements and Additions for Natural Gas Units in ERCOT

Retirements of natural gas units for WECC are presented in Figure 3.4: Natural Gas Retirements for WECC. Retirements are significantly lower in the three LG cases. Among the LG cases, total retirements are highest in the C&T LG case, because the CO_2 prices added by the cap-and-trade system increase the cost of using gas over the other two cases. As the CO_2 price increases from 2022 to 2032, additional gas is retired in the C&T LG case. Among the LG cases, however, gas retirements are higher in 2022 in the EPA LG case. This is because in 2022 no coal is retired in the EPA LG case, allowing retirement of older gas units, while a significant amount of coal is retired in the C&T LG case.

Similarly, total gas retirements are highest in the EPA HG case, and almost all gas retirements in the HG cases occur in 2022. This is again because no coal is retired in the EPA HG case, while a significant amount is retired with increasing CO_2 prices in the C&T HG case. Among the HG cases this leaves the C&T HG case with the least gas retirements. Gas retirements in the base HG case are higher because no coal is retired, and the price of gas is high, making it a less attractive fuel.

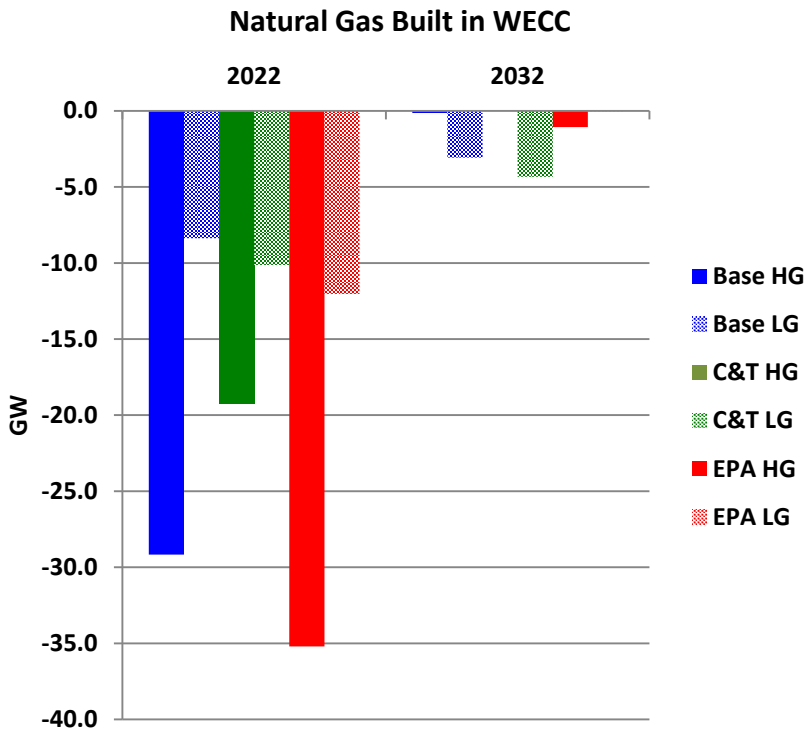

Figure 3.4: Natural Gas Retirements for WECC

Figure 3.5: Natural Gas Additions and Retirements for EI shows that the EI is a different story with combined cycle plants constructed both under high and low gas price cases for all scenarios in 2022 and 2032 with the most construction occurring under cap-and-trade. However, retirements generally exceed new construction in 2022 but the reverse is true for cap-and-trade in 2032 and more balanced in the other scenarios. NGCC is built in New England in all cases. In the Base Case, some NGCC is built in Florida under both gas prices and PJM under low gas prices.

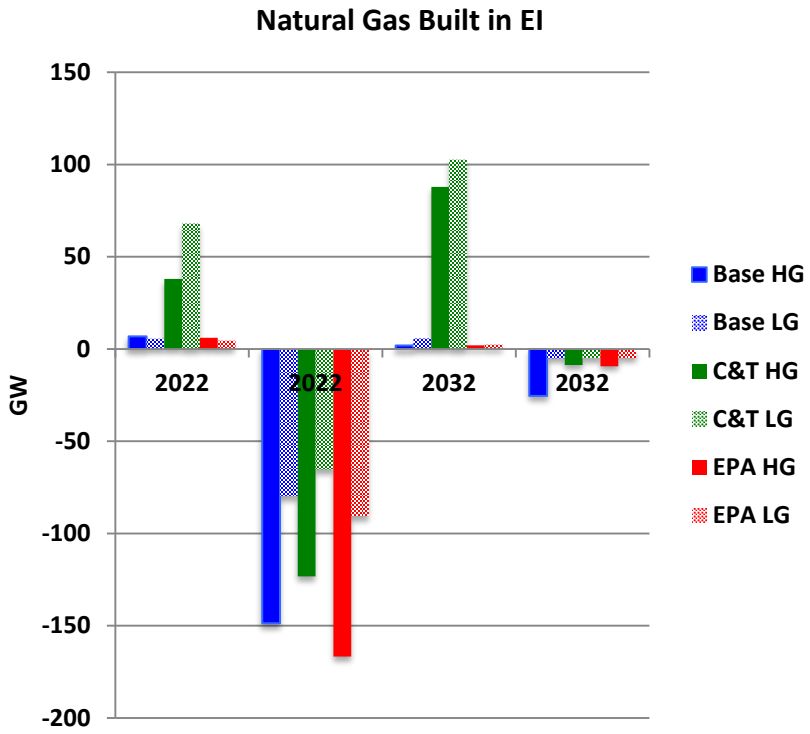

Figure 3.5: Natural Gas Additions and Retirements for EI

3.4.2 Coal

The retirements for coal in ERCOT are shown in Figure 3.6. It can be seen from Figure 3.6 that the C&T LG case has the largest capacity of coal retirement, which is 11.5 GW in 2022 and 4.5 GW in 2032. Comparing the C&T LG case with the other two LG cases, the imposing of CO_2 emission penalties increases the operating cost for coal units; therefore more coal units are decommissioned in the C&T LG case. Similar reasoning maybe used to explain why more coal is decommissioned in the C&T LG case than that in the base HG and EPA HG case.

Comparing the C&T LG case with the C&T HG case, it can be seen that only about 0.5 GW of coal is retired in 2022 in the C&T HG case, which is less than 5% of the capacity of coal retired in 2022 in the C&T LG case. This is because the high natural gas price modeled in the C&T HG case increases the operating costs for natural gas units and results in the dispatching of more coal units. Therefore much less coal is decommissioned in the C&T HG case than that in the C&T LG case. No coal unit is built in any case, because coal units are expensive to build. To replace retired coal, wind and solar units are built in each case. Since more coal is retired in the C&T LG case, natural gas units are built in addition to the building of wind and solar units.

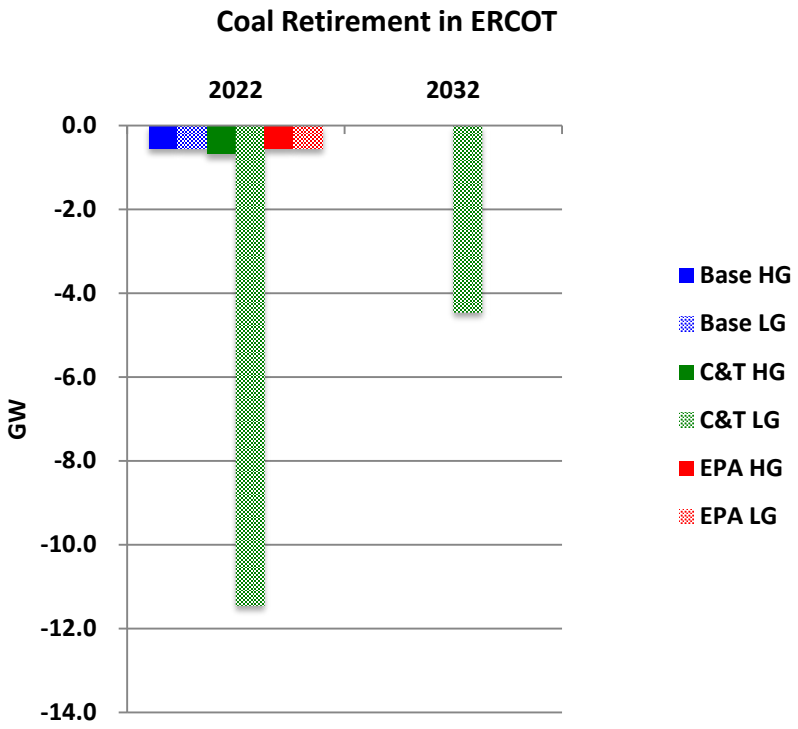

Figure 3.6: Coal Retirements in ERCOT

Coal retirements are shown in Figure 3.7 for WECC. The highest coal retirements occur in the two C&T cases because of the increased cost of burning coal. Almost all coal retirements in these cases occur in 2022. No coal retirements occur in 2022 in the other four cases. In the EPA LG case, coal is retired in 2032 in favor of low cost gas. Less coal is retired in the base LG case because less wind and solar is built to replace it because of the lack of incentives. Coal retirements are lower in the EPA HG and base HG cases because more high-cost gas is retired.

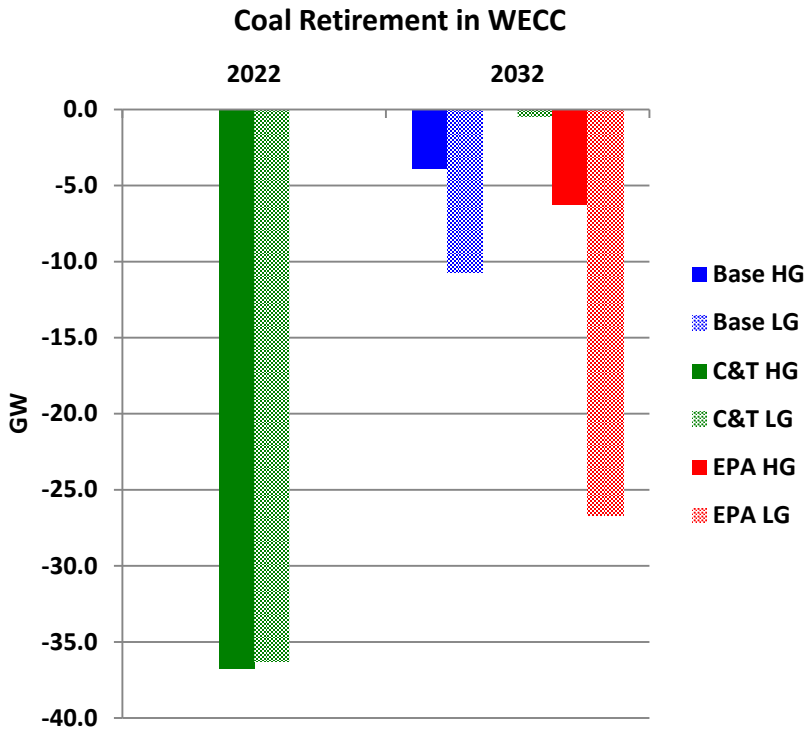

Figure 3.7: Coal Retirements in WECC

Figure 3.8 shows coal retirements for the EI. CO_2 emissions charges force greater retirement of coal units; The PTC allows more units to be retired in favor of renewables. Surprisingly, no new coal is constructed in any of the scenarios, even the base case with high gas prices. Retirement of both existing coal (and single-cycle natural gas plants) is accelerated by low gas prices, the production tax credit for wind and solar, and by cap and trade. It should be noted that no new oil units are built and retirements are substantial over the 20-year time horizon of the study.

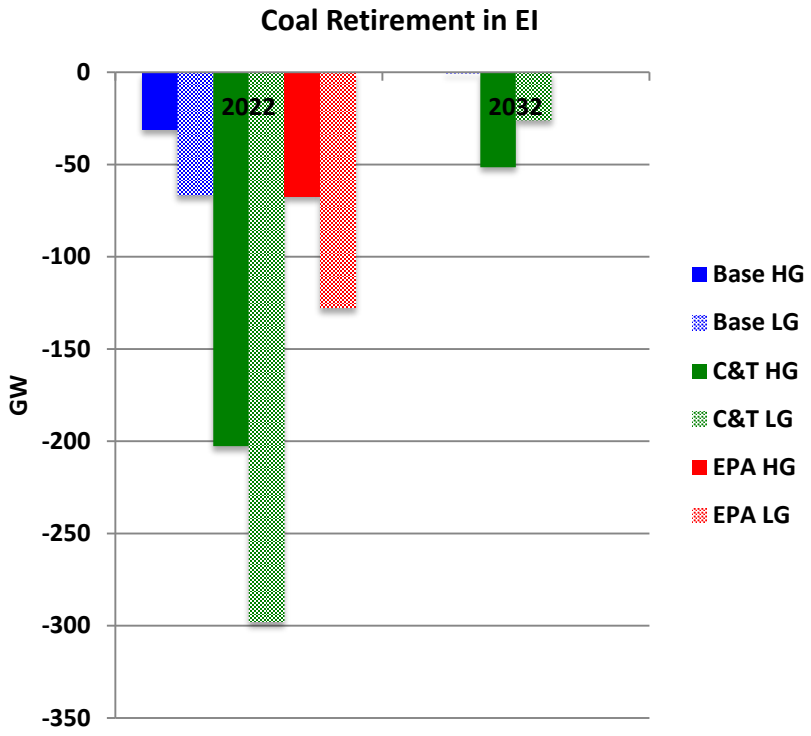

Figure 3.8: Coal Retirements in EI

3.4.3 Wind

The additions for wind generation are shown in Figure 3.9. Since wind is cheap to operate, no wind unit is retired in any of the scenarios studied. In all the six scenarios, when the wind additions from both decades of the study are added, wind reaches its building limit by 2032. From Figure 3.9, it can be noticed that the two C&T cases and the two EPA cases add the same wind capacity in 2022 and 2032, which is the result of the wind and solar incentives modeled in these four cases. In 2022, no wind unit is built in the base LG case while 1.3 GW is built in the base HG case. This is because more natural gas generation is dispatched in the base LG case since the natural gas price is lower in this case. Therefore no wind unit needs to be built in the base LG case in 2022.

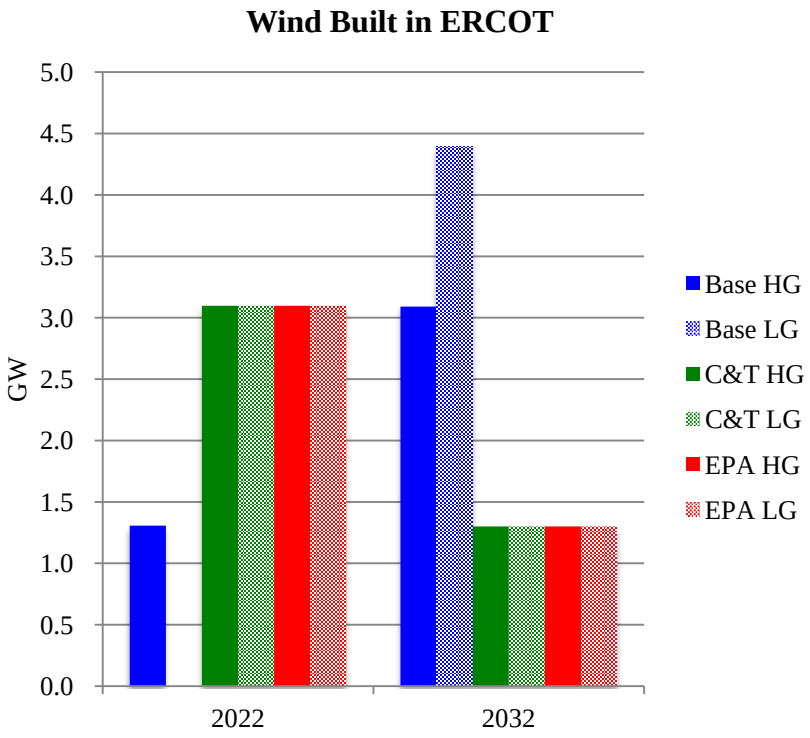

Figure 3.9: Wind Additions in ERCOT

Figure 3.10 shows the wind capacity added to the WECC system. Significantly higher, and equal, amounts of wind are added in the EPA and C&T cases because the renewable incentives make it more economical. A similar amount of wind is added in the base HG case, although more is delayed until 2032. This wind is added even without incentives to replace retired gas plants. The least amount of wind is built, and mostly in 2032, in the base LG case, because this case has the least coal and gas retirements.

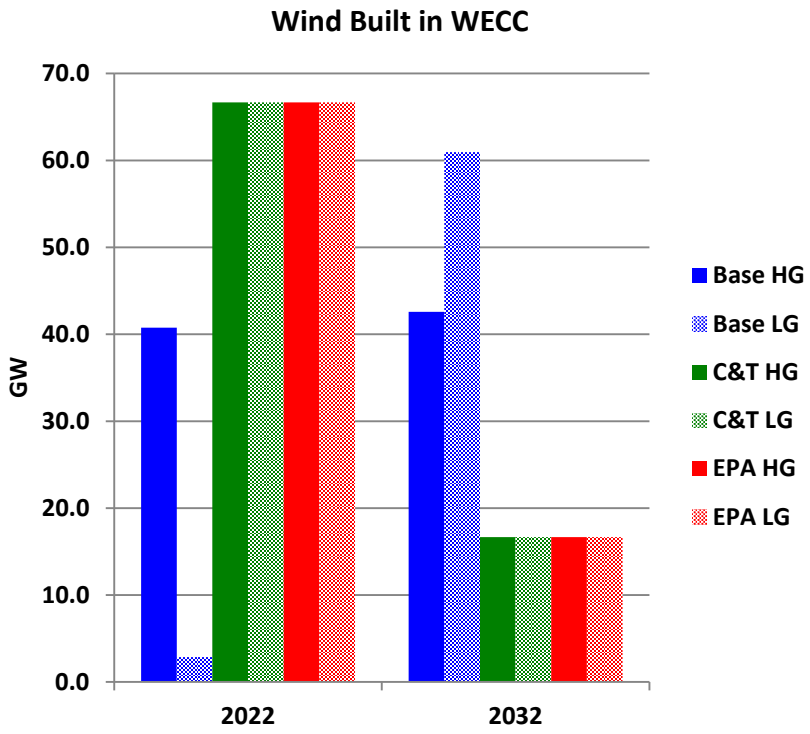

Figure 3.10: Wind Additions in WECC

Figure 3.11 shows wind additions for the EI. The largest share of wind is built in the SPP (mostly Kansas and Oklahoma). Note that the model assumes that the existing high voltage network is in place with no new high voltage lines. The geographic distribution of additional wind is likely to change if new high voltage lines are put in place. Some wind is built in the other regions (except for Florida)

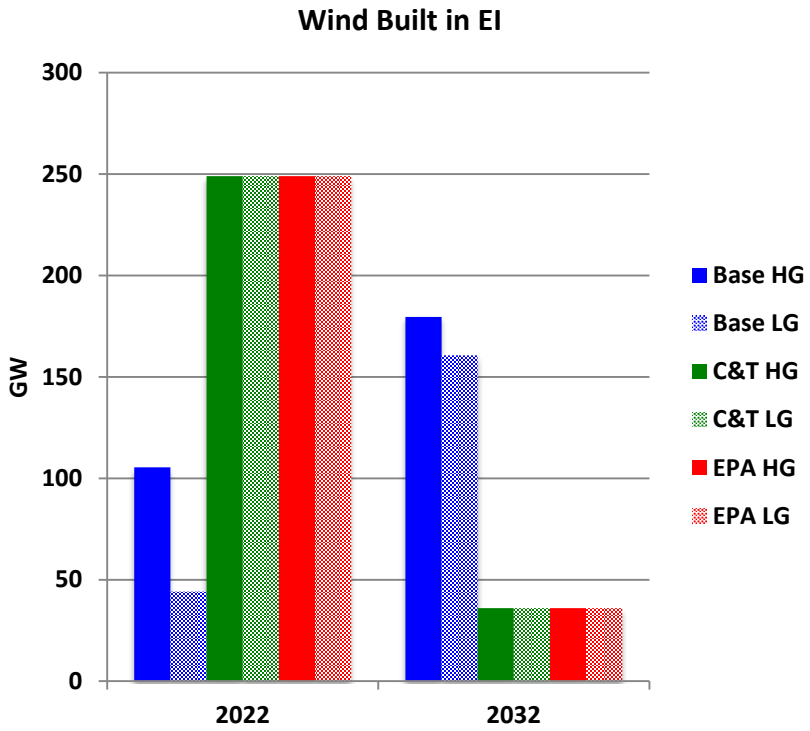

Figure 3.11: Wind Additions in EI

3.4.4 Solar

The additions for solar generation in each year are depicted in Figure 3.12. Except for the base LG case, solar reaches its maximum building limit in all of the other five cases. In the base LG case, natural gas prices are much lower than in the base HG case in 2032; therefore more natural gas generation is dispatched and less solar is built in the LG base case than in the base HG case during the second decade of the study. Since no incentives are modeled in the base LG case, less solar is built in the base LG case than in either of the two-C&T or in either of the two-EPA cases. Meanwhile, for the two base cases and the two EPA cases, solar units are only built in the second decade of the study. This is the result of the projected reduction in the capital cost of solar and the corresponding decline in the capital recovery for solar in the second decade of study as shown in Table 3.2.

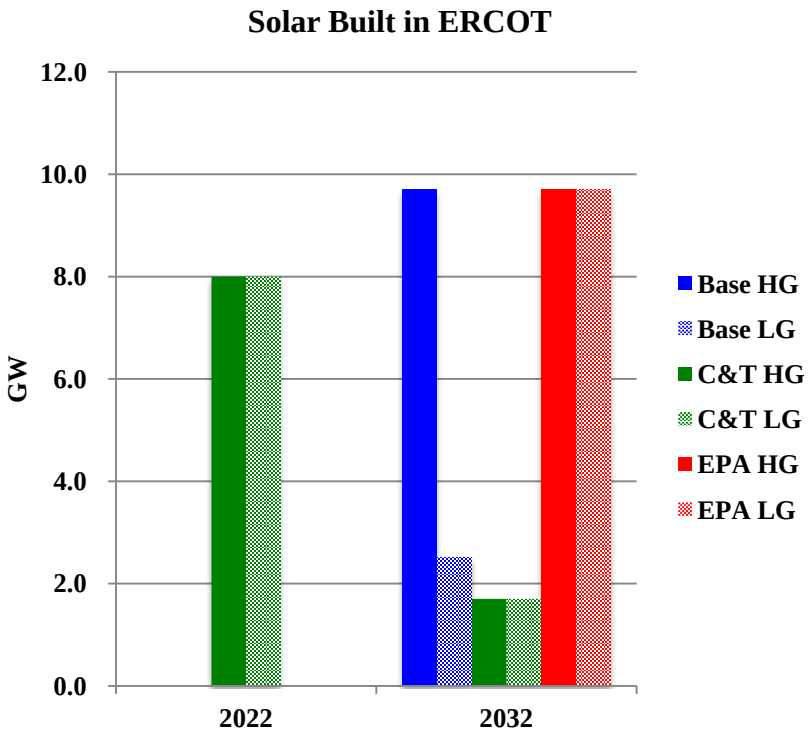

Figure 3.12: Solar Additions in ERCOT

The highest amounts of solar added, Figure 3.13, occur in the two C&T cases, because of the availability of renewable incentives coupled with prices on CO_2. In the LG C&T case, some of the solar capacity is delayed until 2032, when its capital cost is lower. Much less solar is built in the base HG case, and none at all in the base LG case, because neither incentives nor CO_2 prices are in place to make it attractive. Solar is built in the EPA cases, where the incentives are in place, to replace retired fossil plants.

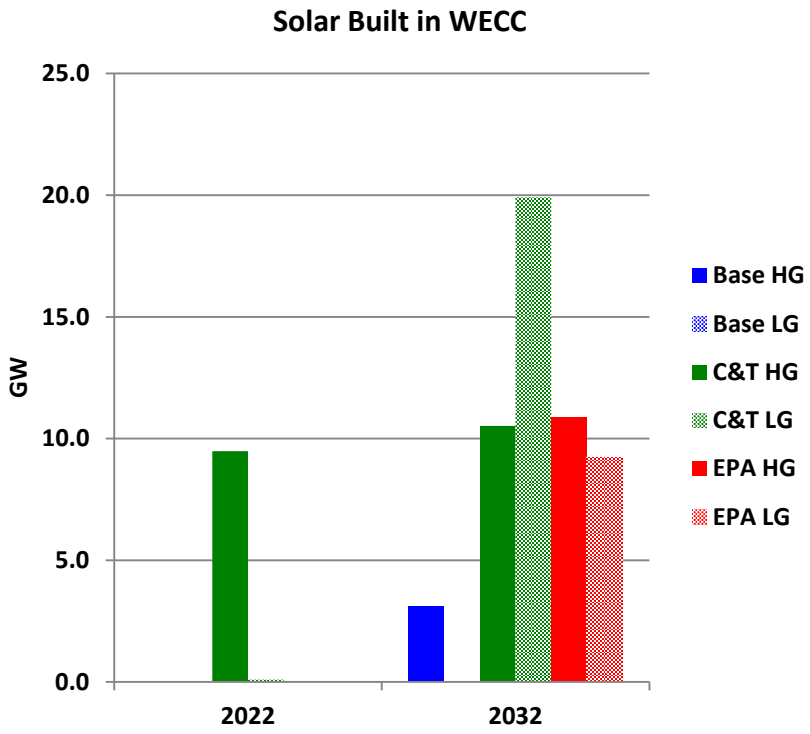

Figure 3.13: Solar Additions in WECC

Solar additions are shown for the EI in Figure 3.14. Surprisingly, by 2022, solar is constructed in all cases except the low gas price base case. By 2032 solar is added in all cases, but the most is added in cases with the production tax credit. Solar investment occurs mostly in Florida, but with the production tax credit, solar is built throughout the Southeast.

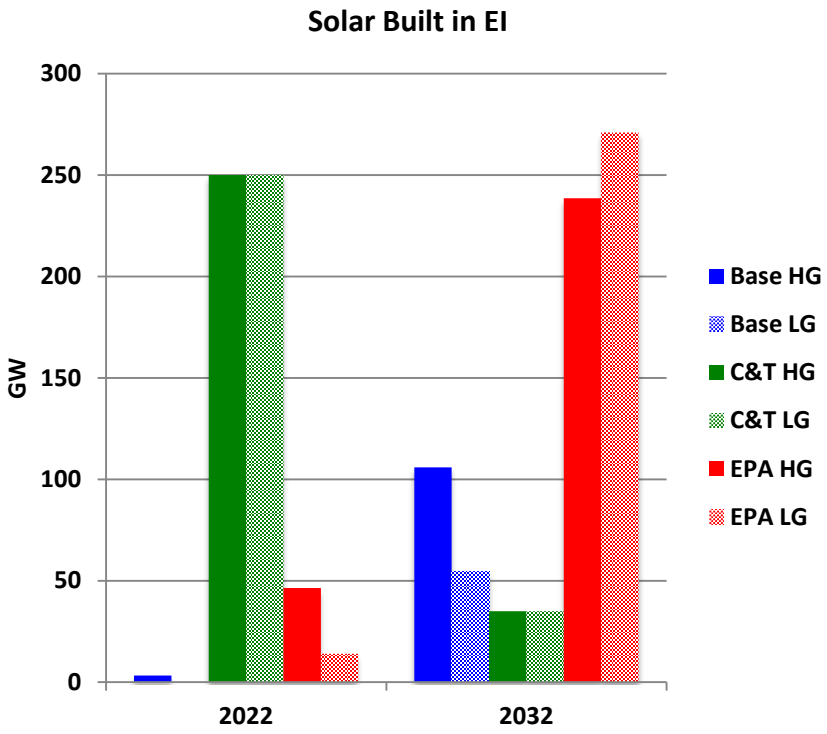

Figure 3.14: Solar Additions in EI

3.4.5 Nuclear

The additions for nuclear are shown in Figure 3.15. Since nuclear is cheap to operate, no nuclear unit is decommissioned in any case. As shown in Figure 3.15, nuclear is only built in the HG cases, which is because more natural gas generation is dispatched in the LG cases and no nuclear unit needs to be built in the LG cases. Among the three HG cases, the C&T case has the largest addition of nuclear capacity. This is expected since the imposition of a CO_2 emissions prices and the positing of high gas price decreases the dispatch of coal and natural gas generation in the C&T HG case. As solar and wind reach their building limits in 2032, nuclear units need be built to serve the demand.

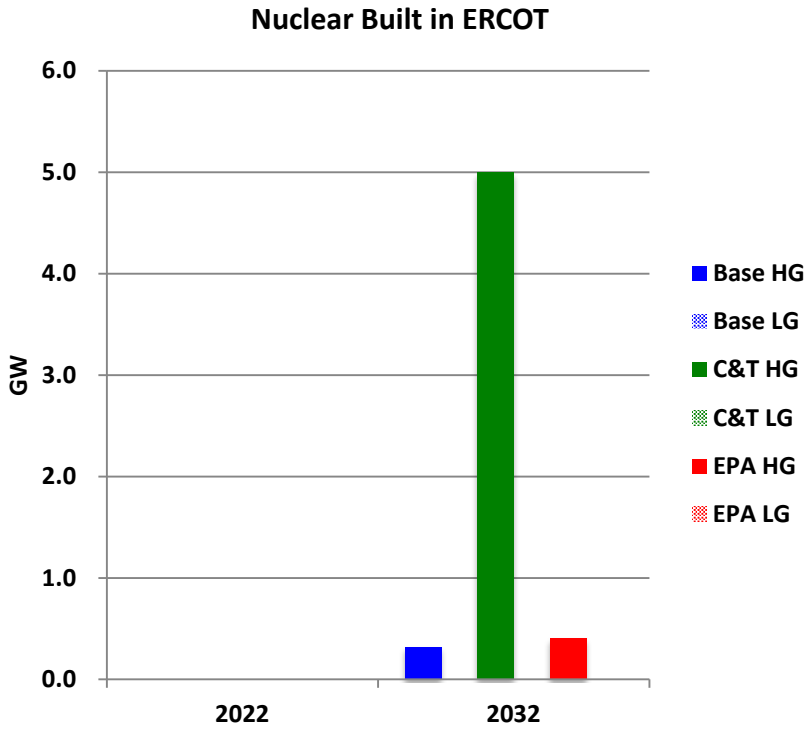

Figure 3.15: Nuclear Additions in ERCOT

Figure 3.16 shows nuclear additions for WECC. One additional nuclear plant is built in the WECC system in the C&T HG case. In this case, retirements of coal plants because of CO_2 prices, and retirement of gas plants because of high gas and CO_2 prices, make a nuclear facility economical in 2032.

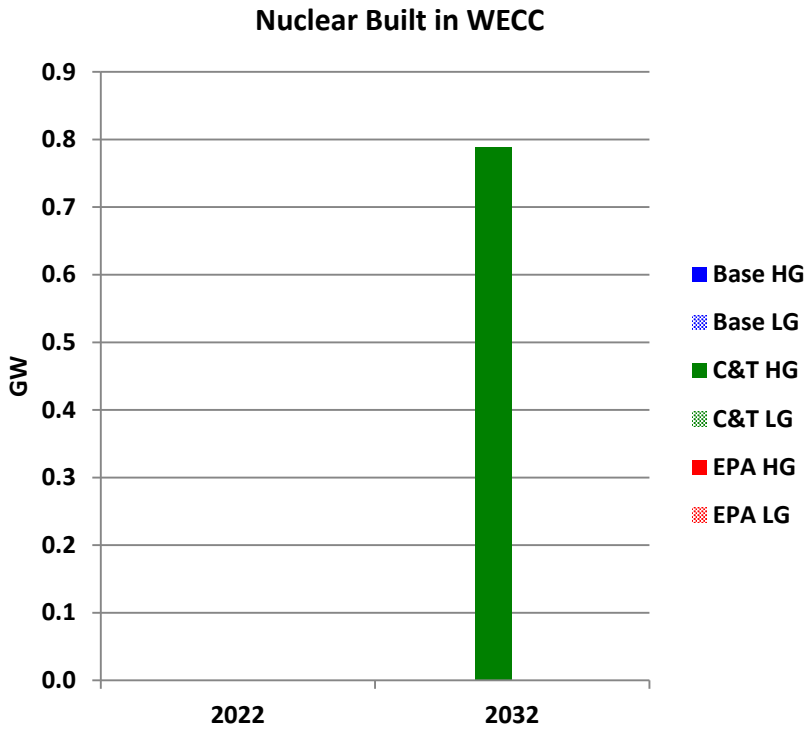

Figure 3.16: Nuclear Additions in WECC

Figure 3.17 shows nuclear additions in the EI. Nuclear is built only in the Kerry-Lieberman High Gas case. The explanation for this result is that, when capacity limits for Solar and Wind are reached, nuclear is cheaper than NGCC at $14 gas.

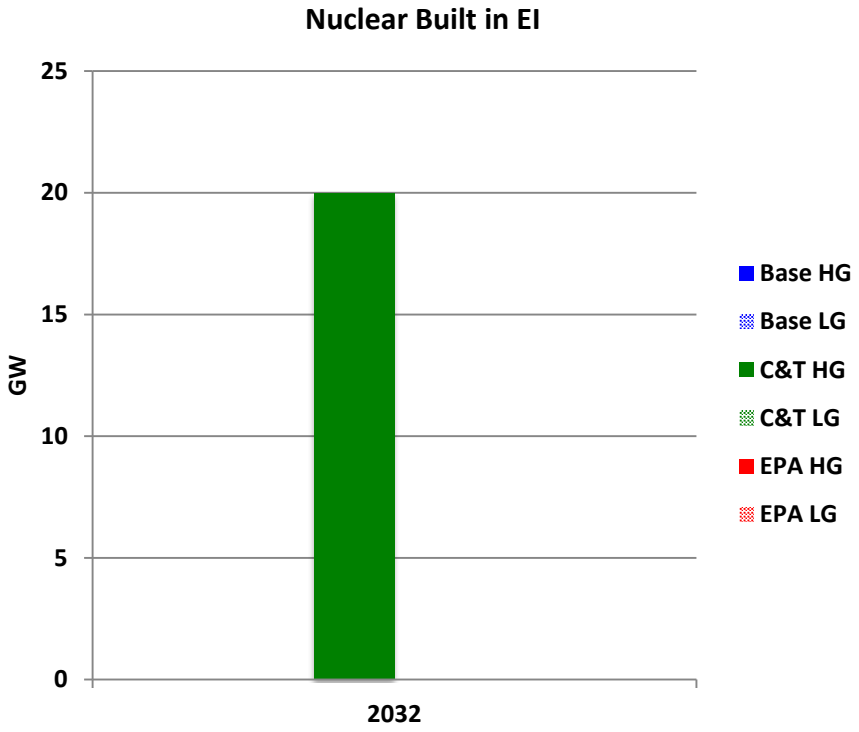

Figure 3.17: Nuclear Additions in EI

3.4.6 Wholesale Prices, Total Energy Generated and Total CO_2 Emissions

Figure 3.18 to Figure 3.21 show the total energy generated and average wholesale prices for each case. By 2032, as shown in Figure 3.18, the three LG cases have higher total energy generated than the three HG cases. This result is consistent with the results for wholesale prices; as the wholesale prices in the HG cases are all higher than those in the LG cases by 2032, which can be seen in Figure 3.21, long-term price response would cause demand to decrease in the HG cases. Among the three LG cases, the EPA case has the largest total energy generated by 2032, with the base case coming second and C&T case following next. This is also consistent with the results for wholesale prices. With CO_2 emission prices modeled, the C&T case has the highest wholesale prices among all the LG cases. The EPA LG case has the lowest wholesale prices among the three LG cases, which is the result of the solar and wind incentives modeled in this case.

The similar pattern can be also found in the three HG cases: the C&T HG case has the lowest energy generated and highest wholesale prices. It is interesting to note that the wholesale prices and the energy generated in 2032 are very close in the base HG case and EPA HG case. In year 2032, in both of these two cases, wind and solar reach their building limits and the capacity of nuclear built is similar. Since no coal or natural gas

units are built or retired in 2032 in these two cases, the generation mix in the two cases is very similar. This is why the wholesale prices and energy generated in these two cases are very close.

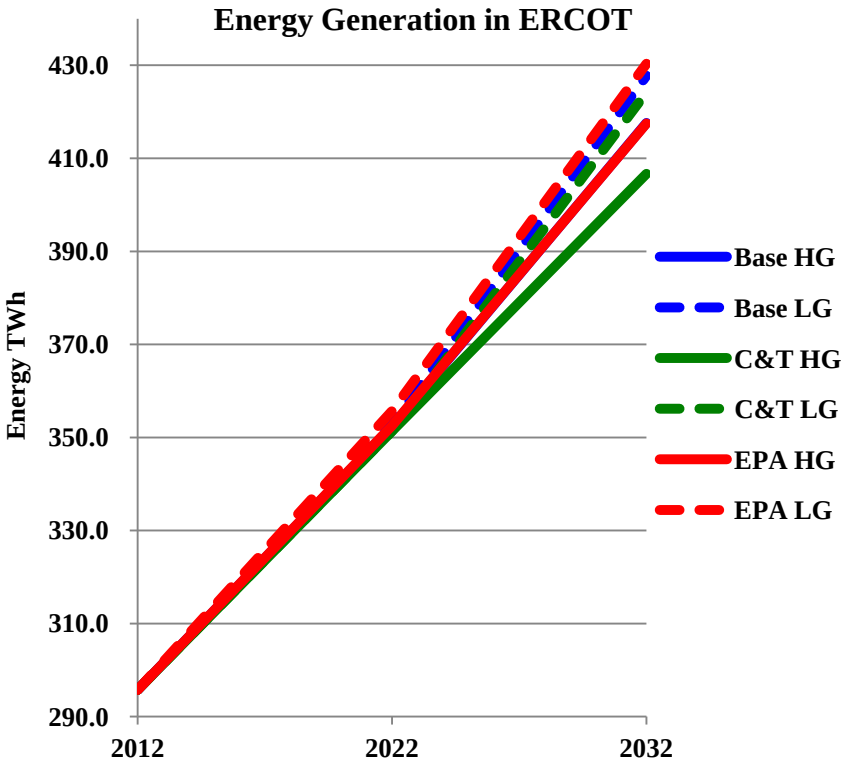

Figure 3.18: Total Energy Generated in Each Case for ERCOT

Figure 3.19 shows the total energy production in each case for WECC. The production corresponds to the wholesale prices shown in Figure 3.22. Variations in production among the cases are not very significant except for the reduction in the 2032 HG C&T case, which has a significantly higher wholesale price in 2032.

A similar but less severe pattern is shown for the EI in Figure 3.20.

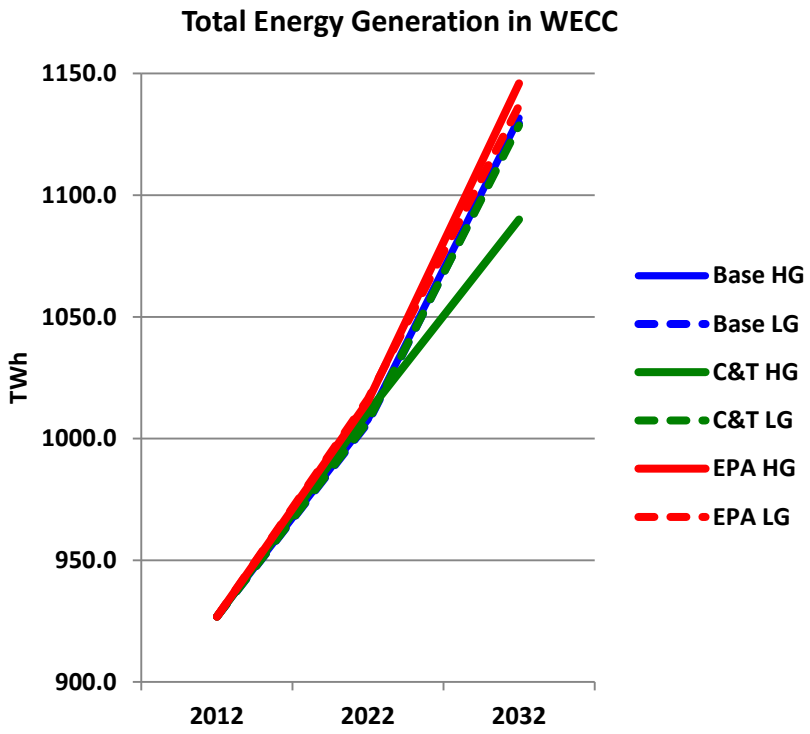

Figure 3.19: Total Energy Generated in Each Case for WECC

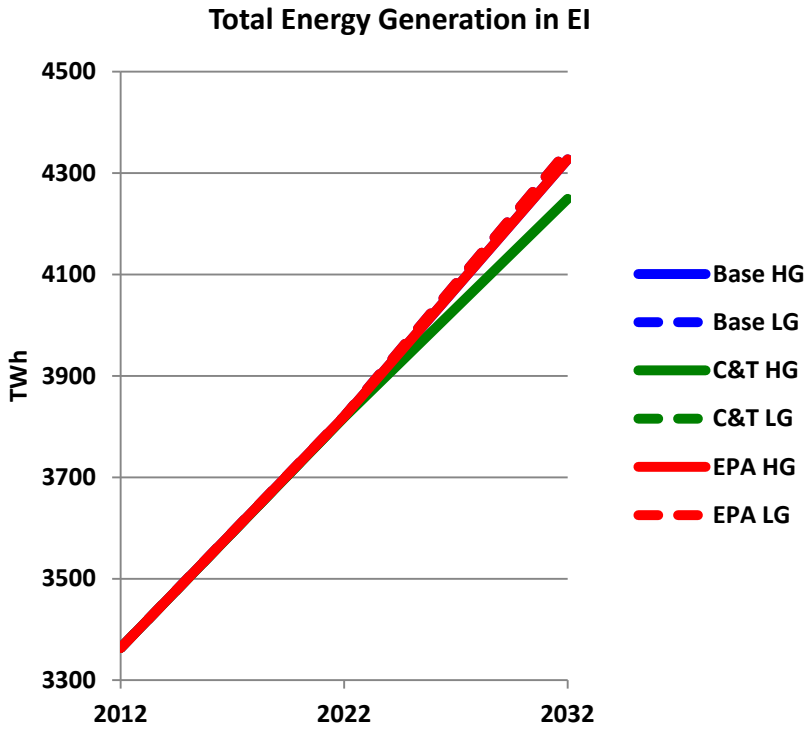

Figure 3.20: Total Energy Generated in Each Case for EI

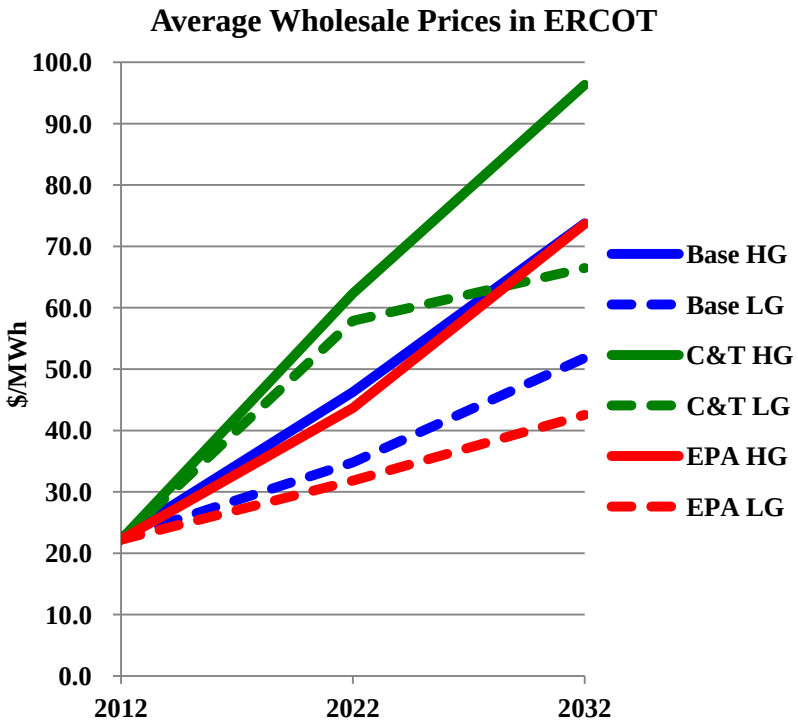

Figure 3.21: Average Wholesale Prices for Each Case for ERCOT

Average wholesale prices for WECC shown in Figure 3.22, are lowest for the two EPA cases. This is because of the low operating costs of the renewable generators that were added with incentives in this case. The price for the HG EPA case is higher in 2022 than the LG EPA case, because gas prices are higher, but by 2032 so much gas has been retired that the two prices converge. Significant renewable capacity was also added in the C&T cases, but the wholesale price is increased significantly by the price of CO_2. Because of this the C&T cases have the highest average prices.

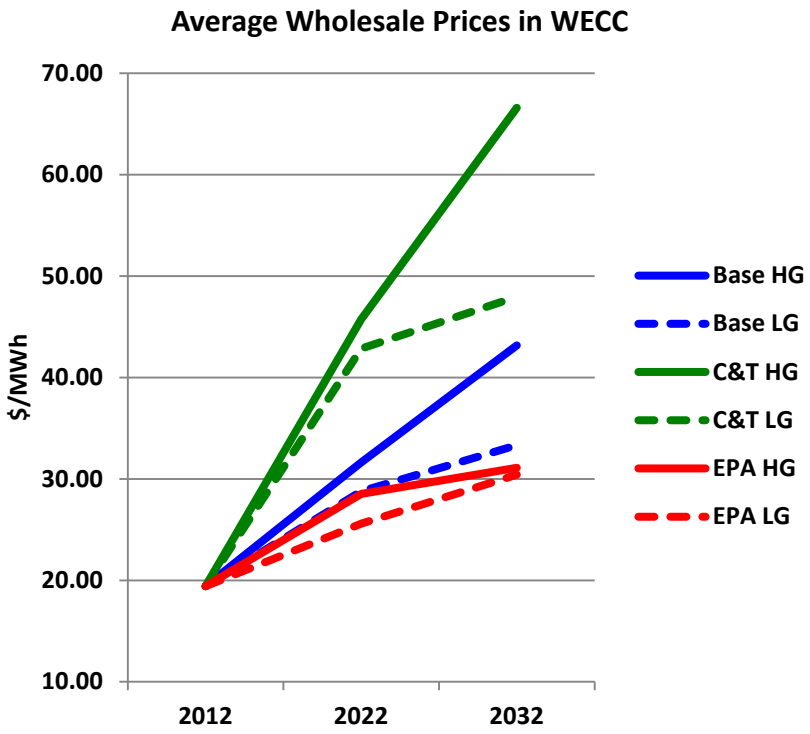

Figure 3.22: Average Wholesale Prices for Each Case for WECC

Average wholesale prices for the EI are shown in Figure 3.23. Cap and Trade (C&T) would increase LMP dramatically. EPA regulations lower prices in part because of PTC for renewables compared to the Base cases.

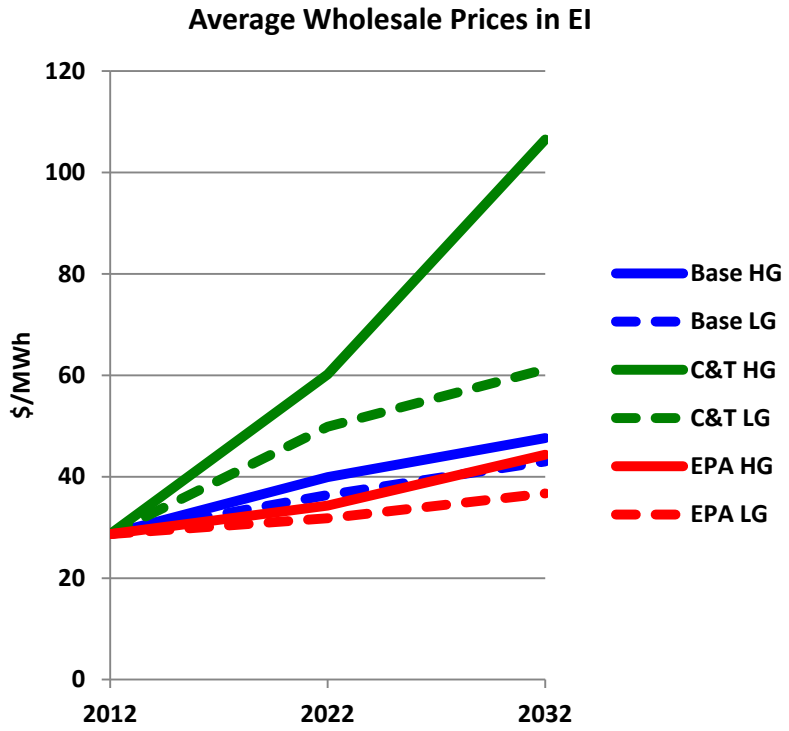

Figure 3.23: Average Wholesale Prices for Each Case for EI

The total CO_2 emissions in the ERCOT system for each case are depicted in Figure 3.24. Among all the six cases, the two C&T cases have the lowest total CO_2 emissions, which is the result of the CO_2 emissions penalties modeled in these two cases. The CO_2 emissions in the C&T HG case are higher than that in C&T LG case, which is because of the higher natural gas price modeled in the C&T HG case shifting power dispatch from future gas to existing coal. The total CO_2 emissions in the EPA LG case are lower than that in the LG base case. This is the result of the incentives for wind and solar modeled in the EPA LG case, The EPA regulation has no affects in the EPA LG case since the low natural gas price prevents coal from being built.

Comparing the HG base case with the EPA HG case, the total CO_2 emissions in the HG base case are higher in year 2022 but converge to the same level as that in the EPA HG case in year 2032. In year 2022, more wind is built in the EPA HG case, which decreases the CO_2 emissions in the EPA HG case. However, in year 2032, wind and solar reach their building limit in both cases and similar capacity of nuclear is built in the two cases. Since no coal or natural gas unit is built or retired in 2032, the generation mix in the two base cases are very similar. Therefore, the total CO_2 emissions in the two base cases are close.

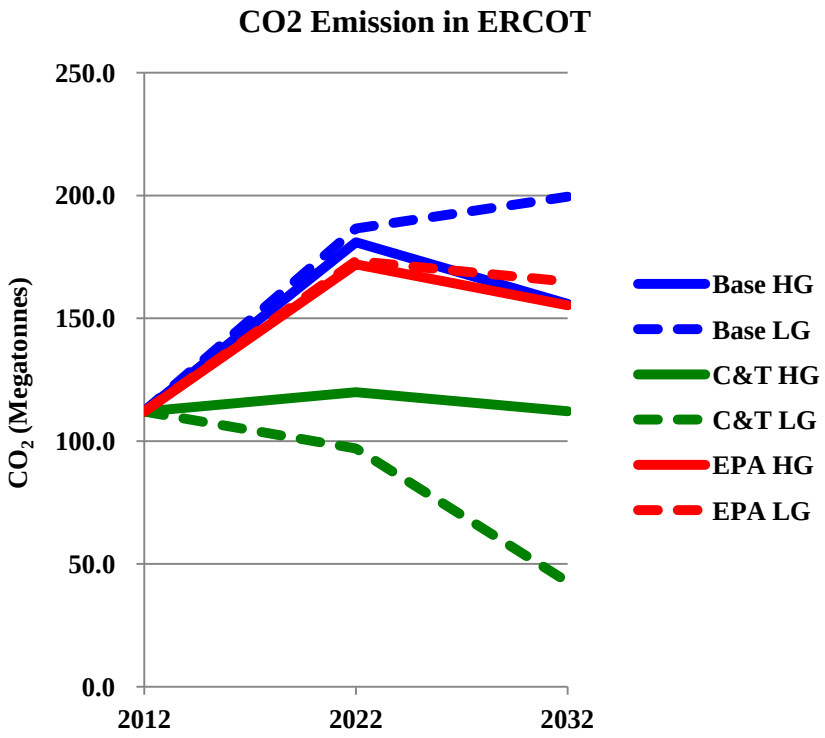

Figure 3.24: Total CO_2 Emissions in ERCOT System

Figure 3.25 shows the CO_2 emissions in the WECC system for the six cases studied. The highest emissions occur in the base cases, with the base LG case being the highest. In the base LG case, almost no renewables are built and very little coal and gases are retired. Low gas prices alone will not provide reductions in CO_2 in the WECC system.

Lower emissions for the C&T and EPA cases indicate that the policies those encompass, which were intended to reduce CO_2 emissions, had some success. The C&T cases, with incentives for renewables and prices on CO_2 emissions, significantly reduced CO_2 emissions below 2012 levels in both cases. The EPA LG case, with incentives for renewables, elimination of new coal plants, and a low price for natural gas, resulted in decreased emissions, but 2032 emissions were greater than those in 2022. The EPA HG case allowed emissions to continue increasing beyond 2012 levels, but at a slower rate than the base cases.

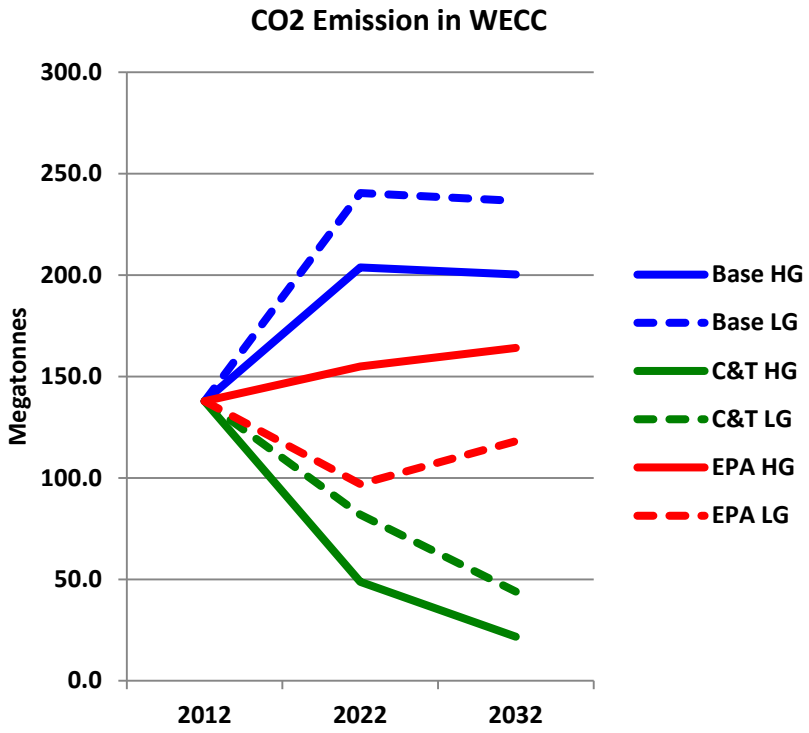

Figure 3.25: Total CO_2 Emissions in WECC System

Figure 3.26 shows CO_2 emissions for the EI. Note that EPA lowers CO_2 not by eliminating coal but because of PTC. In the Base Case, older NG units are eliminated in the HG case, which lowers CO_2 emissions in 2032, though less fuel switching occurs. In the C&T case, higher gas prices result in less Coal to NG fuel switching, which increases CO_2 emissions.

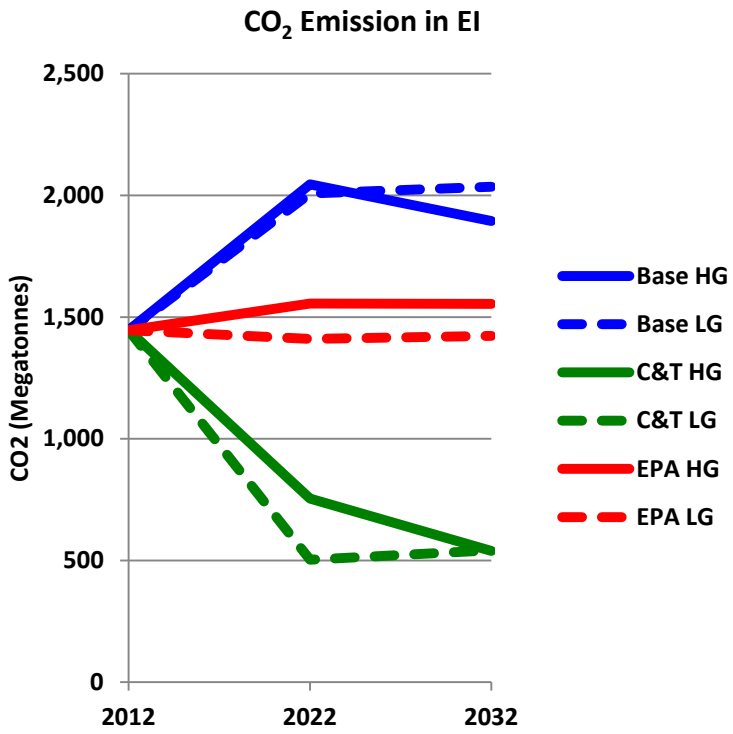

Figure 3.26: Total CO_2 Emissions in EI System

4. CONCLUSION

This research depends critically on detailed network reductions for the ERCOT (Texas), WECC (Western States), and EI (Eastern Interconnection) systems. To maintain acceptable accuracy in line flows for the Eastern Interconnection needed for optimal investment in generation, the research showed that a model with more than 5,200 busses was necessary. Since the full EI network is much more tightly connected than the ERCOT and WECC systems, it is expected that the errors in the PF and OPF solutions for the equivalent for EI will be larger than that for the ERCOT and WECC systems when the percentage of buses retained for the equivalent is the same for each model. The results of the model evaluations demonstrated that a 279-bus equivalent for ERCOT has more than acceptable accuracy in terms of both PF and OPF solutions, indicating that even a smaller equivalent would likely be acceptable. For the WECC system, a similar size system, a 300-bus equivalent, is adequate for performing an optimal generation investment study.

To assess the response of long-term generation investment to the future environment, an environment that is uncertain, studies are conducted using six possible scenarios. Each future (case) consists of three simulation years: 2012, 2022 and 2032, an interval which is based on the assumption that each investment cycle takes ten years and generation is optimized in 2022 and 2032 for conditions in that year. The simulation year 2012 is assumed to have generation as built today.

The cases studied in this report are described as follows. The first case is referred to as the base case. In the base case, no environmental regulation or subsides for renewable energy are included.

In the second case, a CO_2 emissions price is added to represent a cap-and-trade auction for CO_2. This cap-and-trade auction for CO_2 is assumed to have a price cap similar to that proposed in the Kerry-Lieberman Bill. This case is referred to as the cap-and-trade (C&T) case. In the C&T case, the CO_2 price starts at 36.94 $/ton in 2022 and rises to 60.18 $/ton in 2032, equivalent to the Kerry-Lieberman price cap. Besides modeling CO_2 emissions prices, subsides for wind and solar generation are included. An incentive of 22 $/MWh for wind and solar generation is included to model the Federal Renewable Electricity Production Tax Credit [28].

Similar to the C&T case, the third case also includes the production tax credit incentives for wind and solar generation. However, instead of cap-and-trade, the EPA proposed rule aimed at regulating CO_2 emissions from power plants is included, a rule that is expected to be finalized later in 2012. This rule requires all new fossil-fuel-fired generation of 25 MW or larger to emit no more than 1000 lbs. of CO_2 per MWh. Since coal-fired plants cannot meet this standard, the standard effectively prohibits the construction of new coal plants. Therefore, in the third case, no new coal-fired plants can be built in 2022 and 2032. The third case is referred to as the EPA case.

All of the three cases are simulated with two different sets of gas prices, yielding six futures in total. The first set of gas prices is referred to as the high gas price set, which is 2.5 $/MMBTU in 2012, 7 $/MMBTU in 2022 and 14 $/MMBTU in 2032. The gas price of 2.5 $/MMBTU modeled in 2012 is based on the assumption that the costs of extracting

shale gas start to rise by 2022 and so the gas price increases to 7 $/MMBTU. Then in 2032, the gas price converges to the world price of about 14 $/MMBTU. The gas price of 14 $/MMBTU may seem large, but the gas price was in the neighborhood of 15 $/MMBTU in 2005.

The second set of gas prices is referred to as low gas price set, which is 2.5 $/MMBTU in 2012, 4.77 $/MMBTU in 2022 and 5.86 $/MMBTU in 2032. This set of gas prices is based on estimates by the EIA [27].

Based on the different sets of gas prices used, the scenarios studied can be categorized into two groups. The cases that are run with the high gas price set are referred to as high-gas-price cases (HG) and similarly the cases that run with low-gas-price set (LG) are referred to as low gas price cases.

The results suggest that alternative policies may have very different outcomes in terms of electricity prices and CO_2 emissions that vary across regions of the continental United States.

First consider fossil fuels. For natural gas, only combined cycle plants are constructed across all scenarios with substantial retirements of single cycle plants by 2022. There is no new construction in ERCOT until 2032 and then only in the scenario with low gas prices and cap-and-trade. There is no new gas generation constructed in WECC under any scenario. The EI is a different story with combined cycle plants constructed both under high and low gas price cases for all scenarios in 2022 and 2032 with the most construction occurring under cap and trade. However, retirements generally exceed new construction in 2022 but the reverse is true for cap and trade in 2032 and more balanced in the other scenarios. Surprisingly, no new coal is constructed in any of the scenarios, even the base case with high gas prices. Retirement of both existing coal (and single-cycle natural gas plants) is accelerated by low gas prices, the production tax credit for wind and solar, and by cap and trade. No new oil units are built and retirements are substantial over the 20-year time horizon of the study.

For renewables, wind and solar are encouraged by high gas prices, cap and trade, and the production tax credit. No wind is retired under any of the scenarios. In ERCOT, wind is added by 2022 in all but the low gas price base case but more is added in all cases by 2032. For WECC, wind is added in all cases, mostly by 2022. For the EI there are very large additions under all scenarios, mostly in Kansas and Oklahoma, but some additions in all states except Florida. Note that the model assumes that the existing high voltage network is in place with no new high voltage lines. The geographic distribution of additional wind is likely to change if new high voltage lines are put in place. For solar, by 2022, small amounts are constructed in ERCOT only if cap and trade is implemented, and small amounts are constructed in WECC only in the high gas, cap-and-trade scenario. But, surprisingly, by 2022 in the EI solar is constructed in all cases except the low gas price base case. In the EI by 2032 solar is added in all cases, but the most is added in cases with the production tax credit. Solar investment occurs mostly in Florida, but with the production tax credit, solar is built throughout the southeast. It should be noted that, though no nuclear construction takes place by 2022, substantial nuclear construction takes place by 2032, but only with high gas prices and cap and trade. Thus, policies can

change how much new generation is built, what types of plants are built, and what types of plants are retired.

Across all regions, electricity prices are highest under cap and trade combined with high natural gas prices and lowest with the production tax credit for wind and solar combined with low natural gas prices. Aggregate CO_2 emissions shown in Figure 4.1 are lowest with low natural gas prices combined with cap and trade and the production tax credit for wind and solar, and highest with high natural gas prices under the base case.

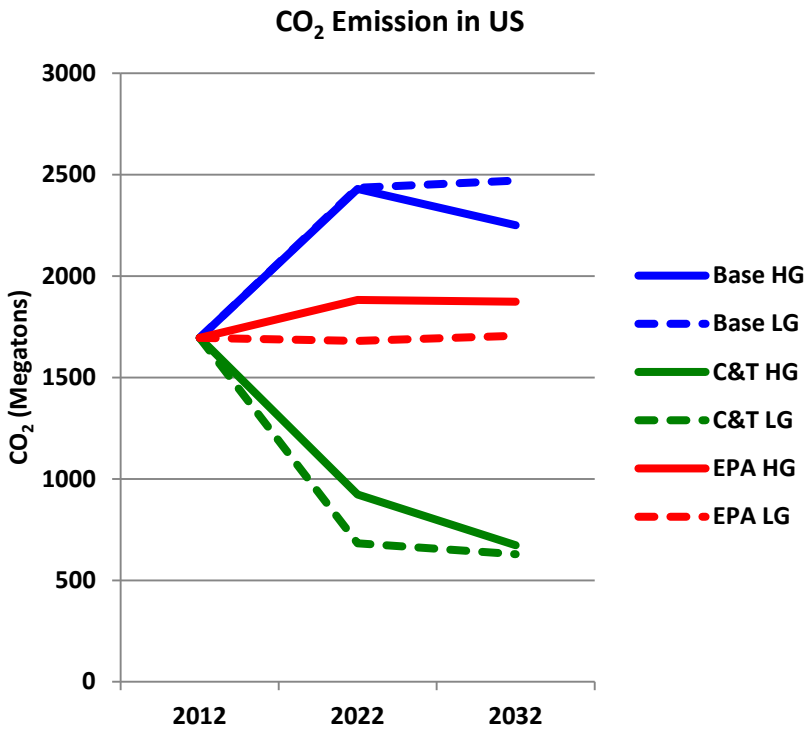

Figure 4.1: CO_2 Emission for Contiguous U.S.

A number of caveats are important in interpreting these results. First, the model assumes that a smart grid is in place in 2022 and 2032 that allows demand response. Second, capital costs are estimated far into the future and, for example, while the costs of wind are well understood, recent cost decreases for solar may, or may not, continue. This study assumes that they do. Similarly, there are several technologies proposed that may lower the costs of nuclear plants. If that were to occur, and nuclear became politically feasible, the results would be quite different than those shown here.

Finally, this study represents the first step in making the SuperOPF Planning Tool publically available as open source software similar to MatPower, since the tool has now been used at both Arizona State and at Wichita State to analyze energy futures for ERCOT and WECC respectively for this report.

REFERENCES

[1] William Schulze, et al., “Mapping energy futures using the SuperOPF Planning Tool: an integrated engineering, economic and environmental model,” Dec. 2011.

[2] F. Ma and V. Vittal, “A hybrid dynamic equivalent using ANN-based boundary matching technique,” IEEE Trans. Power Syst., to be published.

[3] P. Dimo, Nodal Analysis of Power Systems, Abacus Press, Kent, England, 1975.

[4] W. F. Tinney and W. L. Powell, “The REI Approach to Power Network Equivalents,” IEEE PICA Conference Proceedings, Minneapolis, pp. 384-390, July 1983.

[5] E. C. Housos, G. Irisarri, R. M. Porter and A. M. Sasson, “Steady State Network Equivalents for Power System Planning Applications,” IEEE Trans. Power App. Syst., vol. PAS-99, no. 6, Nov./Dec. 1980.

[6] J. B. Ward, “Equivalent Circuits for Power Flow Studies,” AIEE Trans. Power Appl. Syst., vol. 68, pp. 373–382, 1949.

[7] W. Snyder, “Load-Flow Equivalent Circuits–An Overview,” IEEE PES Winter Meeting, New York, Jan. 1972.

[8] F.F. Wu and A. Monticelli, “Critical review of external network modelling for online security analysis,” Electrical power & energy systems, vol.5, no. 4, 1983.

[9] S. Deckmann, A. Pizzolante, A. Monticelli, B. Stott, and O. Alsac, “Studies on Power System Load Flow Equivalencing,” IEEE Trans. Power App. Syst., vol. PAS-99, no. 6, pp. 2301–2310, Nov./Dec. 1980.

[10] S. Deckmann, A. Pizzolante, A. Monticelli, B. Stott, and O. Alsac, “Numerical testing of power system load flow equivalencing,” IEEE Trans. Power App. Syst., vol. PAS-99, no. 6, pp. 2292–2300, Nov./Dec. 1980.

[11] R. A. M. V. Amerongen and H. P. V. Meeteren, “A generalized Ward equivalent for security analysis,” SM, 455-5, p.1519, June. 1982.

[12] A. Monticelli, S. Deckmann, A. Garcia and B. Stott, “Real-time External Equivalents for Static Security Analysis,” IEEE Trans. Power App. Syst., vol. PAS-98, No. 2, pp. 498-508, Mar./Apr. 1979.

[13] K. L. Lo, L. J. Peng, J. F. Macqueen, A. O. Ekwue and N. H. Dandachi,”Extended Ward equivalent of external system for on-line security analysis,”, IEE 2nd International Conference, Hong Kong, Dec. 1993.

[14] J. Machowski, A. Cichy, F. Gubina and P .Omahen, “External subsystem equivalent mode for steady-state and dynamic security assessment,” IEEE Trans. Power Sys., vol. 3, No. 4, Nov. 1988.

[15] L. A. Zhukov, “Construction of power system electromechanical equivalents,” Izv. Akad. Nauk SSSR, Energy. and Transp., No. 2, 1965.

[16] E. H. Allen, J. H. Lang, and M. D. Ilic,"A Combined Equivalenced-Electric, Economic, and Market Representation of the Northeastern Power Coordinating Council U.S. Electric Power Systems," IEEE Trans. Power Syst., vol. 23, no. 3, pp. 896-907, Aug. 2008.

[17] H. K. Singh and S. C. Srivastava, “A Reduced Network Representation Suitable for Fast Nodal Price Calculations in Electricity Markets,” IEEE Power Engineering Society General Meeting, vol. 2, pp. 2070-2077, June 2005.

[18] X. Cheng and T. J. Overbye, "PTDF-based Power System Equivalents," IEEE Trans. Power Syst., vol. 20, no. 4, pp. 1868-1876, Nov. 2005.

[19] HyungSeon Oh, “A New Network Reduction Methodology for Power System Planning Studies,” IEEE Trans. Power Syst., vol. 25, no. 2, pp. 677-684, May 2010.

[20] D. Shi and D. J. Tylavsky, "An Improved Bus Aggregation Technique for Generating Network Equivalents," IEEE PES General Meeting, July 2012, San Diego, USA.

[21] D. Shi, et al., “Optimal generation investment planning: Pt. 1: Network Equivalents,” to be published.

[22] R. Zimmerman, C. E. Murillo-Sanchez, and D. Gan, MATPOWER: A MATLAB Power System Simulation Package. Ithaca, NY, 2008. [Online]. Available: http://www.pserc.cornell.edu/matpower/.

[23] The Mosek Optimization Tools Manual, [Online]. Available: http://docs.mosek.com/6.0/tools/index.html.

[24] D. Shawhan, et al., “Engineering, economic, and environmental simulation of power-sector policies: a preliminary application to carbon dioxide, sulfur dioxide, and nitrogen oxide emission regulation,” Rensselaer Working Papers in Economics, 2012.

[25] Loan Programs of Office, U.S. Department of Energy, [Online]. Available: https://lpo.energy.gov/?page_id=31.

[26] C. Dahl, A Survey of Energy Demand Elasticities in Support of the Development of the NEMS, 1993. [Online]. Available: ftp://eia.doe.gov/pub/oiaf/elasticitysurvey/elasticitysurvey_dahl.pdf.

[27] EIA, ”Annual energy outlook 2012 with projections to 2035,” DOE/EIA-0383(2012), Jun. 2012. [Online]. Available: http://www.eia.gov/forecasts/aeo/pdf/0383(2012).pdf.

[28] Database of State Incentives for Renewables & Efficiency, [Online]. Available: http://dsireusa.org/incentives/incentive.cfm?Incentive_Code=US13F.

[29] Price, J.E.; Goodin, J., Reduced network modeling of WECC as a market design prototype. *2011 IEEE Power and Energy Society General Meeting*, pp. 1-6.

[30] J. Jung, C. C. Liu, S. Tanimoto, and V. Vital, “Adaptation in Load Shedding under Vulnerable Operating Conditions”, *IEEE Trans. Power Syst.*, vol. 17, no. 4, pp. 1199-1205, Nov. 2002.

[31] N. P. Yu, C. C. Liu, and J. Price, “Evaluation of Market Rules Using a Multi-Agent System Method”, *IEEE Trans. Power Syst.*, vol. 25, no. 1, pp. 470-479, Jan. 2010.

[32] CAISO 2007 Transmission Plan, January 2007. [Online]. Available: http://www.caiso.com/1b6b/1b6bb4d51db0.pdf.

[33] Price, J. and A. Sheffrin, “Adapting California’s Energy Markets to Growth in Renewable Resources”, paper 2010GM0783, IEEE PES Annual Meeting, July 2010.

[34] James Price, 240 Bus WECC Model Data, www.pserc.wisc.edu/documents/publications/reports/2010_reports/WECC240%20data%20for%20IEEE%20PES%202011GM0942.zip.

[35] Energy Visuals, FirstRate Generator Cost Database, [Online]. Available: http://www.energyvisuals.com/products/firstrate.html.

[36] R. Zimmerman, C. E. Murillo-Sanchez, and D. Gan, MATPOWER: A MATLAB Power System Simulation Package. Ithaca, NY, 2008. [Online]. Available: http://www.pserc.cornell.edu/matpower/.

[37] D. Kirschen, G. Strbac, and I. Ebrary, Fundamentals of Power System Economics. New York: John Wiley & Sons, 2004, pp. 141-200.

[38] F. Li and R. Bo, “DC OPF-based LMP Simulation: Algorithm, Comparison with AC OPF, and Sensitivity,” IEEE Trans. Power Syst., vol. 22, no. 4, pp. 1475–1485, Nov. 2007.

[39] B. Stott, J. Jardim, and O. Alsac, “DC Power Flow Revisited,” IEEE Trans. Power Syst., vol. 24, no. 3, Aug. 2009.

[40] A. Wood and B. Wollenberg, Power System Generation, Operation and Control. New York: Wiley, 1996.

[41] J. Glover, M. Sarma, and T. Overbye, Power System Analysis and Design: 4th Edition. Thomson Engineering, 2011, pp. 281-333.

APPENDIX 1:

Gen	Gen										
BusNum	GenID	GenCostModel	GenFixedCost	GenIOA	GenIOB	GenIOC	GenIOD	GenFuelCost	GenVariableOM	GenFuelType	GenUnitType
30	H	Cubic	0	0	9.492	0	0	1.786	0.806	Coal	ST (Steam Turbine)
30	L	Cubic	0	0	9.492	0	0	1.786	0.806	Coal	ST (Steam Turbine)
31	2	Cubic	0	0	10.175	0	0	20.754	4.665	(Diesel,FO1,FO2,FO4	IC (Internal Combustion)
31	H	Cubic	0	0	9.492	0	0	1.786	0.806	Coal	ST (Steam Turbine)
31	L	Cubic	0	0	9.492	0	0	1.786	0.806	Coal	ST (Steam Turbine)
32	2	Cubic	0	0	10.644	0	0	20.754	4.665	(Diesel,FO1,FO2,FO4	IC (Internal Combustion)
32	H	Cubic	0	0	9.741	0	0	1.948	0.775	Coal	ST (Steam Turbine)
32	L	Cubic	0	0	9.741	0	0	1.948	0.775	Coal	ST (Steam Turbine)
33	H	Cubic	0	0	9.741	0	0	1.948	0.775	Coal	ST (Steam Turbine)
33	L	Cubic	0	0	9.741	0	0	1.948	0.775	Coal	ST (Steam Turbine)
34	1	Cubic	0	0	10.434	0	0	0.445	2.325	Nuclear	ST (Steam Turbine)
35	1	Cubic	0	0	10.434	0	0	0.445	2.325	Nuclear	ST (Steam Turbine)
36	1	Cubic	0	0	10.434	0	0	0.445	1.129	Nuclear	ST (Steam Turbine)
37	1	Cubic	0	0	10.434	0	0	0.445	1.129	Nuclear	ST (Steam Turbine)
38	1	Cubic	0	0	10.434	0	0	0.445	2.563	Nuclear	ST (Steam Turbine)
39	1	Cubic	0	0	10.434	0	0	0.445	3.875	Nuclear	ST (Steam Turbine)
40	1	Cubic	0	0	10.434	0	0	0.445	2.563	Nuclear	ST (Steam Turbine)
41	1	Cubic	0	0	10.434	0	0	0.445	2.563	Nuclear	ST (Steam Turbine)
42	1	Cubic	0	0	10.434	0	0	0.445	1.354	Nuclear	ST (Steam Turbine)
44	1	Cubic	0	0	8.665	0	0	7.649	0.827	Natural Gas	Combustion Turbine Part)
45	1	Cubic	0	0	8.665	0	0	7.649	0.827	Natural Gas	Combustion Turbine Part)
46	1	Cubic	0	0	8.665	0	0	7.649	0.827	Natural Gas	Combustion Turbine Part)
47	1	Cubic	0	0	8.665	0	0	7.649	0.827	Natural Gas	Part)
48	1	Cubic	0	0	8.665	0	0	7.649	0.827	Natural Gas	Combustion Turbine Part)
49	1	Cubic	0	0	8.665	0	0	7.649	0.827	Natural Gas	Combustion Turbine Part)
50	1	Cubic	0	0	8.665	0	0	7.649	0.827	Natural Gas	Combustion Turbine Part)
52	1	Cubic	0	0	11.071	0	0	7.531	2.357	Natural Gas	GT (Gas Turbine)
53	1	Cubic	0	0	11.071	0	0	7.531	2.357	Natural Gas	GT (Gas Turbine)

Each column in the table above is described below:

Gen BusNum — Number of the bus to which the generator is attached.

Gen GenID — Generator ID number; single character ID used to distinguish multiple generators at the same bus.

GenCostModel — The type of model this generator is currently using. It can be cubic, piecewise linear or none. In the test, all generators are set to have cubic cost models.

GenFixedCost — The fixed operating cost of the generator.

GenIOA, GenIOB, GenIOC, GenIOD — Parameters used to model the cubic cost characteristic of the generator. The cubic cost model used is:

$$C(p) = GenIOA + GenIOB \cdot p + GenIOC \cdot p^2 + GenIOC \cdot p^3$$

	where $C(p)$ is the generator total fuel cost and p the active power output of the generator.
GenFuelCost	The fuel cost for the generator.
GenVariableOM:	Operations and Maintenance costs for the generator.
GenFuelType	An informational field that can be set to the type of fuel the generator uses.
GenUnitType	An informational field that can be set to reflect the generator type, such as combined cycle, steam, hydro, etc.